



SAPIENZA
UNIVERSITÀ DI ROMA

Faculty of Mathematical, Physical and Natural Sciences

Department of Earth Sciences

Approaches of data analysis from multi-parametric monitoring systems for landslide risk management

Candidate: Matteo Fiorucci

Advisor: Prof. Salvatore Martino

Co-advisor: Prof. Alberto Prestininzi

XXX CYCLE



DIPARTIMENTO
DI SCIENZE DELLA TERRA

SAPIENZA
UNIVERSITÀ DI ROMA



DOTTORATO DI RICERCA
IN SCIENZE DELLA TERRA

al nonno Gerva
al nonno Nino

Abstract	5
Extended Abstract	6
1. Introduction	8
2. State of art	10
3. Proposed methodology for data analysis	22
3.1. Observation-Based Approach	24
3.2. Statistic-Based Approach	24
3.2.1. Rate analysis in monitoring strategies	28
3.3. Semi-Empirical Approach	31
4. Test-sites	34
4.1. Acuto test-site	35
4.1.1. General setting and geological framework	37
4.1.2. Geomechanical survey and slope stability analysis	39
4.1.3. Multi-parametric monitoring system	48
4.2. Peschiera Spring slope	53
4.2.1. General setting and geological framework	53
4.2.2. Multi-parametric monitoring system	57
5. Results of multi-parametric data analysis	61
5.1. OBA approach analysis	61
5.2. SBA approach analysis	106

5.3. SEA approach analysis	125
6. Discussion	129
7. Conclusion	138
8. References	141
Aknowledgements	146

Abstract

In the last decades, several approaches were proposed accounting for early warning systems to manage in real time the risks due to fast slope failures where important elements, such as structures, infrastructures and cultural heritage are exposed. The challenge of these approaches is to forecast the slope evolution, thus providing alert levels suitable for managing infrastructures in order to mitigate the landslide risk and reduce the “response” time for interventions.

Three different strategies can be defined in this regard: an Observation-Based Approach (OBA), a Statistic-Based Approach (SBA) and a Semi-Empirical Approach (SEA). These approaches are focused on searching relations among destabilizing factors and induced strain effects on rock mass.

At this aim, some experiments are being performed at different scales in the framework of consulting activities and research projects managed by the Research Centre for the Geological Risk (CERI) of the University of Rome “Sapienza”. These experiments are testing different kind of sensors including extensometers, strain gauges, rock-thermometers, interferometers, optical cams connected to Artificial Intelligence (AI) systems, for detecting changes in rock properties and detecting stress-strain changes, as well as pluviometers, anemometers, hygrometers, air-thermometers, micro- or nano- accelerometers and piezometers for detecting possible trigger of deformational events.

The results of this Ph.D. thesis demonstrate that the data analysis methods allowed the identification of destabilizing actions responsible for strain effects on rock mass at different dimensional scale and over several time-window, from short- to long- period time scale. Furthermore, the three approaches were to be suitable to recognize precursor signals of rock mass deformation and demonstrated the possibility to provide an early warning.

Extended Abstract

Negli ultimi decenni diversi approcci di analisi dei dati, provenienti da sistemi per il monitoraggio ambientale, sono stati proposti per l'implementazione e la gestione dei sistemi di *early-warning* applicati alla mitigazione del rischio da frana laddove fenomeni rapidi coinvolgono infrastrutture strategiche come le reti viarie, ferroviarie e acquedottistiche.

In quest'ottica, la presente tesi di Dottorato ha indagato e confrontato tra loro tre differenti tipologie di analisi dati: una osservazionale (*Observation-Based Approach* – OBA), una statistica (*Statistic-Based Approach* – SBA) ed una semi-empirica (*Semi-Empirical Approach* – SEA). L'attenzione è stata posta sulla ricerca di relazioni tra fattori destabilizzanti la stabilità di ammasso e le deformazioni risultanti. Più in particolare il primo approccio, quello Osservazionale, si basa sulla ricerca di relazioni oggettive di causa-effetto tra fattori predisponenti e/o innescanti e le deformazioni di versante ad essi implicabili. Il secondo approccio, quello Statistico, applica funzioni di cross-correlazione a tutte le serie dei parametri monitorati cercando una significatività statistica ed una correlazione alle variazioni dei loro *rate* nel tempo. L'ultimo approccio, il Semi-Empirico, si basa su modelli reologici semplificati e sulla loro calibrazione nel tempo effettuata al fine di predire ed anticipare il momento di rottura di un versante. Gli approcci proposti sono stati studiati per metterne in luce tre caratteristiche principali: l'abilità di individuare segnali precursori di fenomeni di frana; la capacità di analizzare e determinare relazioni causa-effettive tra fattori predisponenti l'instabilità di ammasso e le deformazioni risultanti; la possibilità di essere considerati validi nella strutturazione di un sistema di allertamento precoce in grado di gestire la sicurezza delle opere infrastrutturali esposte al rischio e dei loro utenti.

Con questo scopo sono stati strumentati due sistemi di monitoraggio multi-parametrico in altrettanti *test-site* scelti nell'ambito delle attività di ricerca e consulenza svolte dal Centro di Ricerca per i Rischi Geologici CERI, di Sapienza Università di Roma. Un primo *test-site* è quello della cava abbandonata di Acuto (Frosinone – Italia),

dove si hanno fenomeni di *rock fall* che coinvolgono l'ammasso roccioso alla scala del blocco di roccia o della parete di cava sub-verticale e intensamente fratturata. Un secondo *test-site* è invece quello del versante delle Sorgenti del Peschiera (Rieti – Italia), dove fenomeni di deformazione gravitativa profonda (DGPV) operano a scala dell'intero versante che ospita al suo interno le gallerie drenanti dell'acquedotto di Roma. I sistemi di monitoraggio installati in questi due casi di studio, hanno previsto l'utilizzo di diversi sensori: estensimetri, *strain gauges*, termocoppie da roccia, interferometri, camere ottiche dotate di Intelligenza Artificiale, stazioni meteo, accelerometri e micro-accelerometri, piezometri. I dati provenienti da questi sistemi sono stati gestiti mediante i tre approcci proposti nell'ottica di individuare i fattori predisponenti od innescanti le deformazioni di ammasso.

I risultati discussi nella presente tesi di Dottorato dimostrano che i tre metodi di analisi proposti hanno permesso l'identificazione di azioni destabilizzanti responsabili delle deformazioni dell'ammasso roccioso, su scale dimensionali diverse e su diverse finestre temporali, dal breve al lungo termine. In particolare, i tre approcci sono risultati utili a identificare le forzanti continue (come la temperatura, il livello idrico di falda, i fenomeni di *creep*) e le forzanti transienti (come la pioggia, il vento e le vibrazioni indotte). L'approccio osservazionale è risultato utile nell'individuare forzanti continue, cicliche oppure impulsive che predispongono l'instabilità di ammasso nel breve-medio termine. L'approccio statistico è invece risultato utile nell'individuare e calcolare la variazione dei *rate* dei fattori innescanti rispetto le deformazioni indotte nel corto e medio termine. L'approccio semi-empirico ha permesso di individuare il *trend* reologico di lungo periodo dei fenomeni di *creep* agenti sul lungo periodo.

Infine, i tre approcci proposti sono risultati adatti a riconoscere i segnali precursori della deformazione dell'ammasso roccioso e hanno dimostrato la possibilità di fornire un *early-warning* per mitigare il rischio geologico connesso alla presenza delle infrastrutture quali elementi esposti al rischio.

1. Introduction

This Ph.D. thesis is focused on the comparison among three different approaches for analysing data from multi-sensor and multi-parametric monitoring systems devoted to mitigate the landslide risk that involve main infrastructures. These different approaches are tested for their suitability in providing strategies to fixed alert levels aiming at reducing the “advice time” for interventions in the infrastructures safety management.

During the last decades, several approaches were proposed accounting for early warning systems to manage in real time risk due to fast slope failures where important elements, such as structures, infrastructures and cultural heritage are exposed. Three possible approaches can be followed to this aim: an Observation-Based Approach (OBA), a Statistic-Based Approach (SBA) and a Semi-Empirical Approach (SEA).

The OBA is based on searching objective cause-to-effect relations among predisposing and/or triggering factors and induced effects; the SBA is based on searching statistically significance cross-correlations among different parameters and their rate variation to point out anomalies of continuous or cumulative values; the SEA is based on simplified rheological models and their time-by-time calibration.

These methodologies have been tested for analysing data from multi-parametric and multi-device monitoring systems installed in two test-sites. The expected result is to fix and define alert detection strategies suitable for mitigating the geological risk and reducing the response time for interventions, in the frame of risk management policies.

The monitoring systems are managed in the framework of technical consulting activities and research projects carried on by the Research Centre for the Geological Risk (CERI) of the University of Rome “Sapienza”. These experiments are experiencing different kind of sensors including extensometers, strain gauges, rock-thermometers for detecting changes in rock properties and detecting stress-strain changes; as well as

rain gauges, anemometers, hygrometers, air-thermometers, micro- or nano-accelerometers and piezometers for detecting possible triggers.

In Chapter 4, the main features of the test-sites are presented and the operating multi-parametric monitoring systems are described. The general results of data analysis from multi-parametric monitoring system are presented in Chapter 5. For each data analysis approach, the main specific results are summarized, after the discussion on data series, and their strengths are highlighted. Discussion on results follow in Chapter 6, where suitability and usefulness of approaches is treated in order to ponder the application of them at various landslide phenomena with the aim to provide an early warning system for the safety of infrastructures.

2. State of art

Gravity-induced instabilities from natural slope and cliff represent a topic of interest regarding the monitoring of fast to very fast failures, including rockslides or rock falls from natural and artificial slopes (Cruden & Varnes, 1996). The relevance of such events is mainly related to the short advice-time that should be necessary to transmit alarm signals for early warning in case of exposed infrastructures (such as railway, highways, pipelines and aqueducts), since no significant displacements are generally detectable before failure occurrence.

The recognition of pre-failure events by multi-parametric monitoring systems in natural contexts is an important target to mitigate the geological risk due to abrupt failures. Changes in stress conditions of rock masses due to impulsive or viscous deformations can cause rapid and violent failures able to widely affect slopes and generate landslides or hypogeous collapses (Evans et al. 2006). The pre-failure behaviour of rock masses represents a complex geomechanical topic because the stress and jointing conditions as well as the joint setting can strongly constrain pre-failure effects, such as fractures generation, opening or closing of joints and rearrangement of the stress field.

The pervasive nature of the landslides combines unpredictability and infrequency of disaster. These favour clearly a cautious investment strategy from decision makers since in numerous situations, hazard mitigation or vulnerability reduction unveils a high socio-economic cost for an uncertain far-off benefit. For these risk situations, multi-parametric monitoring systems, linked to early-warning procedures, appear a very good solution in prevention plan. Monitoring offers a temporary strategy to ensure public safety prior to more definitive remediation or vulnerability reduction works. It provides at least delay for appropriate decision making, timely action and important investments to be planned (Bigarré et al., 2011).

The setting-up of a multi-parametric monitoring system towards an identified ground movement hazard requires correct identification of the most relevant factors, in

regard to the physical mechanisms potentially driving the instability, so as to classify them in a hierarchy according to their role, impact, chronology and causality effect, relatively to the considered phenomenon. It is possible to distinguish (Klein et al., 2008):

- a) *worsening factors*: they promote but do not cause occurrence of the phenomenon;
- b) *triggering factors*: they directly cause the occurrence of the phenomenon;
- c) *precursor signals*: they mark irreversible acceleration and short term appearance of the hazard.

This may conduct to monitor very heterogeneous physical variables, i.e. ranging from water table level in an observation borehole to GPS monitoring, passing by seismic ground shaking and ground temperature. This multi-parameter approach leads to the definition of vigilance and alarm variables linked to the measurements: a vigilance variable will be typically associated with a worsening or even a triggering factor depending on the relevant case. Whereas the alarm variables will allow initiation of an alert procedure associated with possible occurrence of the phenomenon (for instance acceleration of the sliding movement, opening of fractures)(Klein et al., 2008).

Other authors (Gunzburger et al., 2005) identify three different factors which contribute to making a rock mass prone-to-failure, with particular attention to surface temperature fluctuations to preparing rockfalls phenomena. The distinction between immediate causes and less-immediate ones (like gradual weathering) stems from the fact that the former acts directly, whereas the latter exerts a slow cumulative effect and therefore requires a long period of time to become effective and ultimately induce a major consequence. It is possible to distinguish:

- a) *preparatory factors*: causes of medium- to long-term changes in resistance or disturbing forces. In order to be efficient, their small and almost imperceptible effects must be cumulated up until rupture;

- b) *trigger factors*: changes over the short-to-medium term and constitute the most direct causes of failure;
- c) *predisposition factors*: characteristic of the typology of the slope. Some slopes are in fact more conducive than others to rockfall activity, due to background factors such as topography (height and steepness of valley walls), vegetation, lithological parameters, and fracture geometry and density. Unlike *preparatory* and *trigger factors* that are defined by their action period, *predisposition factors* do not exhibit any evolution over time; instead, they serve to define the general framework of the slope that incites, to varying degrees, the onset of instabilities.

Distinction among the aforementioned typologies of factors has been made based on their physical nature: mechanical, hydrological, thermal or geochemical phenomena.

Monitoring of these factors before failure time in addition with the failure detection (and of the potential aftermaths if necessary) provides the most coherent approach at least during the stage of design. Monitoring of the stakes is even more important as the latter may be at the origin of a new induced hazard (Kilburn e Petley, 2003).

In this regard, there are several strategies to monitor these causing factors and manage the related risk. However, there are two major methods used for natural hazard controls.

The first one (focused on hazard) consists in monitoring precursors of rock failures by multi-parametric monitoring system mainly composed of micro- or nano-accelerometers recording devices as well as by acoustical emission recording. Examples of such multi-parametric monitoring system are present in alpine areas, where rockfalls are common instabilities phenomena probably correlated with permafrost degradation induced by climate changes. At this aim a multi-parametric monitoring system, composed by five tri-axle geophones and a rock thermometer, was installed since 2007. The preliminary data processing, carried out for search cause-effect relations, show the classification and identification of the significant microseismic

events and the analysis of their special-time distribution. The first results indicated a possible correlation between cluster of microseismic events and temperature trend (Amitrano et al., 2010). Similar multi-parametric monitoring system was operating at La Clapiere rockslide, an high-scale mountain slope instabilities in the southern French Alps. The multi-devices system was composed of four three-component seismic stations, four Global Position System (GPS) and three weather stations. Data analysis was performed by combining the results of monitoring devices with geological investigation, with the aim to investigate the unstable rock mass behaviour (Gaffet et al., 2010).

The second strategy (mainly focused on vulnerability) consists in observing the landslide source areas as well as the threatened infrastructures, by using optical devices (among which camera, laser scanner, and interferometer) capable of detecting fast morphological changes or abnormal and unexpected objects hazardous for the monitored infrastructure. A first example of these applications are present in (Antonello et al., 2004), where an innovative technique for the remote assessment of ground displacements, based on radar interferometry (GB-InSAR), has been tested in recent years on a number of selected case sites. Several applications of the system have been conducted on a number of mass movements located in Italy for the measurement of the superficial ground displacements of different landslide types, in terms of failure mechanism, materials involved, kinematics, water content and deformation rates. This second strategy was also applied at Mt. Pucci cliff (Italy), where an integrated approach to the geomechanical characterization of coastal sea cliffs was performed through field-based geomechanical survey and multi-parametric remote sensing monitoring systems, including terrestrial laser scanner (TLS) InfraRed Thermography (IRT) and radar interferometry technique (GBInSAR), with the aim to characterized the rock mass and evaluate the role of the surveyed joint sets in inducing slope instabilities (Martino e Mazzanti, 2014).

Some authors tried to combine the two strategies for a common purpose, using innovative devices. In fact remote sensing monitoring instruments such as Terrestrial

Laser Scanner (TLS) and interferometric radar (GBInSAR), capable to inspect an unstable slope with high spatial and temporal frequency, was coupled with microseismic monitoring system that provide a deeper insight of stress and strain conditions within the rock mass. The capability to detect microseismic events is a key for understand the slide kinematics and triggering mechanism of future collapses (Arosio et al., 2009).

Great relevance is assumed by multi-parametric monitoring systems applied to risk mitigation that involve strategic infrastructures (such as highways, railway and aqueducts) or main workplace (such as mines and yards for underground excavation). A first example can be found in Linglong gold mine (China) work areas, where the main transport roadway (MTR) is involved in excavation-induced deformation changes due to dynamic collapse of large-scale mined-out areas. In this scenario a multi-parametric monitoring system, composed by subsidence level devices, multiple-point displacement devices, convergence measurement of cross-section devices, stress measurement devices, acoustic emission (AE) monitoring devices have been installed with the aim to the safe and reliable operation of the main transport system (Lai et al., 2006). Thanks to the results of the monitoring system, the authors divided the deformation process into three interesting periods:

- a) *quiet period*: where the inner rock mass is relatively quiet with no apparent AE. This means that the rock mass is stable;
- b) *burst period*: where AE from the rock mass becomes suddenly active at a certain time, but it reverts to the quiet state after a short time;
- c) *continuously active period*: where AE occurrence is relatively active. The large event rate, AE and energy release rate increase sharply.

In Europe, decades of mining have left extensive underground cavities beneath or near urban areas. To ensure post-mining risk management and public safety, numerous real time microseismic monitoring systems were installed. The goal is to detect remote rock mass fracturing processes, precursory events and phases of

accelerating rock mass deformations and collapses (Contrucci et al., 2010). A permanent multi-parametric monitoring system, including high-resolution microseismic network coupled to a surface field-displacement measurement system, was installed in French to improve the knowledge of the large-scale ground failure phenomena caused by old underground mining works. This system is able to transmit a large amount of data for on-line processing that provide daily insight into the evolution of geological system (Contrucci et al., 2011). Multi-parametric monitoring system focused on micro-seismicity activities can also be applied to the safety of hydropower station. In Southwest China (Xu et al., 2015), an high-resolution microseismic monitoring system was established in deep underground caverns to assess the instability of underground caverns and resolve the complex subsurface conditions of the highly fractured rock mass. This system was devoted to define correlations between measured microseismic activities and excavation damage zones in the surrounding rock mass. The monitoring results demonstrate that microseismic events mainly occurred in high-stress-concentration regions. This comprehensive method, which incorporates microseismic monitoring, numerical analysis, traditional monitoring and field observations, is promising for predicting the deformation and instability of surrounding rock masses in the underground caverns. Multi-parametric monitoring system was also applied to soil slide phenomena that represent a hazard for two important railway lines. In this case, the landslide is monitored by an array of displacement measurement system including GPS units, a ShapeAccelArray (SAA), satellite InSAR, and crack extension metres, as well as an array of piezometers. This system provide near real-time displacement data on which an early warning system is calibrated for detecting changes in landslide annual displacement cycles and potential acceleration (Macciotta et al., 2016).

The researches described above, are based on data analysis approaches aiming to find the trigger factors of the landslide movements searching cause-effect relationships on multi-parametric monitoring raw data series. To improve these traditionally strategies, some authors propose an innovative approach based on the seismic noise

rate analysis. In fact, changes in base noise level or in Fast Fourier Transform (FFT) amplitude are symptom of an increase or a variation of the monitored values. A first example of this methodology is in multi-parametric monitoring system, composed by displacement devices and seismic sensors, of an unstable vertical rockslide in a natural cliff in southern France. Seismic noise analysis showed a steady increase in the high frequency base noise level in the signal recorded by the sensor installed on the unstable rock slice during the weeks preceding the collapse. High frequency seismic noise base level seems to represent subcritical crack growth. Drop of the seismic noise amplitude was concomitant with the later stages of instability. In this study case, the seismic rate analysis approach has worked very well in the perspective of risk mitigation, recognizing precursory sequences of collapse (Got et al., 2010). Similar analysis was conducted for monitoring the unrest of active volcanoes. In fact, the base level activity of volcanoes can be detected by continuous monitoring of minimum amplitude of all spectral components, filtering the transitory signal related to weather and environmental conditions. The application to data recorded at three different volcanoes demonstrates the ability of this methodology to clearly distinguish volcanic background activity from signs of re-activation and provide an early warning for volcanic eruption (Vila et al., 2006).

The middle latitudes, and the Mediterranean basin, are particularly subjected to considerable daily and seasonal thermal variations as reflection of intense solar radiation. In spring and autumn seasons, air temperature excursions can frequently exceed tens of degrees. This seemingly negligible effect can influence the long-term behaviour of fractured rock masses operating as thermal fatigue process and acting as preparatory factor for rock failure and slope instabilities. In these environmental contexts, multi-parametric monitoring system have been installed in order to quantify the influence and magnitude of thermo-mechanical effects on slope stability. With this aim, block stability in the Cliff of the Masada monument was studied using field mapping, mechanical analysis and a multi-parametric monitoring system composed by displacement, pressure, temperature, relative humidity devices. A monitoring period

of one year has point out a linear un-reversible displacement trend that is interpreted as the block response to regional micro-seismicity. A pronounced cyclic displacement trend is also shown to be a response to climatic changes on the cliff wall. All data from monitoring system was analysed by direct comparison between displacement values and temperature, humidity and pressure values to highlight the triggering factors of deformation (Hatzor, 2003). An improvement was done, in the same study case, comparing thermally and seismically induced sliding mechanism of block. In fact, physical and mechanical lab-tests were carried out to provide the assumed depth of penetration of the heating front during seasonal cycles of exposure as well as the thermal expansion coefficient of the rock mass. These values allow quantifying the expected thermally induced displacement rate of the block. Cycles of earthquake vibration was numerically simulated. Numerical modelling found that for a time window of 5000 years, the observed 200 mm displacement is more likely to have been thermally controlled, rather than seismically. The results imply that in climatic regions where temperature amplitude over a seasonal cycle is sufficiently high, thermally induced displacements play an important role in rock slope erosion and stability (Bakun-Mazor et al., 2013). In areas characterized by temperate climate, as in France, thermal and geotechnical in situ measurements were carried out in order to examine surface thermomechanical phenomena and their potential contribution to rock fall triggering. The test site was equipped with different kind of devices to record the temperature variation in the rock-mass and the potential induced effects. Furthermore, laboratory test were conducted for testing the fatigue processes that afflict the rock mass. The measured data were analysed based on analytical solutions and numerical modelling, following and observational strategies (Merrien-Soukatchoff and Gasc-Barbier, 2017).

Some authors observed that hazardous rockfalls occur during periods when known trigger factors (such as precipitation, seismic activity and freezing conditions) are absent. These authors have been suggested that these rockfalls may occur due to solar heating of rock surface, which can cause an outward expansion. Thanks to data from

multi-parametric monitoring system, including thermal and displacement devices, it was possible to assess the magnitude and temporal pattern of thermally induced rock deformation. A thermodynamic analysis has revealed that daily seasonal and annual temperature variations are sufficient to drive cyclic and cumulative opening of fracture with consequent detachment of rock (Collins e Stock, 2016). Other important studies have been carried out to know the importance of rock surface temperature related to sub-surface and depth temperature of rock mass exposed to solar radiation. In fact, subsurface temperature in rocks naturally fluctuate under the influence of local weather conditions. These fluctuations can provide a natural hazard in term of landscape evolution. Two main contributors to the heat balance have been identified: i) heat flux entering the rock mass through conduction; ii) the incoming shortwave solar radiation (Gunzburger e Merrien-Soukatchoff, 2011). Multi-parametric monitoring system was applied also to the Randa (Switzerland) rock slope instabilities, revealing seasonal deformation trend. In fact, relative dislocation rates across active fractures increase when near-surface rock temperatures drop in the fall and decrease after snowmelt as temperature rise. This temporal pattern was observed with different devices at the ground surface and in depth, representing the behaviour of the entire instabilities. Numerical modelling was carried out taking into account measured displacement values and thermal forcing in order to study objective relations between them (V. Gischig et al., 2011; V. S. Gischig et al., 2011a, 2011b).

Multi-parametric monitoring systems, focused on rock mass temperature, have also been applied to preservation of sites relevant for natural heritage. The goal of these systems was to explore diurnal, seasonal and annual temperature oscillations at the shallowest part of the rock mass and to acquire an insight into the heat balance both at the surface and within the rock mass. At this aim, several thermocouples were embedded at different positions and at various depths. Numerical models, calibrated on monitoring data series, reproduced the existence of thermally drive strains after quasi-cyclic (reversible) movements and irreversible (plastic) strains demonstrating

that temperature oscillations can be regarded as a main contributing factor to the total displacement rate at a rock wall scale (Greif et al., 2016).

Authors studied the influence of thermal factors on seismic response of unstable rock column. At this aim, a multi-parametric system, coupling seismic and thermal devices, was installed in French Alps. Spectral analysis of seismic noise allowed several resonance frequencies to be determined, ranging from 6 Hz to 21 Hz. Seismic noise monitoring pointed out that resonance frequencies fluctuate with time, under thermomechanical control. For seasonal cycles, changes in frequency are due to the variations of the bulk elastic properties with temperature. At daily scale, increase in fundamental frequency with temperature has been interpreted as resulting from the rock expansion inducing a closure of the rear fracture rock bridges, hence stiffening the contact between the column and the rock mass. Conversely, the rock contraction induces a fracture opening and a decrease in resonance frequency. These results were obtained analysing data from monitoring system and performing a direct comparison between thermal and/or rainfall record and seismic time series with the purpose of finding objective relations (Bottelin et al., 2013).

Following the wide literature background, integrated monitoring systems should be designed and arranged for a comprehensive aim including to satisfy the following requirements: i) investigation or detection of the sites at different evolutionary stages (forward prevention), corresponding to different distributions of the landslide hazard; ii) definition and control of parameters to forecast the short-term evolution of gravity-driven instabilities (e.g. high-velocity landslides) as well as to plan alert systems (real-time prevention).

Such a design strategy guarantees that a very relevance role is played by monitoring over time different physical processes that can contribute to geological risk mitigation at different scales, i.e. involving different typologies of infrastructure (Fig. 1).

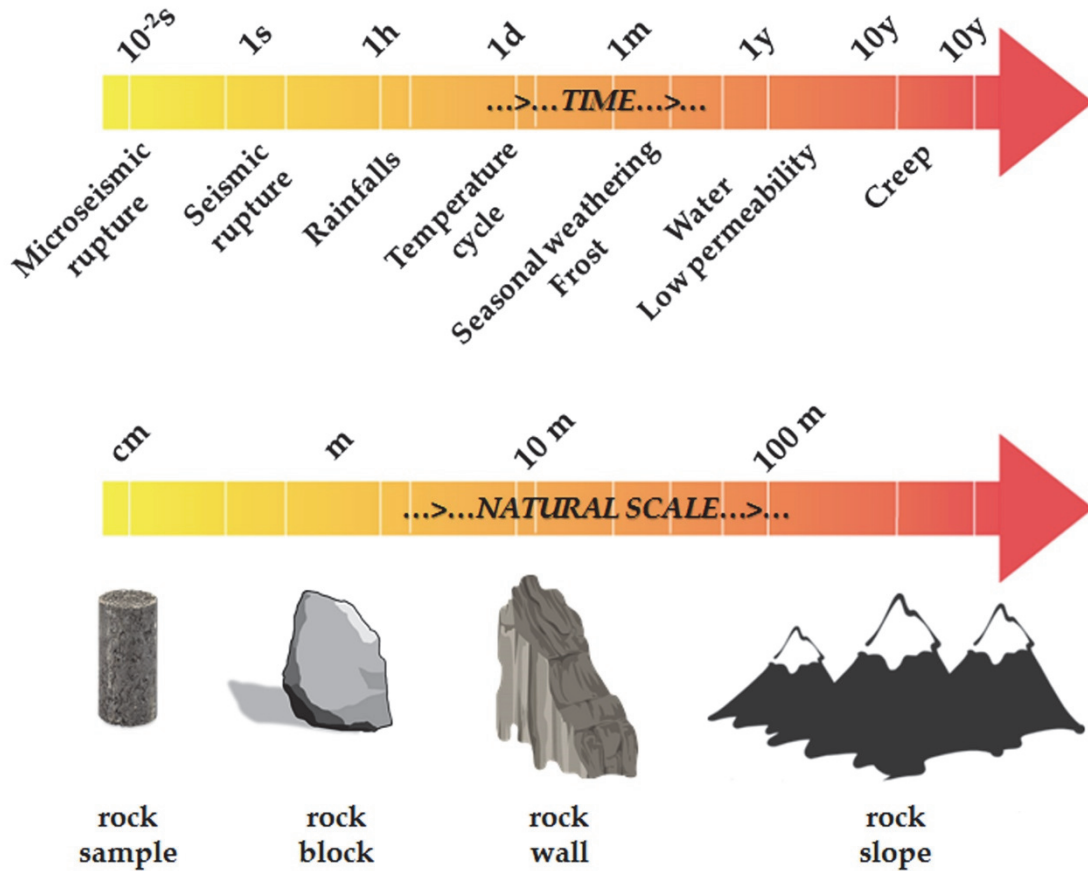


Fig. 1: Schematic timetable of some heterogeneous physical processes contributing to the occurrence of geological instabilities. From left to right: transient – quasi-static scale (upper). Schematic table of various scale of several geological context in which the heterogeneous physical processes are acting (bottom). Modified from (Klein et al., 2008).

In the last years, virtualization technologies and web applications introduced new solutions for managing applications, to store and process important amount of data, while ensuring seamless access to the data whenever and wherever needed, to all persons involved in the collaborative work. On this recent informatics trend in based the Cloud monitoring concept (Bigarré et al., 2011). Monitoring systems for early warning need huge data sets to be managed in very short time by (semi)automatic data-flow-to-data-processing analyses. This concept involves the development of computerized multi-parametric monitoring systems. Peculiarity of Cloud Parametric Monitoring Systems (CPMS) are: (i) redundancy of the measurement data; (ii)

secondary relevance of the *a-priori* understanding of cause-effect relations of the monitored phenomena; (iii) reconstruction of *ex-post* relations between destabilizing causes and/or forcing factors and induced effects; (iv) quantification of alert levels and connected control index for infrastructure management. In this way, CPMS can be designed as a part of a Wireless Sensor Network (WSN) for real-time data transmission (Fantini et al., 2015; Rosi et al., 2011). Feasibility, simplicity and low costs are key points to appreciate monitoring strategies; nonetheless, specific research should be devoted in evaluating the efficiency of different approaches also in an integrative perspective. In this regard, main criteria for a suitability evaluation are: i) delay-time from event occurrence (detection) to data processing (info-flow) to alert signal (warning); ii) number of true vs. false positives or negatives; iii) how to turn the alert detection into intervention procedures or strategies, in real to delayed time respectively.

Within the general framework just presented, the following dissertation aims at performing a comparative analysis of heterogeneous environmental data by testing three different approaches for multi-parametric data management through CPMS: Observation-Based Approach (OBA), Semi-Empirical Approach (SEA) as well as statistical (in clouding analysis) ones (SBA).

Final goal is to determine the suitability of each approach in providing the relation between *trigger factors* and related stress-strain effects for a better comprehension of the gravity-driven slope deformations evolving toward failures or general collapses. The expected result of these relational analyses is to best-tune control indexes for identifying several alert levels suitable for mitigating the geological risk and reducing the “advice-time” for interventions, in the frame of risk management policies.

3. Proposed methodology for data analysis

The installation of a multi-parametric monitoring system allows to acquiring important information on the evolution of a physical system. More in particular, in this Ph.D. thesis the attention is focused on the evolution of two different kind of landslide slopes. At this aim, the multi-parametric monitoring systems are commonly designed including the use of different type of devices focused on the same target.

Three main approaches are proposed and applied for the treatment of the recorded monitoring data: an Observation-Based Approach (OBA), a Statistic-Based Approach (SBA) and a Semi-Empirical Approach (SEA). The first one, OBA, is focused on searching objective cause-to-effect relations among *predisposing* or *trigger factors* and induced effects. This approach is based on well-constrained engineering-geological and evolutionary models; therefore, a site-specific know-how is requested for the considered slope. Such an approach has the great advantage to allow for long-term prediction and for the temporal calibration of the model, thus easily accounting also for changes in the boundary conditions. The second one, SBA, adopts statistically-based cross-correlations among different parameters and/or their rate variation to point out anomalies of trends in case of continuously recorded values (i.e. extensometer, piezometer) as well as scatters in case of discontinuous values (i.e. rainfalls intensity, earthquake records), treated as cumulative values. This approach needs huge datasets to be managed in very short time by (semi)automatic data-flow-to-data-processing analyses, accounting for early warning strategies. The recent development of several contact and remote monitoring technologies, as well as the development of cloud-systems for dataset storage and the increasing capabilities of processors, are making the application of the above described approaches more and more effective and the application of SBA strategy more feasible. The last one, SEA, is based on simplified rheological models and their time-by-time calibration based on long-term monitoring time series. This approach does not need for detailed information about the slope, but only for a good dataset of monitoring data. It may allow for the temporal prediction of

the slope failure, but it fails for slope processes affected by relevant temporal changes of the controlling and triggering factors.

When a geological risk that involve main infrastructure (such as railways, highways and aqueducts) is manifest and detected, this can be mitigated by installing a multi-parameter monitoring system. Design stage of the monitoring system architecture is based on a detailed engineering geological model, defined thanks to direct survey and remote sensing techniques. The data collected by multi-parametric monitoring system, are informatically managed through the constitution of specific cloud-database and analysed following one of three proposed approaches: one by one or by combining together. The challenge of these approaches is to forecast the slope evolution thus providing alert levels, fixing threshold values on monitored parameters, suitable to reduce the response time for interventions in the infrastructures management (Fig. 2).

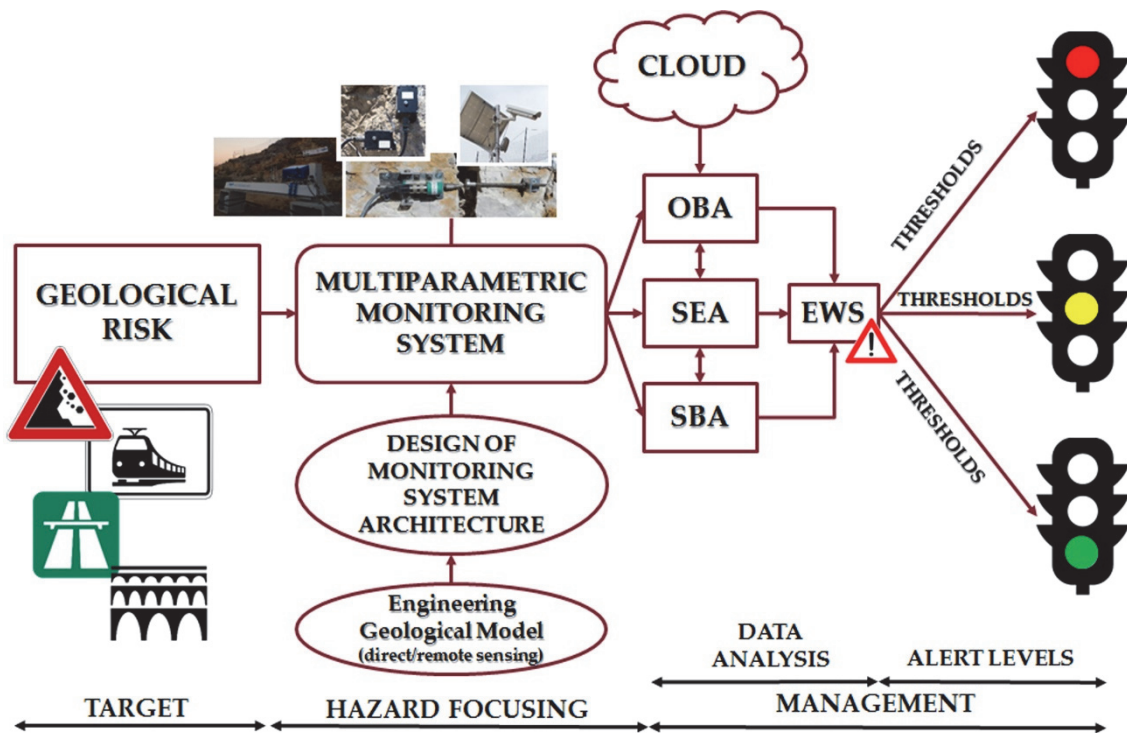


Fig. 2: Flow chart illustrating the role of data management approaches in the frame of geological risks mitigation processes. The data from a multi-parametric monitoring system was processed through one of the three proposed approaches for mitigation of the geological risk by real time early warning system.

3.1. Observation-Based Approach

The Observation-Based Approach (OBA) is focused on searching objective cause-to-effect relations among *forcing triggers* and *induced effects*: in fact, it is assumed that events are chained according to “cause-effect” logic relations.

As a part of a monitored physical system, two types of data are generally available: continuous and discontinuous ones. Continuous data are monitored over time and they have always a measurable value, which may be constant over a certain period but never null. On the other side, discontinuous data are referred to transitory episodes, related to impulsive events that occur with some intensity only at certain times. In order to search for objective correlations among the different monitored data, the discontinuous ones generally represent possible destabilizing triggers while the continuous data can be generally related to the induced effects. Impulsive phenomena can play indeed a trigger role by causing transitory variations of the recorded process evolution trends respect to their absence.

In this framework, OBA analysis approach results particularly suitable to investigate paroxysmal *destabilizing factors* that induce a deformative response in the slope during a short or middle time. For this purpose synoptic graphs and tables, that allow evaluating the evolution of several variables together and establishing their concause, are produced.

3.2. Statistic-Based Approach

The Statistical-Based Approach (SBA), uses statistic correlation functions to output objective relationship between two independent time series, $x(t)$ and $y(t)$. Cross-correlations can be performed among several time-series by testing the reciprocal dependence, i.e. by performing a check for couple of series. The cross-correlation measures the similarity of two series as a function of the lag of one relative to the other.

The cross correlation outputs a statistical coefficient CCF (R_{xy}) whose value increase at increasing coincidence between the time series. The cross-correlation function of two continuous temporal series $x(t)$ and $y(t)$ acquired with sampling step τ , is defined as:

$$R_{xy}(\tau) = \int_{-\infty}^{+\infty} x(t)y(t + \tau)dt \quad [1]$$

For instance, consider two real valued function x and y differing only by an unknown shift along x-axis. Using the cross correlation function is possible to find how much y must be shifted along the x-axis to make it identical to x . The formula essentially slides the y function along the x-axis, calculating the integral of their product at each position. When the functions match, the value of $(x*y)$ is maximized (Fig. 3).

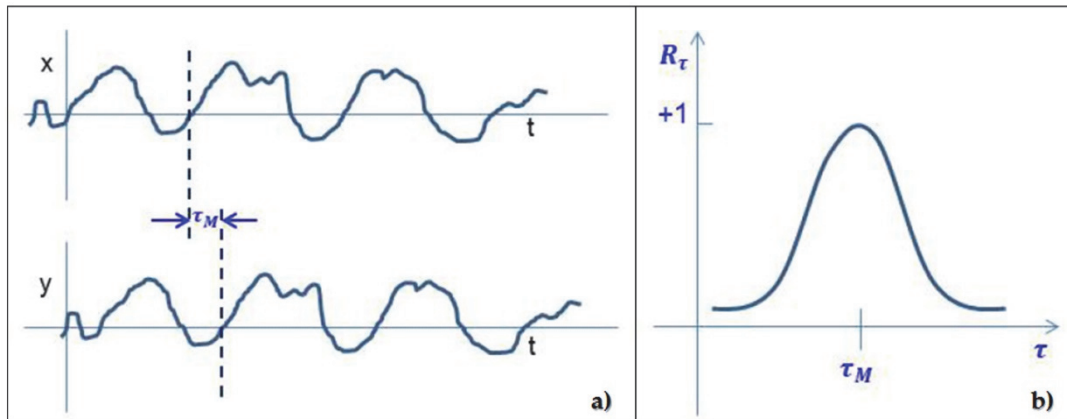


Fig. 3: Graphic illustration of cross correlation function. Two functions $x(t)$ and $y(t)$, with offsets of tm , are compared to each other. Translating $x(t)$ respect $y(t)$ is possible to find a maximum cross correlation coefficient (CCF) when the shift between $x(t)$ and $y(t)$ is minimal.

In Fig. 4 shows some types of cross correlation results for different kind time-series.

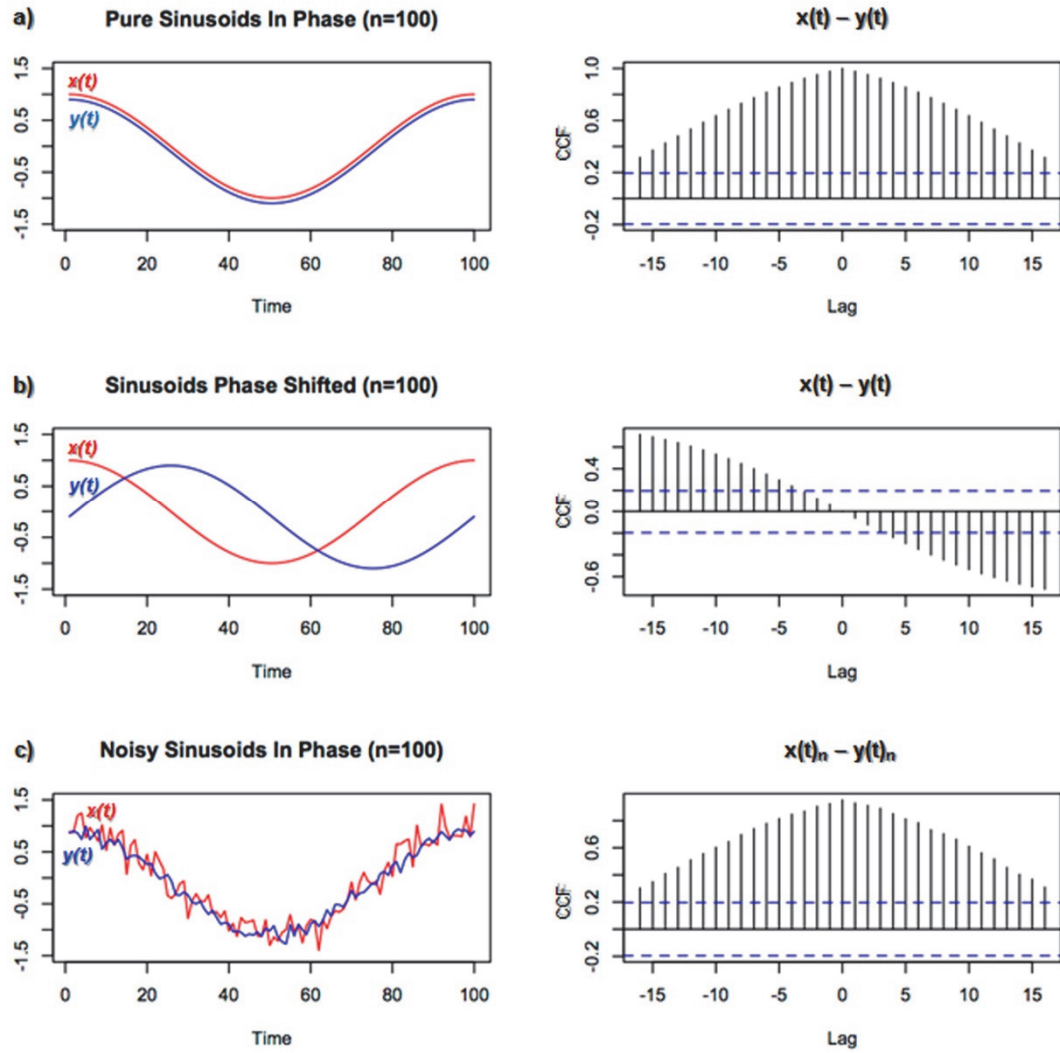


Fig. 4: Examples of different kind of cross correlation results. a) comparison between two in phase sinusoidal functions which show a CCF maximum values for nil time Lag (φ_m is 0) ; b) comparison between two not in phase sinusoidal functions which show a CCF maximum values for time Lag of ± 16 ; c) the same functions have the background noise that causes a loss of cross-correlation symmetry, which, however, is able to return a result similar to the first case.

According to equation [1], the autocorrelation represents the correlation of a signal with a delayed copy of itself as a function of delay. In the other words, the autocorrelation is an exceptional case of a signal which is cross-correlates with itself, i.e. when $x(t)$ is equal to $y(t)$. This function is useful for detecting the presence of periodicity in a series as it highlights whether a constant trend, seasonality or

stochastic component prevails in the analysed time-series of the data. In case of non-periodic functions, CCF is equal to 0; in case of periodic function, also the autocorrelation function shows the same trend result (Fig. 5).

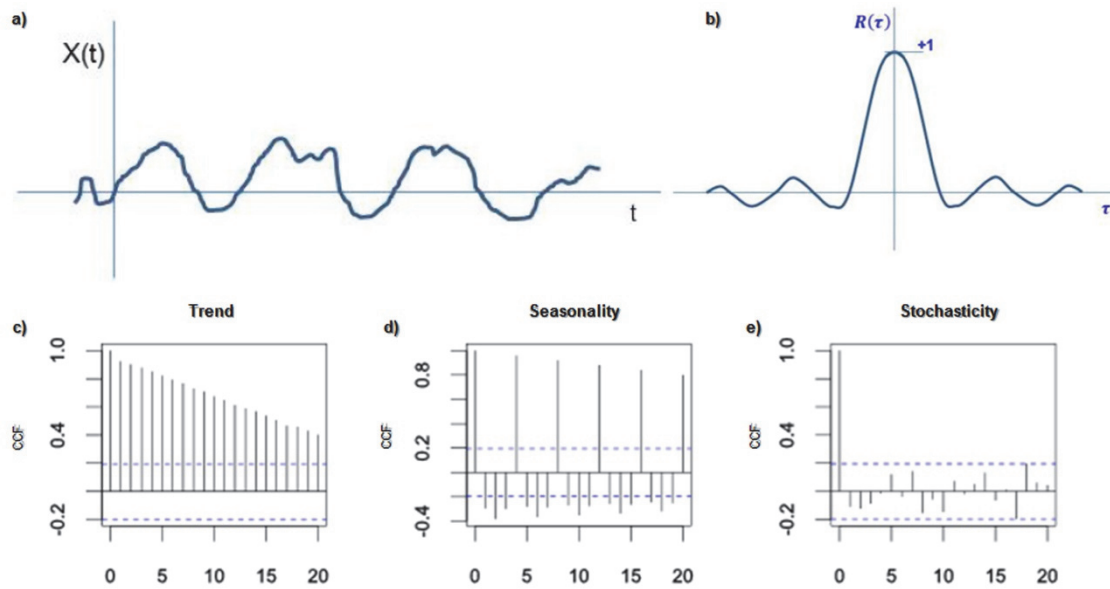


Fig. 5: Autocorrelation result (b) of $x(t)$ function (a) which show period trend due to periodic component of $x(t)$. Typical results of autocorrelation function (c, d, e) that highlights different behaviour of monitored series: the trend is prevalent (c), seasonal repetition is prevalent (d), the series are not correlated and the stochastic behaviour is predominant (e).

The cross-correlation function is widely applied in the Earth sciences. However, specific conditions are mandatory to guarantee its application. In order to process dataset by this tool the continuous time series are requested as well as a constant sampling rate. In the following analysis (see Chapter 5), the cross-correlation function was performed on the different time-series using R open-source software (R Core Team, 2015). This software returns a correlogram as a graphic output, that have CCF value in y-axis and the LAG value in x-axes. This last value, also called k , indicates the time delay between two signals. In fact, after calculating the cross-correlation between the two signals, the maximum peak of the cross-correlation function indicates the point in time where the signals are best aligned. Two dotted lines are also depicted that represent the statistical significance threshold (Fig. 6).

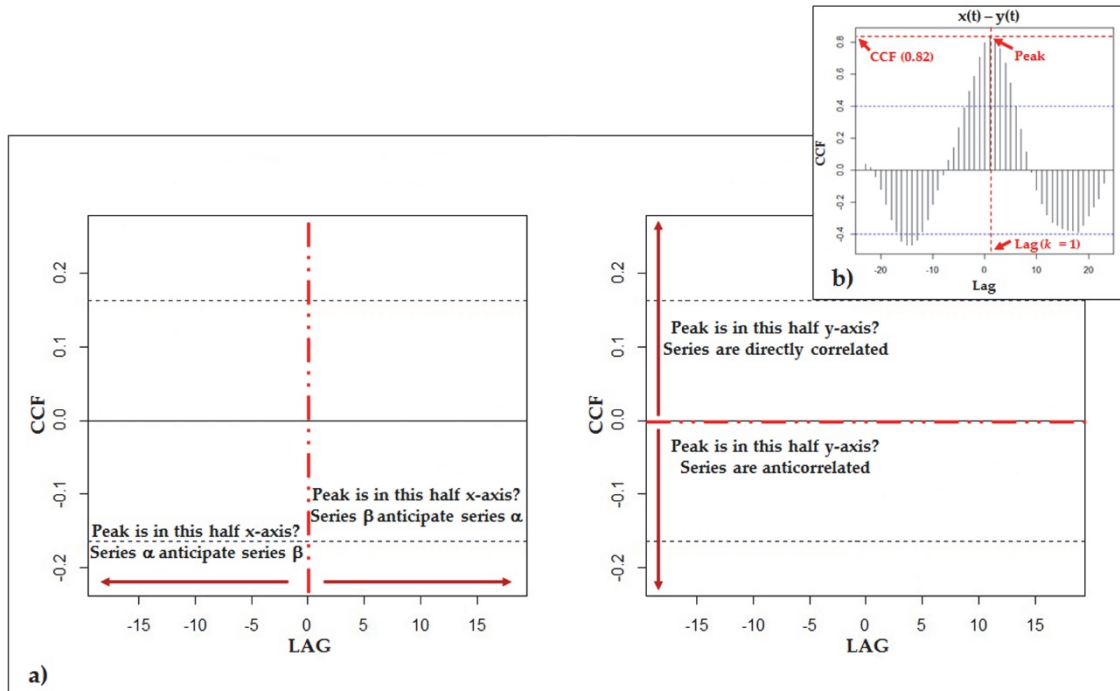


Fig. 6: Illustration representing how read the correlogram and the interpretation of the peak (a) and example of correlogram obtained with R software. In y-axis is shows the CCF value and in y-axis is shows the Lag value: $y(t)$ anticipates $x(t)$ of Lag time equal to 1 (that correspond to sampling step of series) (b).

3.2.1. Rate analysis in monitoring strategies

SBA strategies of data analysis was carried out using the rate of monitored data time series.

Variation of process rates can be detected by analysing the continuously recorded, not considering measured absolute values but computing the intensity of their variation over time. In this regard, increasing rates indicate a transgressive process that could evolve toward a paroxysmal phase; on the contrary, decreasing rates can be attributed to regressive processes that reduce the possibility of failure occurrence within a short-middle time window. Finally, constant rates identify stationary processes not yet evolving toward critical stages but anyway prone to do this in a long-time window (Szwedzicki, 2001, 2003).

Discontinuous monitoring data can be analysed by cumulating the recorded values to derive variation curves characterized by a typical alternating pattern constituted of ramps and flats. The ramps correspond to event occurrences, while the flats indicate the lack events. The analysis of cumulative trends allow switching from zero to non-null values in case of occurrence or not of triggering events.

Rates of continuously recorded data can be measured by performing a linear regression analysis to detect and distinguish suites of events (i.e. sequences or crises) as well as their variations over time. In order to output possible response delays of the system respect to a different kind of forcing actions such an analysis is strongly influenced by the selected "time windows" for computing the rates of recorded values. A correlation coefficient (R^2) can be attributed at each value of the rate that indicates the quality of the data processing allowing to evaluate the effectiveness of a trend within a selected time window, which must consist of at least 3 points. If the recorded data are strongly scattered the computed values of R^2 are very low, so testifying an aleatory variation of the measured variable. On the opposite, if the data are well aligned, the R^2 value increases up to 1, so detecting a well-constrained trend of the monitored effect. In the experimental tests performed so far, $R^2 \geq 0.75$ was considered for indicating a reliable trend in case of both transgressive and regressive process evolutions (Lenti et al., 2012; Szwedzicki, 2003).

In case of a trend analysis, to remove any spikes from the data series before computing the values of the rates mathematic filters should be applied to the data set to perform a data smoothing, especially in very scattered data series.

The following sketch (Fig. 7) illustrates the above described methods for continuous and/or cumulative data analysis.

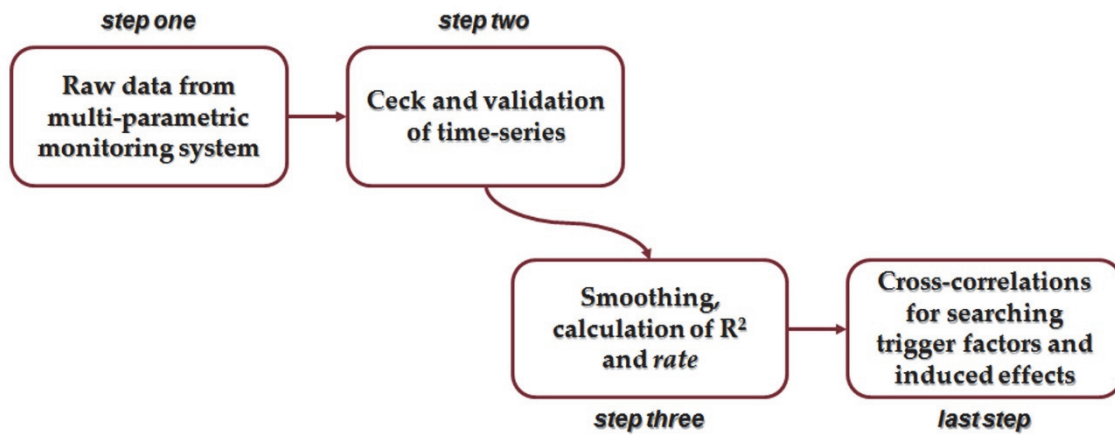


Fig. 7: Flow chart illustrating the analytic process of SBA approach.

The rate of different devices of a multi-parametric monitoring system were automatically computed through a customised script encoded by SAC (Seismic Analysis Code) and FORTRAN software on UNIX platform. The script performs some pre-processing operations on individual time histories. It mainly smoothies the data and removes possible anomalous spikes from installed sensors. After that, it calculates the linear regression, the R^2 factors and the rate on several time series in specific time window (Fig. 8). The so obtained time-series of rate were cross-correlated using R open-source software with the aim to calculating the Cross Correlation Factor (CCF) and the time shift between two rate series (LAG).

The time-series of rate were cross-correlated among them in order to determine which series influences the other and in what time range. Initially, the rate of the measured values was computed for three different time windows (30-20-10 minutes). To get a high resolution statistical analysis, 10-minutes time windows was adopted. The attention was focused on searching the cross-correlation among possible destabilizing factors and related induced deformations.

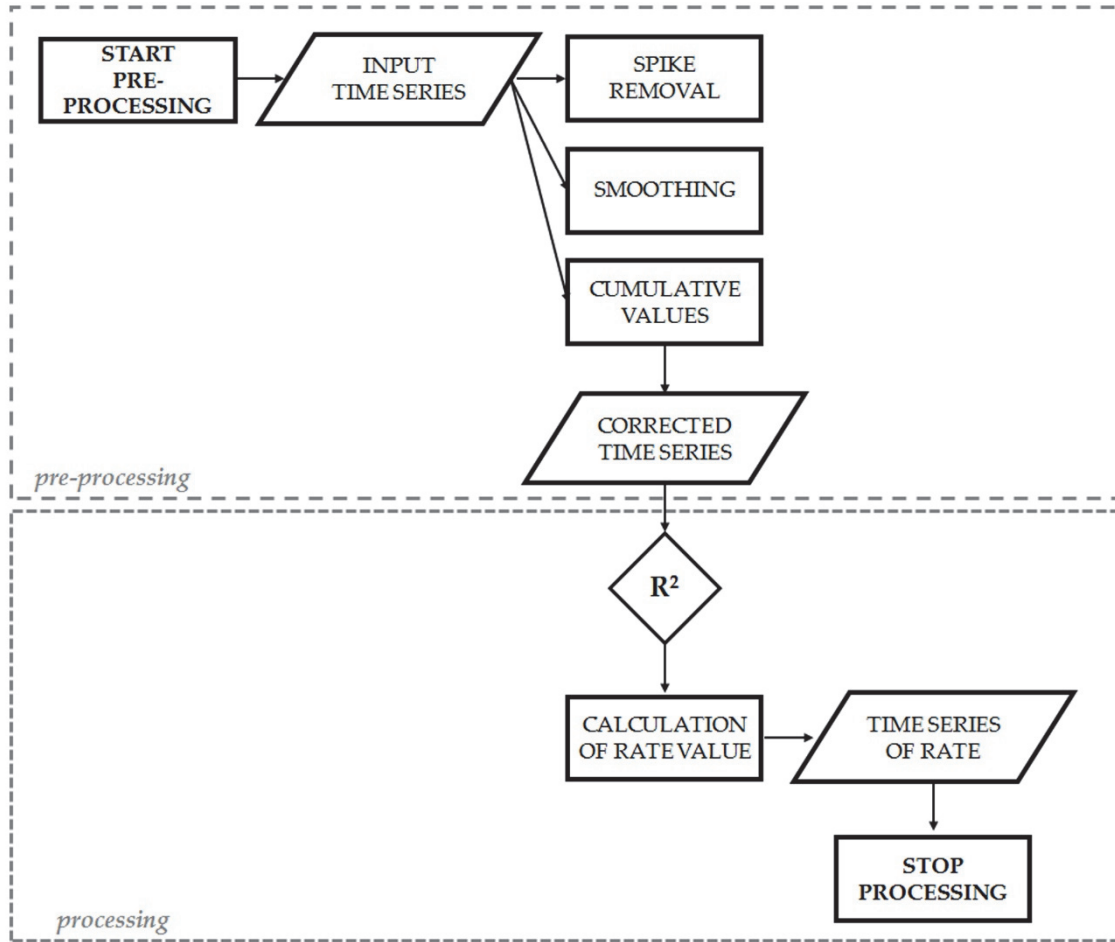


Fig. 8: Flow chart illustrating the tools of the script compiled rate analysis of Acuto dataset, propaedeutic to cross-correlation analysis.

3.3. Semi-Empirical Approach

The Semi-Empirical Approach (SEA) is addressed to predict the time of failure of a given slope based on the hypothesis that such failure represents the final stage of a creeping process. The milestone of this kind of approach is the work by Fukuzono (1985), who took into account results from laboratory experiments finding a relation between velocity and acceleration of surface displacement during the final creep stages under constant stress and temperature conditions. This relation, later validated by Voight (1989), is expressed in the following form:

$$\ddot{\Omega} = A(\dot{\Omega})^{\alpha} \quad [2]$$

The dot superscript represents the time derivative, Ω is the displacement and A and α are two empirical constants. A basic requirement for the application of semi-empirical methods is the collection of displacement data and, in general terms, the monitoring of the landslide behaviour to catch the transition to the tertiary creep phase.

This approach is based on simplified rheological models and their time-by-time calibration in order to predict the time of failure of a given slope based on the hypothesis that such failure represents the final stage of a creep process (Fig. 9).

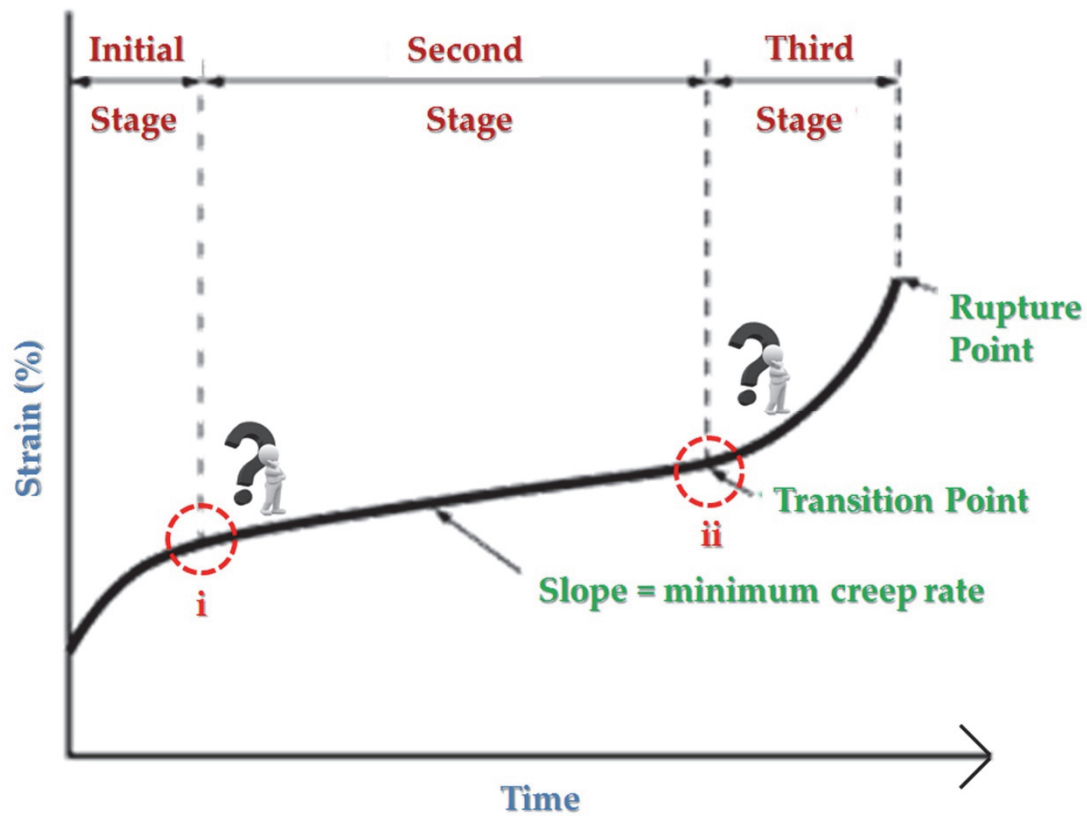


Fig. 9: Creep curve with indicates the three different stages and with highlighted the transition points.

Furthermore, based on the principles expressed in equation 1, different semi-empirical methods, known as Material Failure Forecasting Methods (FFMs), were

developed to forecast the timing of natural hazard events, e.g.(Cornelius e Voight, 1995), such as:

- a) graphical techniques;
- b) log rate *vs* log acceleration techniques;
- c) linearized least-square techniques;
- d) non-linear least square techniques.

These techniques can extensively benefit from the new monitoring technologies that provide robust and dense time histories of ground displacements. The feasibility and reliability of such methods applied to well-constrained case histories have already been tested (e.g. Mazzanti et al., 2014). Same researchers is now involved in a more challenging research, represented by the assessment of the applicability of SEA based on satellite InSAR data, characterized by a relatively low temporal resolution but constantly acquired over wide areas. Preliminary results are reported in a recent study by Moretto et al. (2017),that back-analyzed a relevant number of case histories. Beyond several limits, the Authors highlighted some relevant and positive outcomes, thus suggesting to go further also considering the growing number of SAR satellite constellations and the related reduction of revisit time, i.e. increasing rate of data acquisition.

4. Test-sites

In order to perform a comparative analysis of heterogeneous environmental data, applying and comparing the three approaches introduced before, two case studies have been chosen where designed and installed multi-parametric monitoring system and managing related data.

Both the test-sites, managed by the CERI Research Centre of the University of Rome “Sapienza”, experienced multi-parametric and multi-devices monitoring systems applied to different types of landslide phenomena, which act at different scales, with the final aim to provide a risk mitigation through the early-warning strategies calibrated on monitored data and parameter value thresholds.

In the first test-site, a multi-parametric monitoring system was installed on a specific densely fractured and proneness-to-failure rock block with the aim to understand its behaviour at rock mass scale. In the second one, a multi-parametric monitoring system was installed inside a karstified rock mass where a DGPV creep phenomenon involves an entire slope. In both sites, the management of data from the monitoring systems, is experiencing approaches for mitigating the landslide risk that involves the main infrastructures, i.e. in case of a railway track and of an aqueduct drainage plant respectively.

The first test-site is located at Acuto (central Italy) in an abandoned limestone quarry. The multi-parametric monitoring system was planned and designed during last years in the framework of several experimental activities managed by CERI (Research Centre for Geological Risks of Sapienza University of Rome), in order to test multi-devices installation devoted to carrying out specific experiments by monitoring unstable rock mass under natural and forced conditions for evaluating the suitability of multi-parametric approaches to managing the early-warning for infrastructure targets. The second test-site is located close to Rieti (central Italy) inside the Peschiera Spring slope, where a monitoring system is operating since the 2007 with the aim to mitigate

the landslide risk related to the main drainage plant of Rome aqueduct. The geographical location of two test-sites is reported in Fig. 10.



Fig. 10: Satellite view showing the geographical location of two case studies: 1) Acuto test-site and 2) Pescara Spring slope. The location of Rome is also shown.

4.1. Acuto test-site

The Acuto test-site was planned and designed starting from summer 2015, in the framework of this Ph.D. thesis, to host a multi-parametric monitoring system devoted to mitigate rockfall events from sub-vertical fractured cliff. The data of monitoring system have been mainly analyzed in according with OBA and SBA approaches, as well as secondarily according to the SEA approach.

Thanks to the availability of an abandoned limestone quarry, provided by the Municipality of Acuto, the designed multi-sensor device was installed starting from autumn 2015. The monitoring system began to acquire from April 2016, to test multi-parametric remote techniques for early warning in case of rockfall events threatening

strategic infrastructure. At this aim, a 1-meter long railway track was posed as original target for falling rock blocks.

More in particular, a rock block of size amounting 20 m^3 as a main focus of the multi-parametric monitoring system. The block is bounded and hosts several joints, so providing a high number of discontinuities to be instrumented. A main fracture separates the backside of the block from the rock mass and the general resulting set of the block is protruding respect to the adjacent rock wall where a railway track was positioned. The height of the entire quarry wall is in a range between 15 and 50 m, but the instrumented rock block have a high of about 6 m from ground level (Fig. 11).

Following the flow chart proposed in Fig. 2, the engineering-geological model was reconstructed on the basis of direct and remote surveys. The results have highlighted the main joint sets that predispose the rock block to failure and on which a multi-parametric monitoring system was installed.

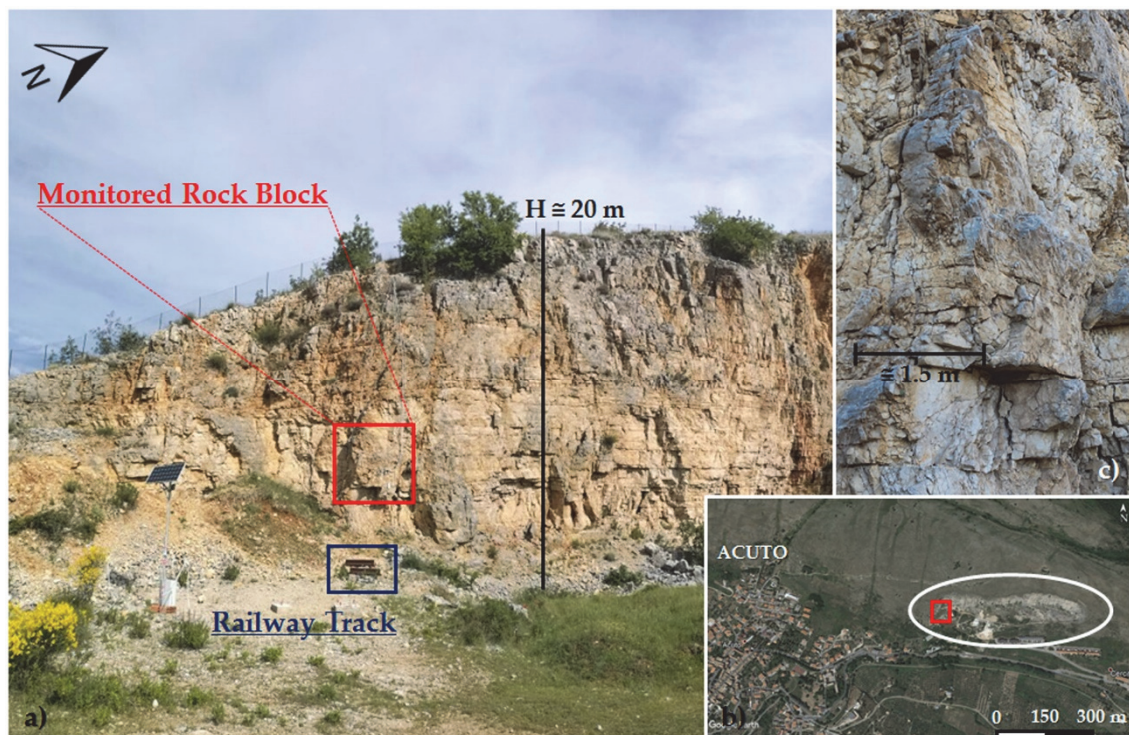


Fig. 11: Panoramic view of the Acuto quarry rock wall. Black frame shows the monitored rock block; red frame shows infrastructure target of the experiments (a). Geographical location (b). Particular of rock block (c).

4.1.1. General setting and geological framework

The municipality of Acuto is located in the western sector of the carbonated ridge of the Simbruini-Ernici Mts., which represent a portion of the Latium-Abruzzo Apennine Chain. This geological structure, longitudinally limited by the Valle Latina valley to SW and by the Val Roveto valley (or Liri Valley) to NE, is essentially a powerful succession of Mesozoic carbonate rocks.

As far as the study area is concerned, during lower Messinian (about 6.8 My ago) migration of the Apennine ridge towards E leads to the chain structure of the sectors: Sibillini Mts., Reatini Mts., Sabini Mts., Latin Valley, Simbruini Mts. and Ernici Mts. (Cosentino e Cipollari, 2006).

In the Quaternary age, an extension of the crustal movement is activate which give rise to the reuse of old thrust structures and the formation of new faults with Apennine orientation. With the extensional tectonic, related to the development of the Tyrrhenian basin, inter-mountain basins are created where Pliocene-Quaternary sediments are deposited (Galadini e Messina, 1994). As far as the structural arrangement of Latium is concerned, different domains converge in it attributable both to the Apennine ridge and to the main volcanic buildings of Quaternary (Mattei et al., 2008) (Fig. 12).

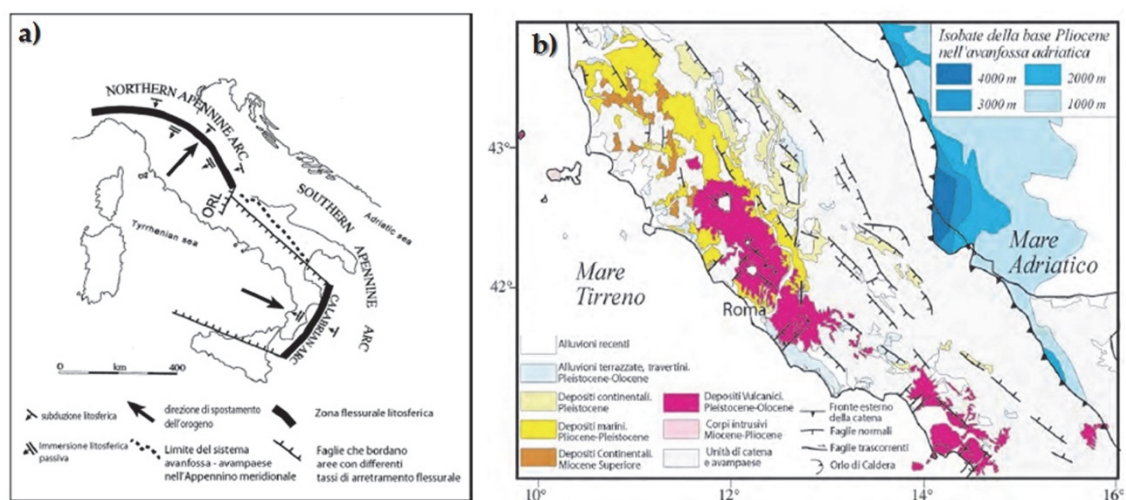


Fig. 12: Structural sketch of Apennine Chain (from Galvani, 2009) a); detailed structural sketch of Tyrrhenian sector (from Mattei et al., 2008) b).

The Apennine reliefs of Latium are characterized by the coexistence of tectonic structures with different orientation and deformation style, whose limit is marked by an important tectonic lineation known as Olevano-Antrodoco line (Parotto, 1980), whose activity is related to upper Miocene – lower Pliocene. In fact, there is a Transition Domain to the Umbria-Marche Pelagic Domain, characterized by predominant scarp and basin sedimentation, and a Latium-Abruzzo platform Domain outcropping in Lepini Mts. and Simbruini-Ernici Mts. (Civitelli et al., 1986; Corda e Mariotti, 1986). The Simbruino-Ernica ridge constitutes a main structural unit that develops in NW-SE direction, delimited to the N by Corneolani Mts., to the WSW by the Valle Latina valley, to the S by Cassino plane, to the E by the Val Roveto valley. The sedimentary sequence outcropping in this sector includes Mesozoic limestone referred to upper Triassic – upper Cretaceous (Devoto, 1970).

The test-site of Acuto is located at an altitude of about 750 m a.s.l. on the Mesozoic reliefs that bounded at N the Latina Valley, that constitute an example of extensional tectonic. The Valle Latina valley separates the Simbruino-Ernica ridge from Lepini Mts. These tectonic lineaments have been set at a zone already subsiding since Miocene (Funiciello e Parotto, 1978). In the Pliocene – Pleistocene a system of normal faults directed NW-SE (Apennine direction) confers to the Graben the same orientation, along which will identify the Latina Valley as know it today. These faults are no longer active but have a rejection of over ten meters (Funiciello e Parotto, 1978).

More in detail (Fig. 13), the Acuto abandoned quarry was totally excavated on a carbonate hill, which is part of the Ernici Mts. ridge. The quarry area is located NE of Acuto village, where Mesozoic calcilutites with rudist crop-out. Bedding, which has a shallow dip out of the quarry face, is offset by NW-SE striking steeply dipping normal faults that have 10 m offset (Accordi et al., 1986). The quarry wall where the monitoring system was installed is SE exposed and corresponds to the NW boundary of the quarry that is characterized by heights ranging from 15 m up to 50 m and by lengths of 500 m.

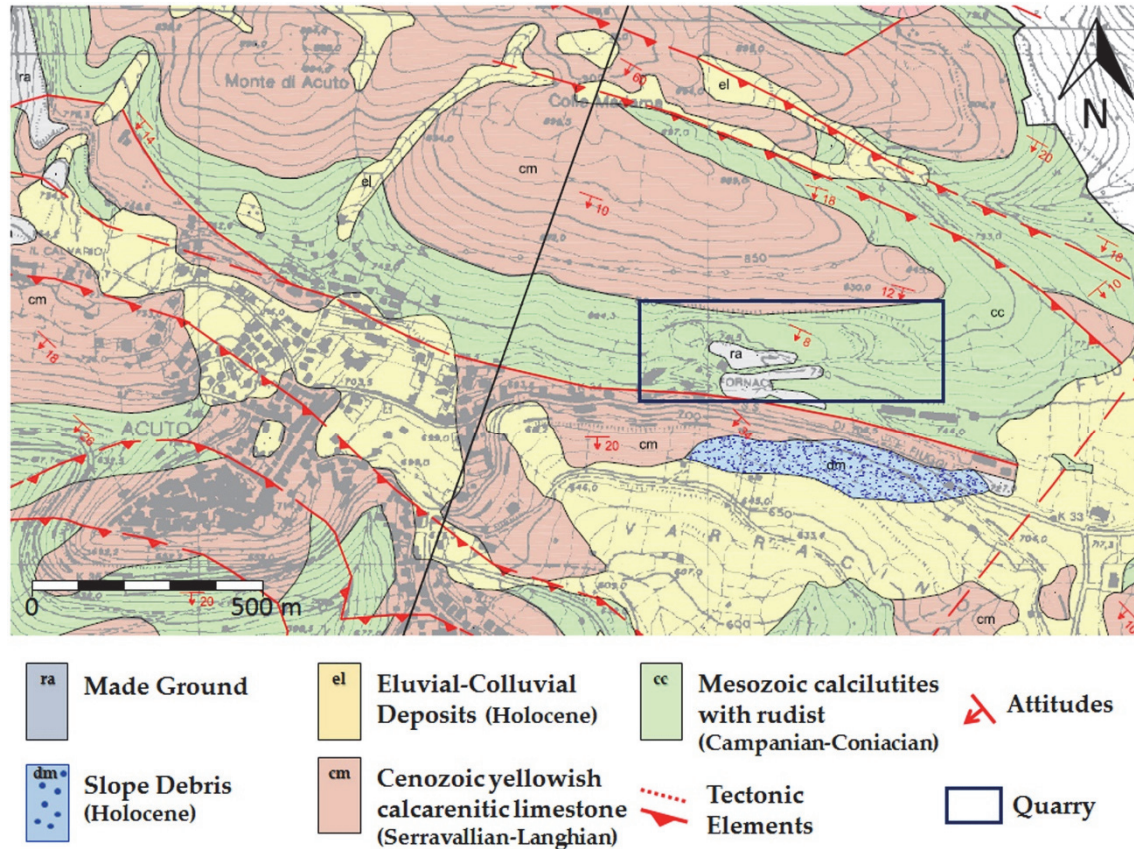


Fig. 13: Geological map of the Acuto area (scale 1 : 10.000), granted by Dr. P. Sarandrea – Geologist.

4.1.2. Geomechanical survey and slope stability analysis

In order to reconstruct an engineering-geological model of the rock wall and correctly design the multi-parametric monitoring system, several direct geomechanical survey and remote measurements were carried out starting from November 2015. On the basis of the results obtained from geomechanical surveys, a slope stability analysis was carried out to establish an hypothetical rock fall time sequence of the partially sub rock block end choose the main joint sets, predisposing the rock block to failure, on which install the monitoring system (Modanesi, 2016).

The geomechanical characterization of the Mesozoic limestone that crop out in the Acuto quarry wall was carried out via a traditional geomechanical survey performed according to the ISRM (2007) standard. This survey was focused on evaluating and dimensioning both the rock mass jointing conditions and the strength properties. To

this aim, the main joint sets of the rock masses together with their attitude, geomechanical properties (i.e., spacing, opening, jointing conditions, standard joint indexes J_v and I_b – ISRM, 1978, 2007) were measured as well as strength parameter values by using a Schmidt Hammer sclerometer and a Barton Comb profilometer.

Due to the reduced accessibility of the sub-vertical rock wall, 3 geomechanical scanlines were performed on the surrounding area and 5 specifically on the rock block. The poles of the measured joints were plotted using the Schmidt equi-areal stereographic projection (lower hemisphere). The attitudes of the main joint sets were deduced, as suggested by ISRM (1978), using Fisher concentration contour lines and attributing a joint set attitude if the concentration value was greater than 5%. Following this approach, five main joint sets (S0 to S4) were recognized (Fig. 14).

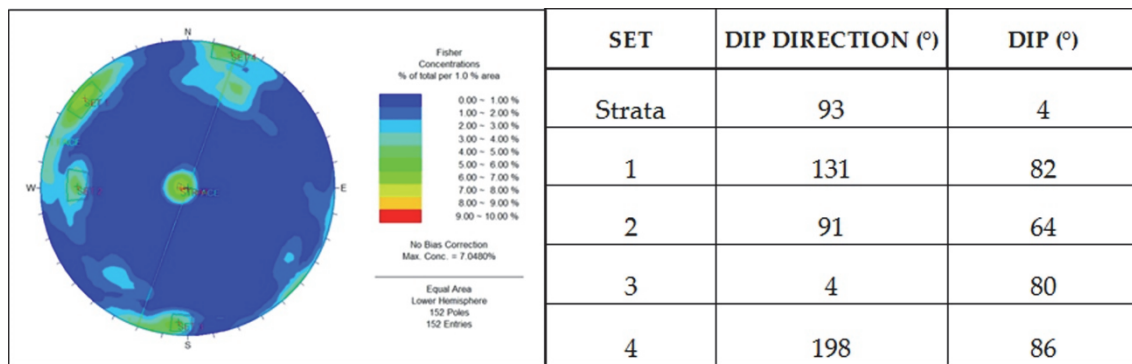



Fig. 14: Main joint sets surveyed through direct geomechanical survey on rock wall and rock block.

The joint roughness coefficient (JRC) and the joint compressive strength (JCS) of the main joint sets were also measured and the values of the intact rock friction angle (ϕ_b) were attributed on the basis of tilt test. Due to the surface alteration of joint sets, the value of residual friction angle (ϕ_r) was also evaluated. In addition, the value of the peak friction angle (ϕ_p) was indirectly calculated using Barton & Choubey (1977) failure criteria (Fig. 15).



SET	JCS (MPa)	JRC	ϕ (°)
Strata	180	3	53
1	120	8	54
2	130	3	49
3	110	4	49
4	140	5	49

Fig. 15: Joint strength features of main joint sets.

Laboratory tests were performed to define the main physical properties of Mesozoic limestone. More in particular, values of weight per unit of volume were evaluated (γ_{sat} : 26.45 kN/m³; γ_n : 26.44 kN/m³; γ_d : 26.43 kN/m³; γ_s : 26.72 kN/m³, porosity: 1.10 %). The average Uniaxial Compression Strength (UCS) of the rock, by Point Load tests, resulted of 130 MPa. According to the Deere & Miller (1966) chart, this value corresponds to a Young modulus of about $6 \cdot 10^4$ MPa. The rock mass properties were defined through the RMRb classification, which assigned to Mesozoic limestone a score of 68.

The direct geomechanical survey was coupled with a remote one to derive a high resolution engineering-geological model of the Acuto quarry wall, with particular attention to rock block. Remote geomechanical surveys were performed using a laser scanner integrated with a high-resolution digital camera and supported by a GPS survey.

Three GPS monographs were preliminary obtained to spatially geocode the rock wall. The new site-specific monographs were installed at fixed reference points for long-term monitoring. To define with very high accuracy and precision the geographical coordinates of the three monographs, statistical tests were performed (i.e. T test, W test, redundancy test and F-test). The error along planar-distance and the elevation error of the three monographs is in the order of some millimeter. The three

monographs were referred to steel topographic nails, fixed to the ground by specific resins.

From November 2015 to July 2016, remote scanning surveys were carried out on the quarry face by two different approaches: i) scanning by Leica Total Station (TS); ii) optical survey by SfM technique (Photo 3D technique). Laser scanner data were collected from the same three different scan positions of GPS monograph in order to reduce the shadow zones and to obtain mm-scale accuracy of the detected points (Fig. 16).

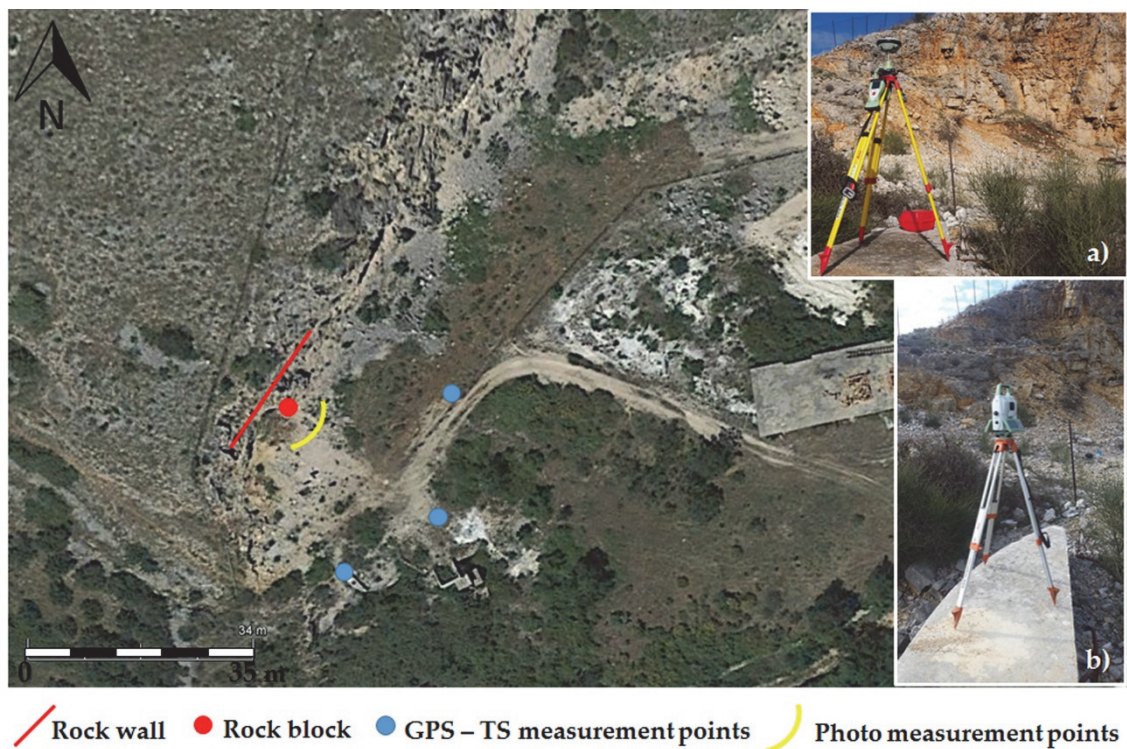


Fig. 16: Satellite view of Acuto test-site with shown the rock wall, the rock block, GPS (a) and Total Station (b) surveys sites, Photo surveys sites (along circular line).

A topographic survey was performed by a Leica MS60 Total Station (TS) in order to geocode all the collected point clouds in the same geographic reference system during the post processing data management. The topographic survey provided high definition geocoded point clouds, processed by the open source software MeshLab and

CloudCompare, which also allowed the alignment of more point clouds. Furthermore, An optical survey was performed by a 3D photos technique, carried out by SfM technique. Four different surveys were performed and carried out with a semi-professional camera. The SfM technique provided high definition geocoded point clouds but also high definition 3D model constructed by texturing and mesh processing of the scanned scenario (Fig. 17).

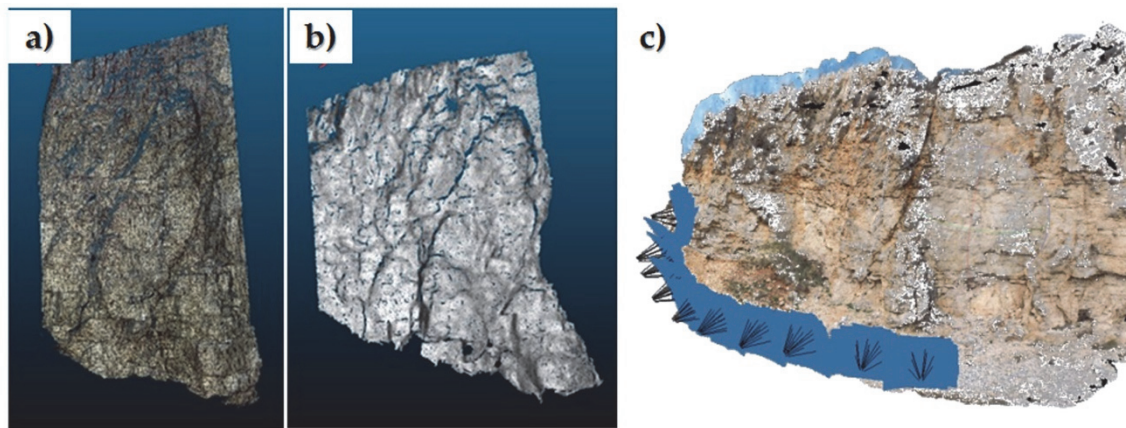


Fig. 17: Point Clouds obtained thanks to analysis with Meshlab open source software: RGB view of monitored rock block (a) and greyscale view one (b). Dense cloud from SfM technique is also shown (c).

The collected data were analyzed by the M3C2 algorithm (Lague et al., 2013), which allows to evaluate differences in distance between cloud point by using the perpendicular constructed on a cloud point, taken as reference. The so reconstructed model was used for two main purposes: (i) comparing point cloud acquired on the same day but with different methods and instrumentation; (ii) drawing up difference topographic maps in order to verify possible differences between November 2015 scan, March 2016 and July 2016 ones. As it regards the first purpose, the aim was to verify the possibility of using 3D photo scan through SfM technology to reconstruct a geocoded point cloud of monitored rock wall. To this aim, TS scan of 16 March 2016 and 3D model built from SfM analysis of the same day were analyzed. The M3C2 algorithm was applied on the alignment and geocoded point clouds, considering as a reference point cloud the one generated by TS scan. These outputs were compared

with the ones obtained by the 3D photos survey to test their reliability. A Gaussian distribution of the surveyed distances was obtained from each measurement; the comparison among the so derived distributions demonstrates that the computed errors are negligible and the main differences result at the boundaries of the sampled 3D domain. Almost 70 % of homologous points considered between the SfM and TS scans show variations less than 1 cm. As it regards the second purpose, the scans captured on 15 December (t_0 time) and 16 March (t_1 time) 2016 have been analyzed to realize a multi temporal differential map. The maximum displacement resulting from the difference of the two scans is of 2.7 cm at the upper part of the rock wall but never at rock block area (Fig. 18).

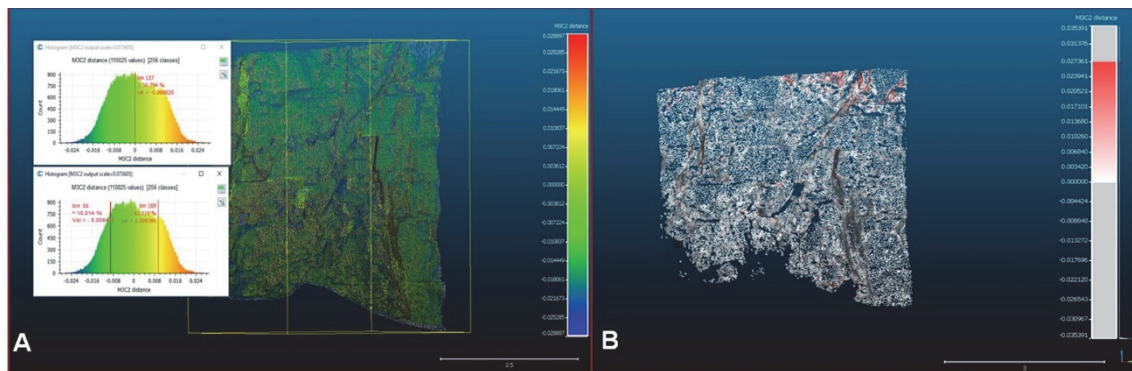


Fig. 18: A) Multitemporal difference map obtained by comparison between same time scans from Total Station and 3D photos analysed with SfM technology. A Gaussian distribution of the surveyed distances was also shown. The 70 % of homologous points to two scans have variations of less than cm. B) Multitemporal difference map obtained by comparison between Total Station and 3D photos analysed with SfM technology for different acquisition time (t_0 and t_1); we see that the maximum displacement is 2.7 cm at the top (red points) of the rock wall.

Both manual and automatic analyses of the point cloud were performed to derive information on the joint pattern features and implement the results of the direct geomechanical survey. Manual analysis and automatic recognition of the *facets* was performed using CloudCompare open source software (Fig. 19). Both analysis identified enough points to depict a surface whose attitude in space can be measured. The results was combined with the ones obtained through direct survey and the main joint sets were recognized.

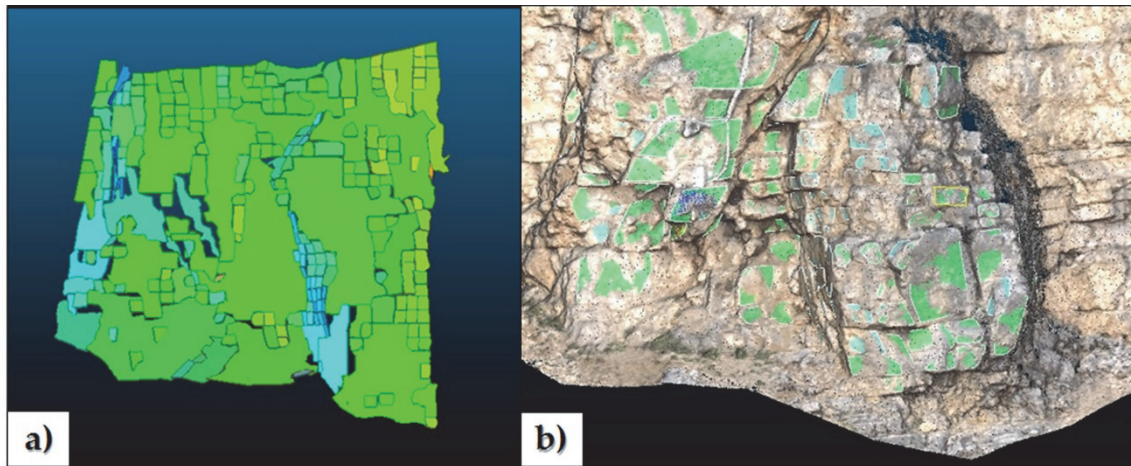


Fig. 19: Automatic analysis of main joint sets using Kd algorithm (developed by Thomas Dewez) (a); manual analysis of the facets and attitude attribution of main joint sets.

Susceptibility analysis to rockfalls was carried out by isolating 18 potentially unstable sub-blocks. on which to perform the Markland test. For each block, kinematic releases were identified by evaluating the attitude of the individual discontinuities that delimit it. The volume of the blocks was also calculated exploiting a specific tool of CloudCompare software (Modanesi, 2016) (Fig. 20).

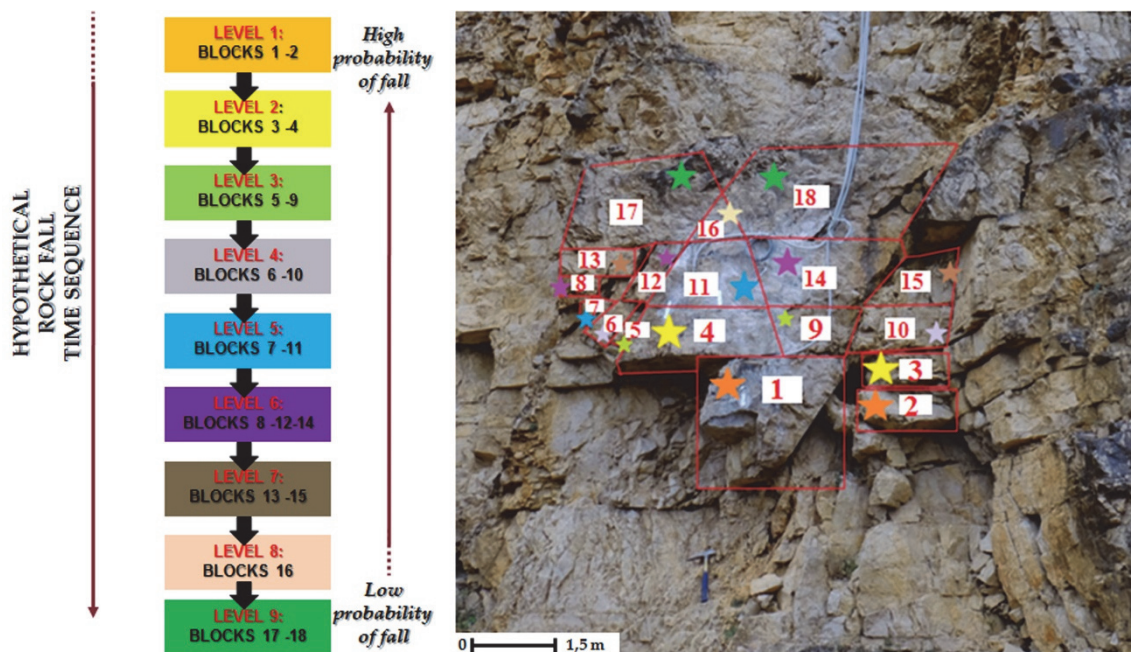


Fig. 20: Rockfall time sequence derived from susceptibility analysis.

The stability conditions of the Acuto quarry wall were analysed by taking into account the results of the geomechanical surveys performed on the rock mass that crops out on the slope face. The primary (strata) and secondary (fractures) joint sets on the rock wall play a fundamental role in controlling the slope instabilities. Four failure mechanisms were therefore considered for the slope stability analysis by taking into account the attitude of the main measured joint sets: (1) rock plane sliding, (2) rock topples, (3) rock wedge slides and (4) rockfalls. For each considered failure mechanism, a preliminary kinematic analysis was performed using the Markland (1972). The tests were performed by considering all of the possible combinations of joint sets and identifying those capable of meeting the established kinematic criteria. The results of the Markland test have define the kinematic condition of each sub-block (Fig. 21).

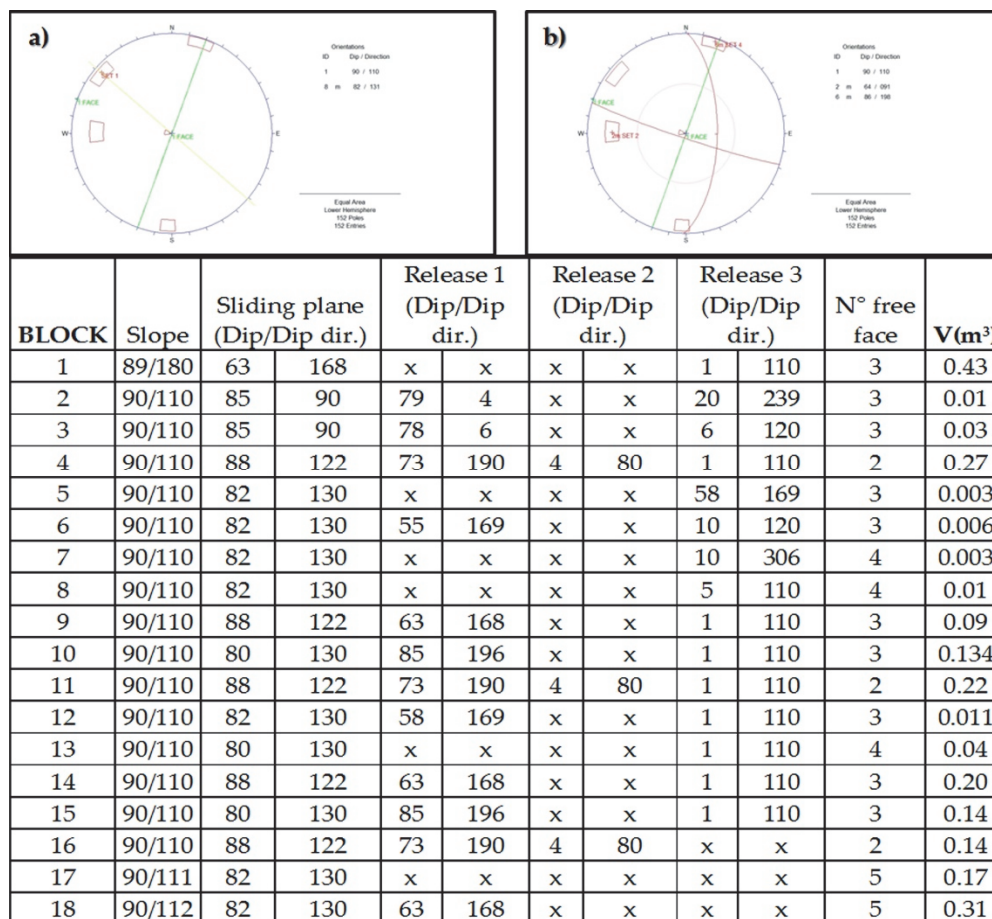


Fig. 21: Kinematic analysis for rock plane sliding (a); kinematic analysis for rock wedge sliding (b).
Summary of kinematic analysis results for each identified sub-block.

The stability analysis was performed under static and pseudo-static conditions (i.e. considering seismic action) in order to attribute a safety factor (SF) under different destabilizing conditions, such as static water pressure within the joint sets. The stability analysis was performed considering a sequential failure of the 18 sub-blocks, presented above. On them, the stability analysis was carried out as if they were released from the lower blocks. The final aim of this analysis was to provide a susceptibility charts different to the variation of the combination of external destabilizing forces. For this purpose 12 scenario was combined for seismic action (k_x – in a range from 0 to 0.253 g) and water pressure (r_h – in a range from 0 to 1). A value of FS (Safety Factor) was attributed for each scenario. The stability conditions were tested on each block only for rock sliding because this mechanisms showed kinematic compatibility based on the Markland tests. In order to describe the variation of FS in different stability conditions for each block, a simple pie chart were reported with highlighted the different conditions (green for $FS > 1.5$; yellow for $1 < FS < 1.5$; red for $FS < 1$) (Fig. 22).

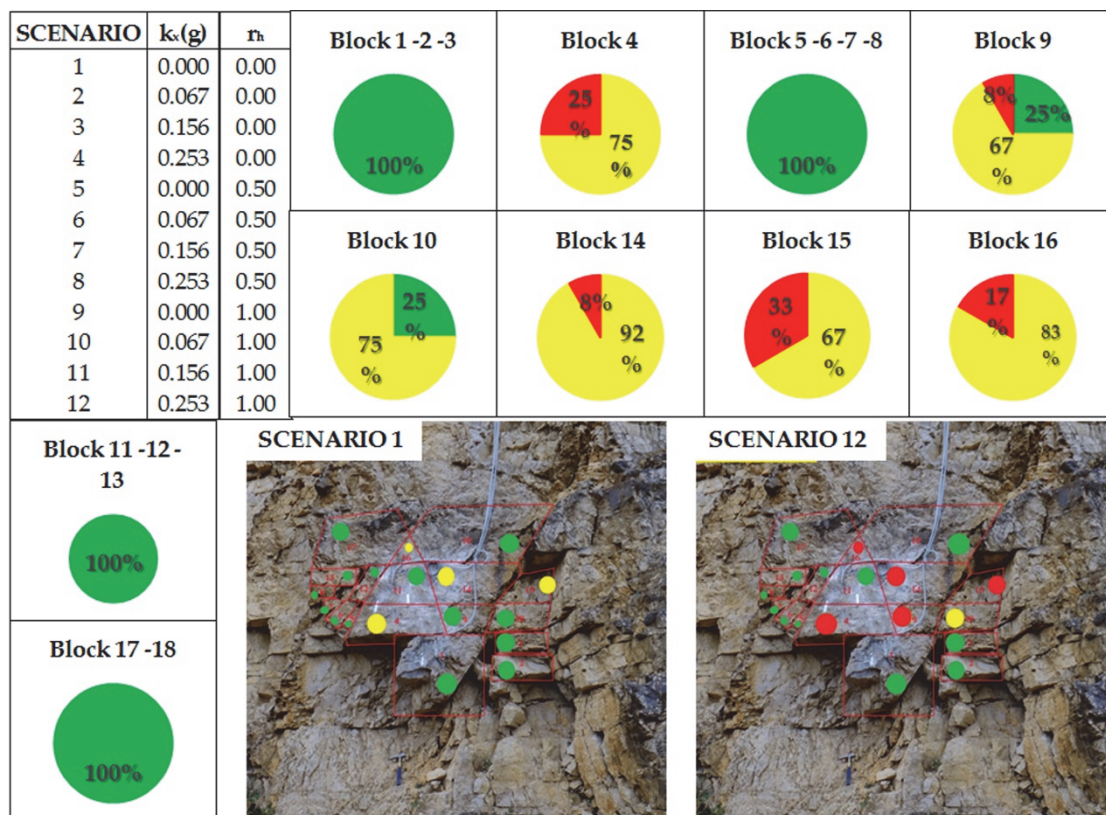


Fig. 22: Results of stability analysis carried out for Acuto rock block. The pie charts shows the statistical distribution of FS, considering each different scenario. Two pictures with FS value for each block for two end-member scenario are also shown.

Based on these analyses, the main joint sets predisposing the rock block to failure was chosen for installing the strain sensors of the multi-parametric monitoring system.

4.1.3. Multi-parametric monitoring system

In the above described geological framework, a multi-parametric monitoring system was installed since November 2015 in order to analyse collected data following the three proposed approach and to infer possible relationships among the detected deformations and possible triggers.

The multi-sensor system consist of (Fig. 23):

- 2 weather stations (a conventional one and an innovative open source cloud system TSA-BOX) equipped with air-thermometer, hygrometer, rain gage and anemometer for wind speed and direction. The stations were installed at foot and at top of the slope;
- 1 thermocouple to measure the rock mass temperature, installed at the centre of the monitored rock block;
- 6 HBM strain-gauges installed on rock matrix and micro-fractures of the rock mass;
- 2 extensometers with 25 mm measure range installed on open fractures (accuracy +/- 0.25 mm);
- 1 extensimeter with 10 mm measure range installed on transversal fracture (accuracy +/- 0.1 mm);
- 1 joint-gauges with 100 mm measure range, installed on a large fracture at the back-side of the monitored rock block;
- 1 optical cam (Artificial intelligence Camera Prototype - AiCP) connected to a customized Artificial Intelligence (AI) system: the AiCP was intended to detect morphological anomalies, such as rock slopes prone to falls, and the presence of unexpected objects along the monitored railway target. The AiCP, which can transmit real-time data, can provide early warning.

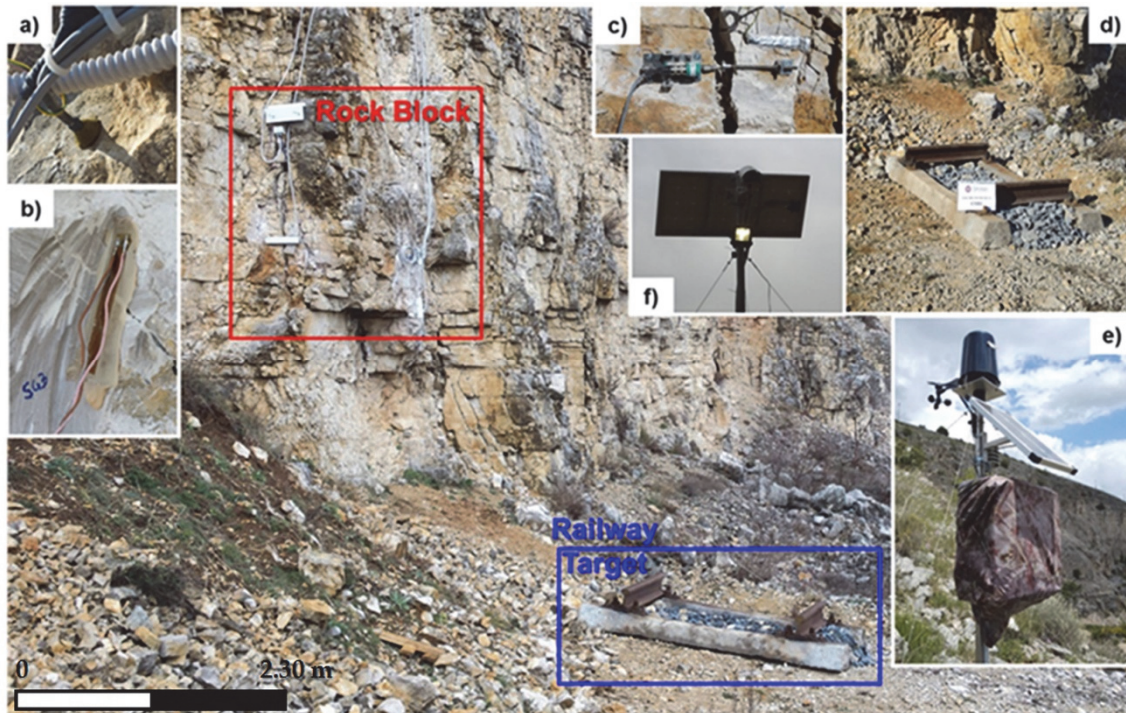


Fig. 23: Monitored rock block (red frame) with the railway track (d) located at its base and used as original target for the optical sensor. Sensors installed on rock block: a) thermometer to measure the rock mass temperature, b) strain-gage, c) extensimeter. In-situ devices are connected to data-logger CR1000 Campbell Scientific with incorporate meteo-station (e). Innovative meteo-station (f) and optical cam are also shown.

More in particular, the monitoring devices were installed on micro-fractures and open-joints, both on frontal face of the block and on backside one, predisposed for rock-fall and wedge sliding phenomena for detecting changes in the stress-strain conditions of the monitored block (Fig. 24).

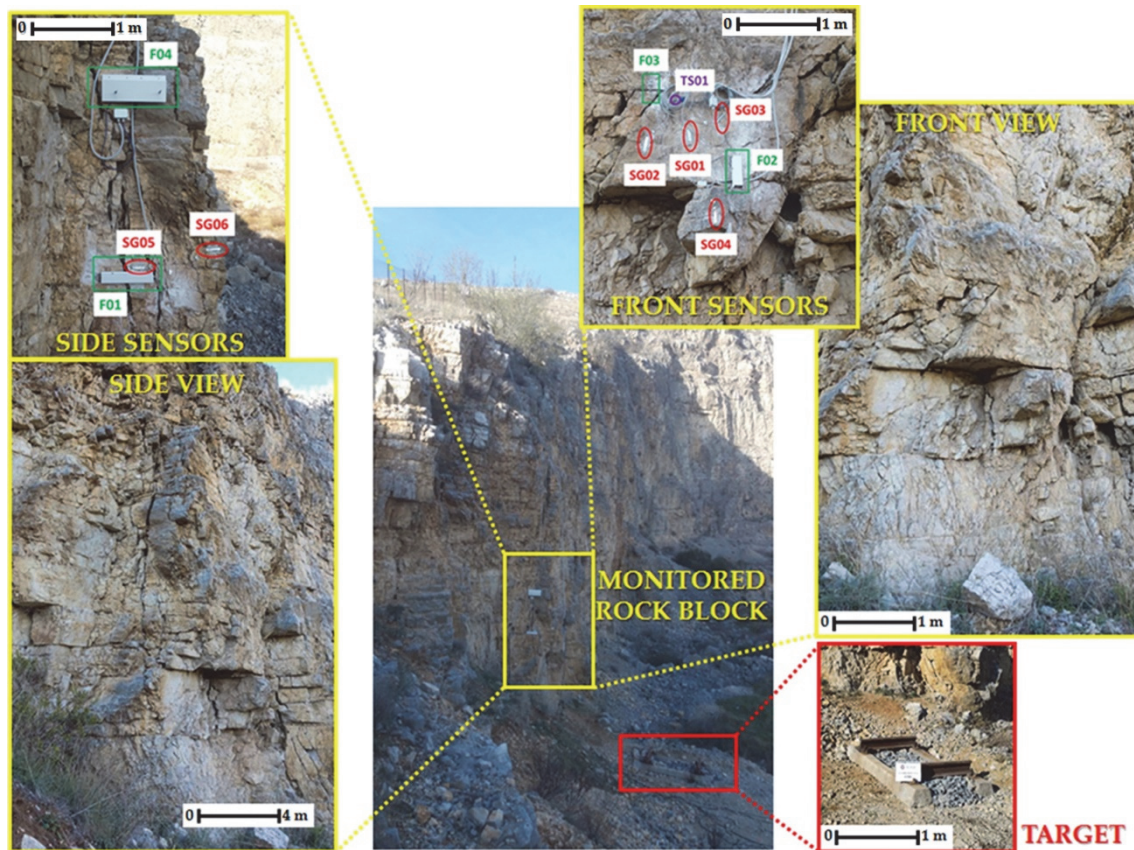


Fig. 24: Detailed view of front and backside of the monitored rock block. The disposition of the strain sensors is shows in two dedicated frame. The infrastructural target of the experiment is also shown.

All the sensors are set to acquire data each minute, starting from April 2016. The recorded data are stored in a local data-logger CR1000 Campbell Scientific, equipped with 24 acquisition channels. The system is completed by an automatic data transmission device, equipped with a GPRS wireless connection system; the data are sent to a local server that allows complete data storage every 4 hours and enables remote control of the dataset (Fig. 25).

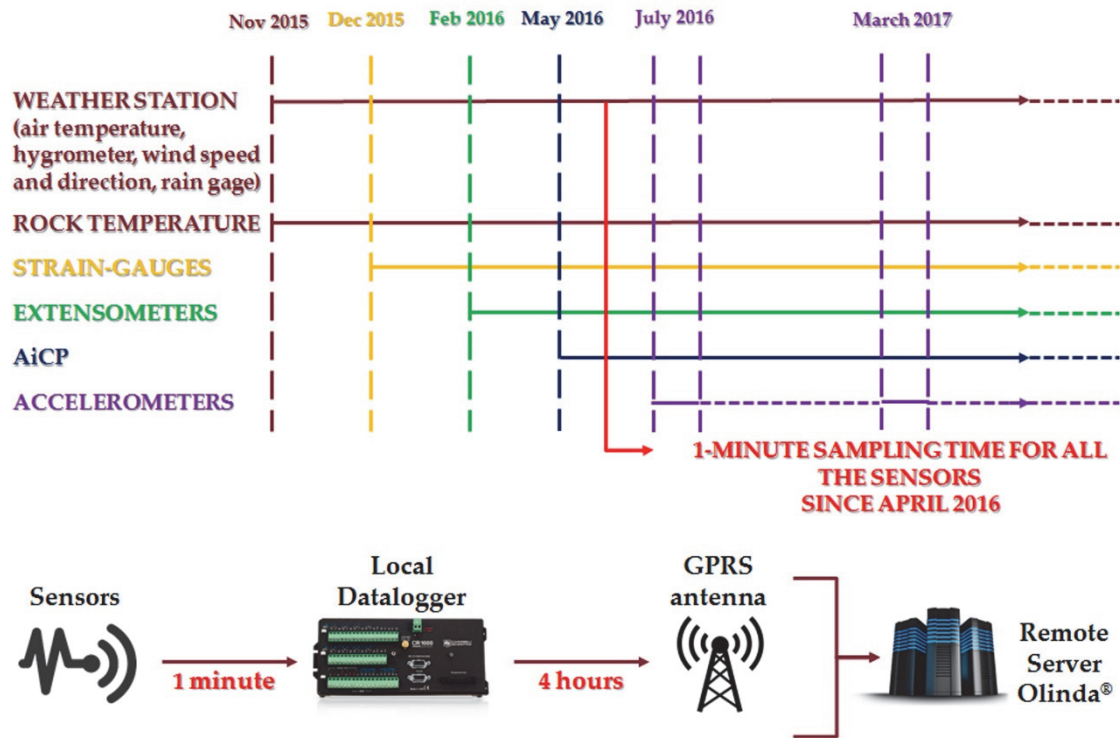


Fig. 25: Timetable of multi-parametric and multi-device monitoring system installation. The automatic transmission system of the data on server for storage and management.

For the forced experiments under a dynamic excitation (see Chapter 5), the monitoring system was implemented with remote and on-rock accelerometers in order to better investigate precursor of rock mass failure. The seismic instruments were kindly provided by ENEA – Casaccia Research Center. More in particular, 6 on-rock sensors mono-axial accelerometers KINEMATRICS FBA11 were installed: 2 on block front side, 2 on block back side, 2 outside the block; they were cable-connected to a KINEMATRICS K2 datalogger, provided with a tri-axial accelerometer, placed at the foot of the slope and acquiring in continuous mode with a sampling frequency of 250 Hz. A Seismic Navigation System (SNS) array, following a recently proposed nanoseismic monitoring approach (Joswig, 2008), was installed in the central part of the quarry, close to the monitored block. This technique allows the identification and location of precursory signals as well as the impact point of rock falls. The aim of nanoseismic monitoring is to locate weak seismic events with negative magnitude, under low SNR (Signal to Noise Ratio) conditions. The installed SNS array consisted of

one central three-component station and three outer vertical stations, positioned with an aperture of 20 m. Each station was equipped with one LE-3Dlite MkII seismometer (Lennartz Electronic GmbH) and one REFTEK 130-01 data-logger that acquired with a sampling frequency of 500 Hz. A further remote sensor implemented into the multi-parametric monitoring system was a terrestrial interferometer installed in front of the selected rock block. Both the accelerometric network and the terrestrial interferometer recorded in continuous mode from 18th July to 21th July 2016, while dynamic actions were applied to the slope for detect instability events. For this purpose, a vibrodyne was located on a concrete base at the foot of the instrumented rock block and was operated to induce frequencies in a range between 5 Hz and 30 Hz with incremental step of 5 Hz interspersed by a pause that had the aim to allow the slope system to reach a new balance after the induced stress (Fig. 26).

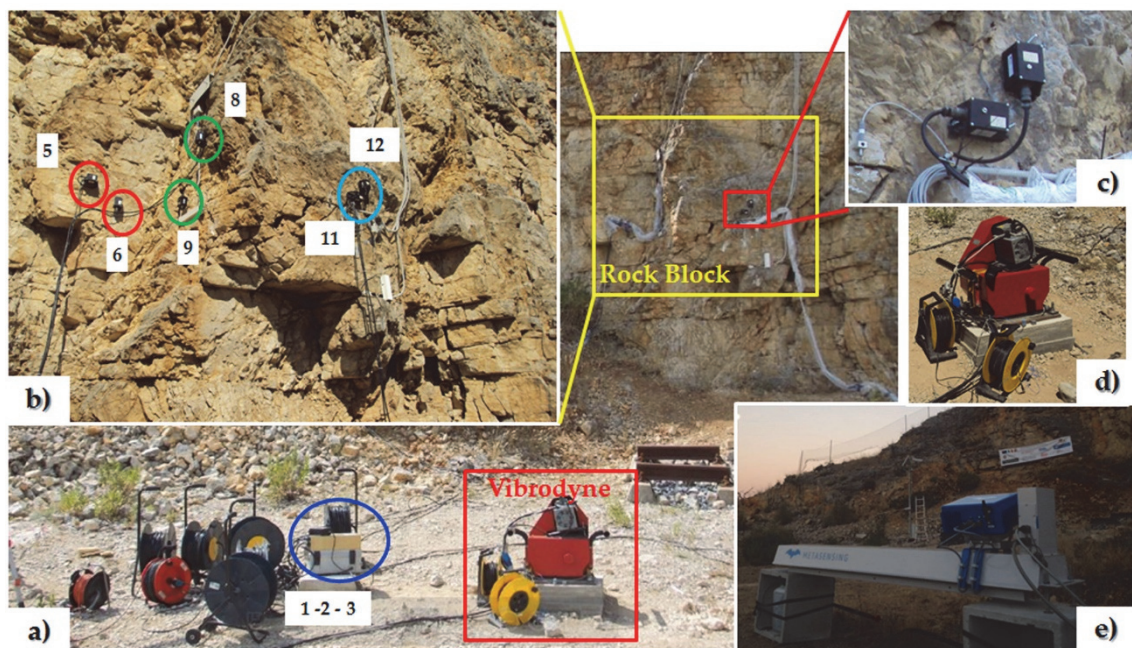


Fig. 26: Devices installed at Acuto test-site for dynamic excitation experiments in July 2016. The rock block is highlighted by yellow frame; the vibrodyne is highlighted by red frame; the Granite Kinematics datalogger, equipped with internal tri-axial accelerometric station, is shown by blue frame (a). Disposition of mono-axial accelerometers on rock wall: two on front side of rock block (light blue frame), two on back-side of rock block (green frame) and two outside the rock block (red frame) (b). Particular of on-rock accelerometers (c), vibrodyne (d) and of terrestrial interferometer are also shown.

4.2. Peschiera Spring slope

The second test-sites consist in the Peschiera Spring slope, which host the main drainage plant of the Rome's aqueduct system managed by ACEA-ATO 2 S.p.A. Italian Company. This slope is affected by a gravitational deformation process consisting in a rock lateral spreading. The deformation mechanism has been characterized through the results of almost a decade of measurements obtained by a stress-strain monitoring system installed inside the tunnels of the plant (Casini et al., 2006; Lenti et al., 2012; Maffei et al., 2005; Martino et al., 2004).

The recognition of pre-failure events by geological monitoring of natural systems is an important focus to mitigate the geological risks due to abrupt failures. The pre-failure behavior of rock masses represents a complex geomechanical topic because the stress and jointing conditions as well as the joint setting can strongly constrain pre-failure effects, such as crack generation, opening or closing of joints and readjustment of the stress field in the rock mass. Specific devices can monitor all of these failure precursors. In this regard, the microseismic approach can be considered as useful tool for mitigating the natural risk in an early warning perspective. With respect to the more traditional seismometric network, microaccelerometers allow detecting vibrations with zero down to negative magnitudes (Butler, 2003).

This technique was here tested in a permanent setting as part of an integrated monitoring system, where it is coupled with more traditional microseismic devices and geotechnical stress-strain sensors, in the aim to manage natural risks. The data of monitoring system have been analyzed in according with OBA and SBA approaches, as well as secondarily according to the SEA approach.

4.2.1. General setting and geological framework

The Peschiera Spring slope corresponds to the south-western flanks of Mt. Nuria (central Apennines). The slope is composed of carbonate ridge related to the Malm-Lower Cretaceous limestone (Ciotoli et al., 2001; Bigi e Costa Pisani, 2002).

The structural setting of the slope is monoclinic, with EW-trending and N-dipping (30° – 40°) strata; many fault lines cross the slope with roughly NS and N35E trends.

The slope hosts a major karst aquifer, which represent the drainage system of the Nuria-Velino-western Fucino and western Marsica (Velino-Sirente) Mts. (total surface area: 1016 km²). The Peschiera-Canetra is the main group of springs in this geological-hydrogeological system (measured total discharge: roughly varying from 18 up to 21 m³/s, according to Boni et al., 1986, 1995). The Peschiera Springs drainage plant is part of the Rome aqueduct system managed by ACEA-ATO2 S.p.A., and represent a main infrastructure object of analysis provided for this Ph.D. Thesis (Fig. 27).

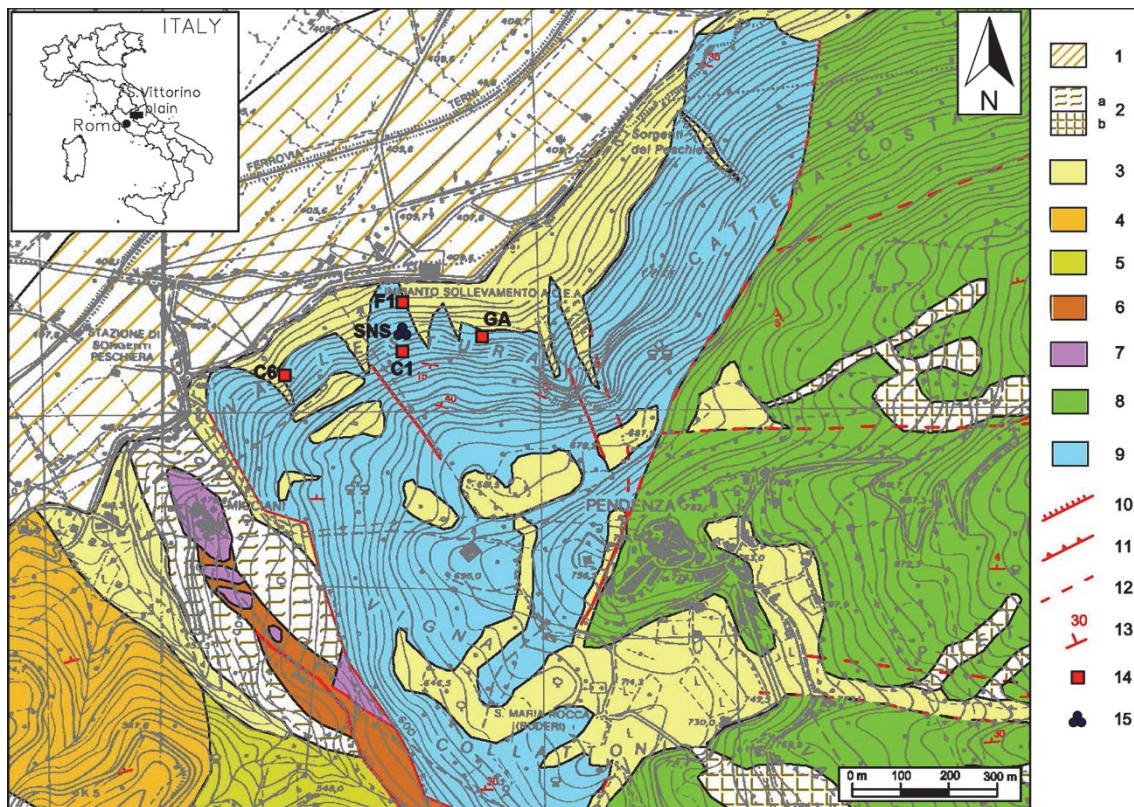


Fig. 27: Geological map of the Peschiera Springs slope: (1) recent alluvial deposits (Holocene); (2) Eluvio-colluvial deposits (Holocene): a silty clays and clayey silts, b reddish soils; (3) Slope debris (upper Pleistocene–Holocene); (4) Fosso Canalicchio Formation (upper Pliocene–lower Pleistocene); (5) Sandy-clayey Flysch (upper Miocene); (6) Marly limestone, marl and calcarenite (lower Miocene); (7) Scaglia formation (upper Cretaceous–lower Miocene); (8) Salpingoporella and Birdseyes limestone (lower Cretaceous); (9) Coral and Echinoids limestone (upper Jurassic); (10) Fault; (11) Thrust; (12) Supposed fault; (13) Attitude of beds; (14) Accelerometric station and (15) SNS array installed within the drainage plant (from Fiorucci et al., 2016).

Geomorphological surveys performed on the slope as well as a digital high-resolution (2 m) elevation model (DEM), derived by a Light Detection And Ranging (LIDAR) radar remote survey, enabled to identify numerous landforms, e.g. scarps, trenches, sinkholes and tension cracks. These landforms are indicative of slow, intense and pervasive slope deformations that affect the entire slope. These deformations correspond to different evolutionary stages that are attributed to different portions of the slope, as demonstrated by data from a stress–strain monitoring system installed at the drainage plant since 2007 (Lenti et al., 2012; Maffei et al., 2005; Martino et al., 2004).

Many scarps with a height varying from 5 to 15 m are present arranged both longitudinal and transverse to the slope. Scarps with a height lower than 5 m typically border longitudinal trenches. These scarps show evidence of recent movements locally. Trenches are generally filled with coarse and heterometric debris, which supplies a wide debris slope and occasional debris cones. Furthermore, a number of sinkholes and depression of variable size can be observed along the entire slope. Most of the sinkholes and depression are downslope of the main transversal scarps or in trenches, whereas other sinkholes and depressions are aligned along open tension cracks. In fact, diffuse evidence of tension cracks can be observed. These tension cracks produce openings in the exposed bedrock, which generally occur without fill, or narrow and elongated depressions, that contain smaller depressions and sinkholes in the sectors having a thicker debris cover or residual reddish soils. The tension cracks may reflect new scarps or the retreat of prior scarps (Martino et al., 2004).

These deformations correspond to different evolutionary stages ascribable to specific portions of the slope, as proved by already published result from a stress–strain monitoring system installed within the drainage plant (Maffei et al., 2005; Martino et al., 2004). In particular, it is possible to recognize three sectors of the slope with ongoing gravity-induced processes: (I) a wide sector, including the southern portion of the slope and its top, with evidences of incipient and low deformations, i.e. in their early evolutionary stage; (II) a western sector, with evidences of mature and not yet advanced gravity-induced deformations, only concentrated close to the main

trenches or scarps and (III) an eastern sector, with evidences of advanced gravity-induced slope deformations, characterized by pronounced landforms, such as scarps, trenches and sinkholes. Based on a frontal 3D view of the slope, the rock mass spreading can be clearly observed in the western portion of the slope, where it is associated with multiple transverse trenches (i.e. continuous transverse scarps combined with longitudinal trenches) that generate a radial displacement field. In the eastern sector, a previous rock mass failure can be observed in the DEM; this failure generated two debris fans clearly visible at the bottom of the slope. The lateral 3D view of the DEM shows that the spreading process attributes a convex shape to the involved portion of the slope, while the scar area of the already occurred failure reveals a concave shape (Fig. 28).

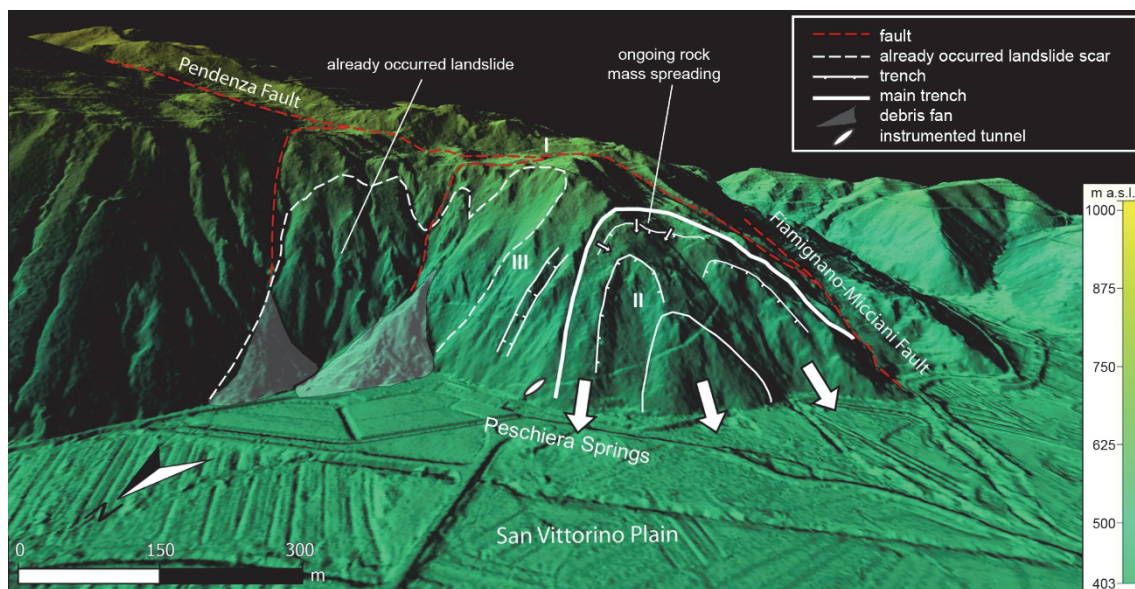


Fig. 28: 3D view of the Peschiera Springs slope obtained from the 2-m-resolution DEM, illustrating the rock mass volume involved in the ongoing landslide processes and showing the main generated landforms. Slope sectors (I, II and III) at different evolutionary stages are also shown. The slope shapes reveal a convexity in the western sector, presently involved in the spreading process, and a concavity in the eastern sector was a general collapse already occurred. Arrows indicate the northward direction of the rock mass movement (from Fiorucci et al., 2016).

The geological-evolutionary model of the slope reflects a complex deep-seated gravitational deformation, which initiates a “sackung” phenomenon (Zischinsky 1969; Savage e Varnes 1987) that continuously evolves from rock mass spreading (Hutchinson 1988) to rock-block mass deformation (Martino et al., 2004). In particular,

rock-mass spreading can be clearly observed in the western portion of the slope, which shows a radial displacement field and is causing transversal scarps and longitudinal trenches (i.e. multiple transversal trenches).

The spreading is associated with the collapse of underground caves due to major karst dissolution within the relieved rock mass, that is, along the subvertical belts (Casini et al., 2006; Maffei et al., 2005). These collapses result in a loss of volume at the surface with depressions and sinkholes. This process dislodged blocks, which increased the jointing of the rock mass. Furthermore, the collapse of underground caves may be triggered by external stresses, such as earthquakes (Maffei et al., 2005). Teleseism events may interact with the dislodged blocks causing a temporary increase in the strain rate that induces displacements along joints up to 2 mm within 24 h (Lenti et al., 2015).

The ongoing deformational process that involves the Peschiera Springs slope also resulted from instrumental measurements performed through a geotechnical stress-strain monitoring system as well as by a traditional seismometric network installed inside the tunnels of the plant since almost 10 years (Lenti et al., 2012, 2015). An alarm system for managing the geological risk of the drainage plant was already tested (Fiorucci et al., 2015; Lenti et al., 2012), based on both frequency of occurrence and cumulative energy of the recorded events.

4.2.2. Multi-parametric monitoring system

A multi-parametric monitoring system was installed since 2007 in order to analyse collected data and to infer possible relationships among the detected deformations and features of the ongoing gravitational processes. The final aim is to mitigate the geological risk that involve the drainage plant and provide an alarm system suitable for infrastructure management.

The stress-strain monitoring system was installed since September 2007 and has been recording the continuous gravitational deformations of the rock mass. This

monitoring system consist of 8 strain gauges installed on structural reinforcements, 7 string extensometers, 14 uniaxial extensometers and 15 uniaxial extensometers. These devices were installed within the tunnels of the Peschiera Spring drainage plant to detect stress-strain effects on structural elements and cracks on both the exposed rock and the tunnel cover. All of the sensors have a displacement resolution of $0.1\ \mu\text{m}$ and were set to automatically record at time intervals of 1 hr. The recorded data are collected by a local datalogger and can be download remotely (Fig. 29).

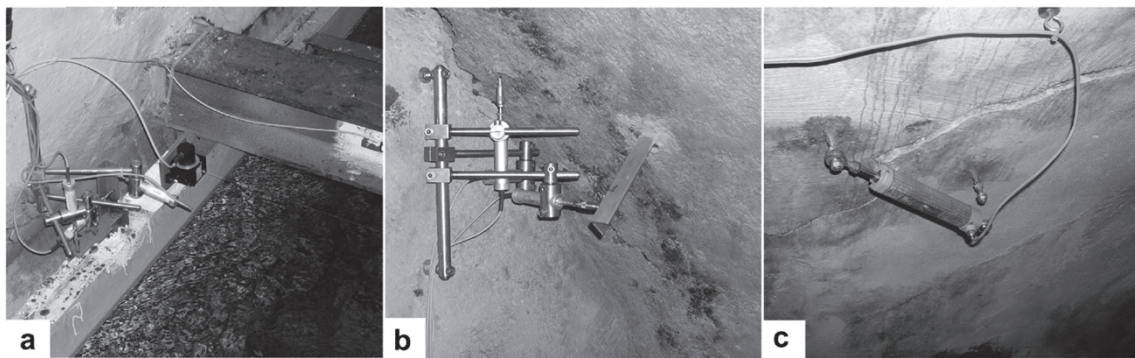


Fig. 29: Examples of the monitoring system devices installed within the drainage tunnels of the Peschiera Spring aqueduct plant: (a) String and triaxial extensometer installation coupled with a strain gauge installed on structural reinforcements; (b) Triaxial extensometer, (c) Uniaxial extensometer.

Starting from September 2008 the multi-parametric monitoring system was implemented with 4 accelerometric station (marked as GA, C1, F1 and C6) always installed within the drainage plant in order to record both earthquakes and microseismic events originated within the slope and related to gravity-induced displacement. Each station is equipped with a three-component accelerometer Kinematics Episensor (dynamic range 155dB+, sensitivity $1.25\ \text{V g}^{-1}$), directly installed on bedrock, connected via cable to a 24-channel digital datalogger Kinematics Granite set to absolute local time through a GPS device and acquires with a 250 Hz sample frequency. The trigger criteria of the datalogger were set to record events characterized by different durations and large-band frequency content (Lenti et al., 2012). The different kinds of events were automatically distinguish thanks to a specific script implemented on Unix-platform. The software allows to classify the events on the basis

of their physical properties, such as time durations, Fast Fourier Transform (FFT), amplitude Arias Intensity (AI) and Peak Ground Accelerations (PGA), and to distinguish among earthquakes and different microseismic events originated within the slope. In particular, microseismic events are distinguished in: (i) failures related to rock mass fracturing, with a duration from 1 to few seconds, and (ii) collapses, with a duration less than 1 s and a typical waveform of impact (Walter et al., 2012a, 2012b). The accelerometric network also records near-field and regional earthquakes as well as teleseism events (Lenti et al., 2015).

During 2013, an experimental SNS (Seismic Navigation System) array (Joswig, 2008) was tested within the slope in an abandoned drainage tunnel with the aim to implement the resolution of the accelerometric network for microseismic events. The SNS records were managed by the NanoseismicSuite (Joswig, 2008; Sick et al., 2014) software that perform a data screening by the “supersonogram”, i.e. a specific spectrogram with noise adaptation that allows to detect weak seismic events with negative magnitude (up to -3 M_L) under low SNR (Signal-Noise Ratio) conditions. Furthermore, stationary noise unrelated to the signal is filtered, allowing for a reliable detection even under challenging noise conditions. The localization of the events is also carried out. The nano-seismic continuous records were measured in five field campaigns with a duration ranging from 1 to 5 weeks. Each station was equipped with one LE-3Dlite MkII seismometer (1 Hz period) by Lennartz Electronic GmbH and one REFTEK 130-01 data logger at 24 bit for channel that acquired in continuous mode with a sample step of 500 Hz. A physical characterization of the signals was carried out by a specific Unix script, implemented with SAC (Seismic Analysis Code), in order to obtain time duration, frequency content, PGA and Arias Intensity (AI) value and distinguish between different kinds of microseismic events.

Based on preliminary results obtained during the five measurement campaigns, a permanent SNS array was designed and installed in last months of 2014 year to replace the temporal one and definitively implement the multi-parametric monitoring system. The permanent SNS array is equipped with six Brüel & Kjær type 8340 accelerometric

sensors, having high sensitivity (10 V g^{-1}) and flat response in acceleration in the frequency range of 0.1-1500 Hz, coupled with 3-modules HBM Quantum X datalogger at 24 bit for channel that acquires in continuous mode at a 600 Hz sampling frequency (Fig. 30).

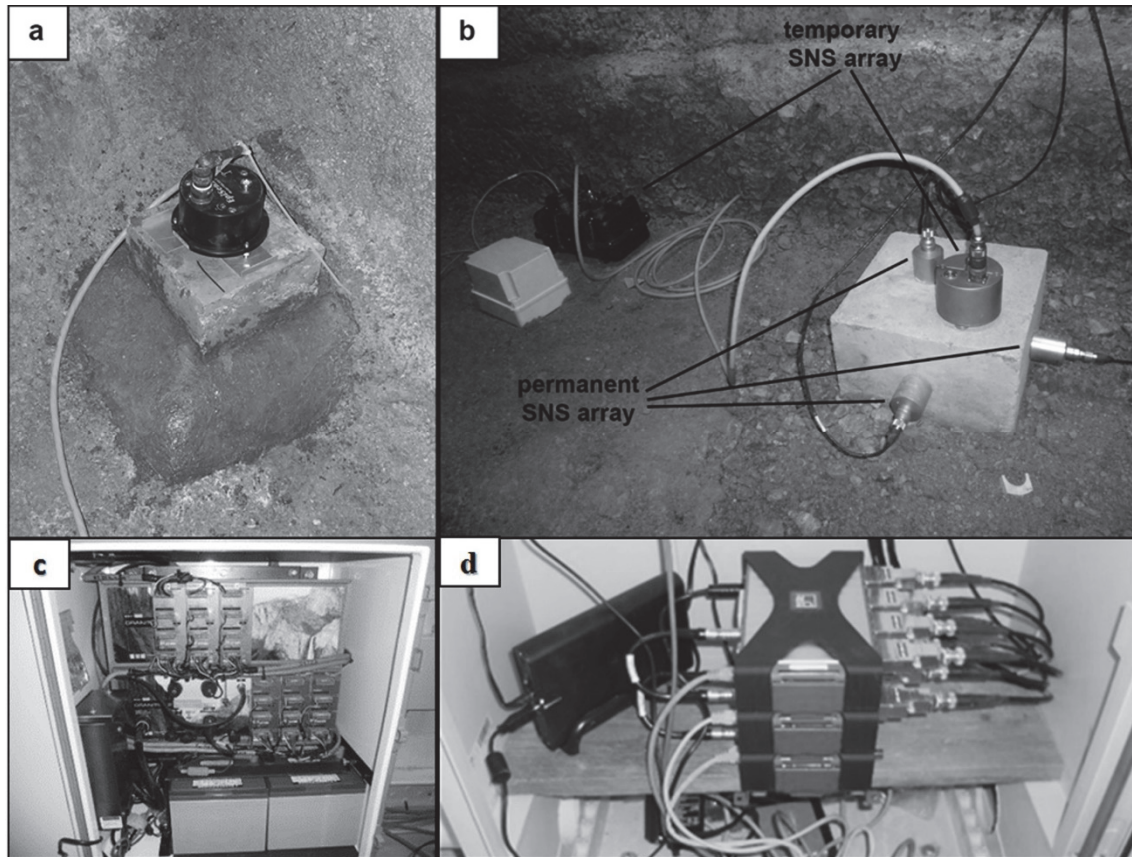


Fig. 30: Seismic monitoring system: a) 3-component KINEMATRICS Episensor installed on rock at the C1 station of the accelerometric network; b) 3-component Lennartz LE-3Dlite MkII seismometer and Reftek 130-01 data logger installed at the central station of the temporary SNS nanoseismic array, 1-component Brüel & Kjær type 8340 accelerometers installed at the central station of the permanent SNS nanoseismic array; c) datalogger Granite Kinematics for accelerometer network; d) Quantum X datalogger devoted to microaccelerometer record (modified from Fiorucci et al., 2016).

Flow discharge measurements were also carried out by ACEA S.p.A., through automatic flow meter recorder at a 1-hour sampling.

5. Results of multi-parametric data analysis

In this chapter, data from multi-parametric monitoring system, installed in both the test-sites, are presented. Data processing was performed following the three proposed approaches. Discussion of obtained results will be shown in the next Chapter.

The experiments planned at the Acuto test-site were performed starting from April 2016 and have been carried out in two different phases, namely “Phase A” and “Phase B”. In the Phase A, weather and stress-strain monitoring were carried out by continuous recording, in order to detect seasonal changes in the rock behaviour due to temperature, wind and precipitation that can influence the rock mass deformations. These specific weather conditions can induce stresses in the rock mass joints, detected by various strain sensors and by optical device. More in particular, a possible cluttering of the railway target can be detected by the AI-tech optical system while precursory sequences of rock failure can be detected by in-situ devices in terms of both stress-strain effects and micro-seismicity. The Phase B of the experiments was performed in July 2016. The monitored rock wall was forced by dynamic actions in order to induce stress-strain effects under controlled conditions.

For the Peschiera Spring slope test-site, data analysis was performed on dataset acquired in the years 2014, 2015 and 2016. Particular attention was paid to the analysis of the data acquired in 2015, because all monitoring systems worked simultaneously and without interruptions (until August 2015). The analysis was focused on findings correlations among groundwater level, microseismic events that are originated inside the slope and gravitational deformation processes that affect the slope.

5.1. OBA approach analysis

During Phase A at Acuto test-site, weather and stress-strain data from multi-parametric monitoring system was analysed by OBA approach, in order to detect daily

and seasonal changes and recognize cause-effect relations between preparatory or trigger factors and related joints displacement.

Phase A start from April 2016, with the simultaneous operation of all sensors that composed the multi-parametric monitoring system. The attention was focused on the strain device installed on the monitored rock block and on the crack-opening trend in relation to climatic forcing. More in particular, the rock block was instrumented with 1 rock thermometer, 4 strain-gauges (SG01; SG02; SG03; SG04) and 2 extensometers (F02; F03) on the front side; 2 strain-gauges (SG05; SG06), 1 extensometer (F01) and 1 joint-gauge (F04) on the backside. Meteorological devices was installed at the top of cliff slope, on the same vertical where the block is located. All sensors were cable-connected with the CR1000 Datalogger (see Fig. 24).

Rock fall can be triggered by several mechanisms. An important role was play by weather-climatic conditions, as well as rainfalls, strong wind and temperature. The role of thermal effects (temperature and solar radiation) on initiating rock deformation, where rock surfaces expand, contract, and eventually fail in response to cyclical temperature variations, was considered in OBA analysis as main deformative factor.

The analysis here presented was carried out in a time of 12 month, where main monthly weather conditions presented values summarized in Fig. 31.

	Air Temperature			Average Thermal Excursion	Rainfall	Wind speed	
	<i>min</i> (°C)	<i>max</i> (°C)	<i>average</i> (°C)	(°C)	(mm)	<i>max</i> (m/s)	<i>average</i> (m/s)
<i>April 2016</i>	3.43	24.37	13.85	9.02	83.00	12.66	2.42
<i>May 2016</i>	4.61	22.29	12.80	9.07	120.40	12.29	2.14
<i>June 2016</i>	10.72	31.45	19.92	8.90	77.40	17.50	1.91
<i>July 2016</i>	12.04	32.53	23.55	10.38	3.40	10.63	1.84
<i>August 2016</i>	14.14	31.89	22.43	11.05	15.80	11.50	1.88
<i>September 2016</i>	10.38	30.84	18.31	10.22	94.00	14.53	1.70
<i>October 2016</i>	5.87	23.74	14.40	8.53	112.40	9.15	2.27
<i>November 2016</i>	0.45	17.84	9.98	7.26	88.80	3.25	1.51
<i>Dicember 2016</i>	-0.87	16.12	7.72	9.38	7.20	12.34	1.99
<i>January 2017</i>	-8.90	11.43	3.23	7.62	38.40	10.28	2.10
<i>February 2017</i>	1.90	15.57	7.70	8.44	42.00	14.73	2.60
<i>March 2017</i>	3.20	21.69	10.48	10.80	31.20	11.45	2.28
<i>April 2017</i>	0.86	21.11	11.47	9.78	44.20	12.74	2.36
<i>May 2017</i>	7.73	24.81	15.39	10.19	71.80	10.93	2.16

Fig. 31: Table summarizing monthly weather conditions in Acuto test-site during monitoring period.

Air temperature, assumed as possible continuous preparatory factors (*sensu* Gunzburger et al., 2005), shows daily and seasonal oscillations typically of latitude and climatic zone in which the case study is located. During summer time air temperature can exceed 30°C, while in winter time may drop below 0°C. Daily thermal excursion follows a trend similar to the average air temperature, showing the highest values (up to 16°C) in the spring and summer period. The lower values (down to 4°C) are concentrated in the autumn and wintertime, in conjunction with the average air temperature decrease (Fig. 32). Lack of data between ends of May 2016 to beginning of June 2016 is due to technical problem to air thermometer.

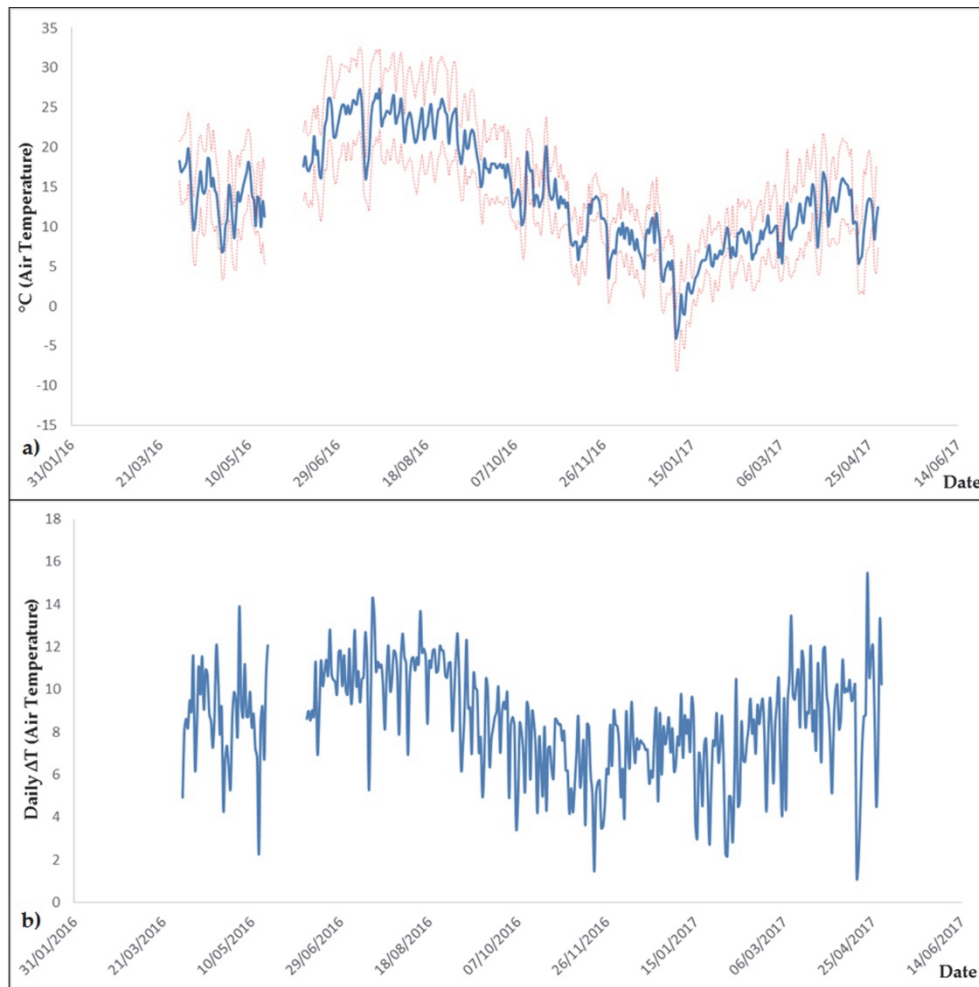


Fig. 32: Time sequence of average daily air temperature (blue line) with shows maximum and minimum value (red dashed lines; a) and daily air thermal excursion (b) at Acuto test-site during monitored period. Lack data is due to technical problem.

The air temperature influences the rock temperature, both in the heating phase and in the cooling phase. In fact, the rock temperature trend follows very well the air temperature trend. This occurs both on a daily and seasonal trend, revealing how the temperature is an external forcing acting continuously on rock mass. In the Acuto test-site, the rock temperature was monitored by the thermocouple installed inside the rock block for a depth of about 5 cm. Similarly to what happens for the air temperature, during summer time rock temperature can exceed 30°C, while in wintertime may drop at 0°C. Daily thermal excursion follows a trend more different to the average rock temperature: in fact, the highest values (up to 14°C) were recorded in the spring and

autumn season; the lower values (down to 2°C) are concentrated in the summer and winter season. The low winter temperature may give rise to freezing effects of rock block, considered as *trigger factors* for micro-fractures and joints deformation (Fig. 33).

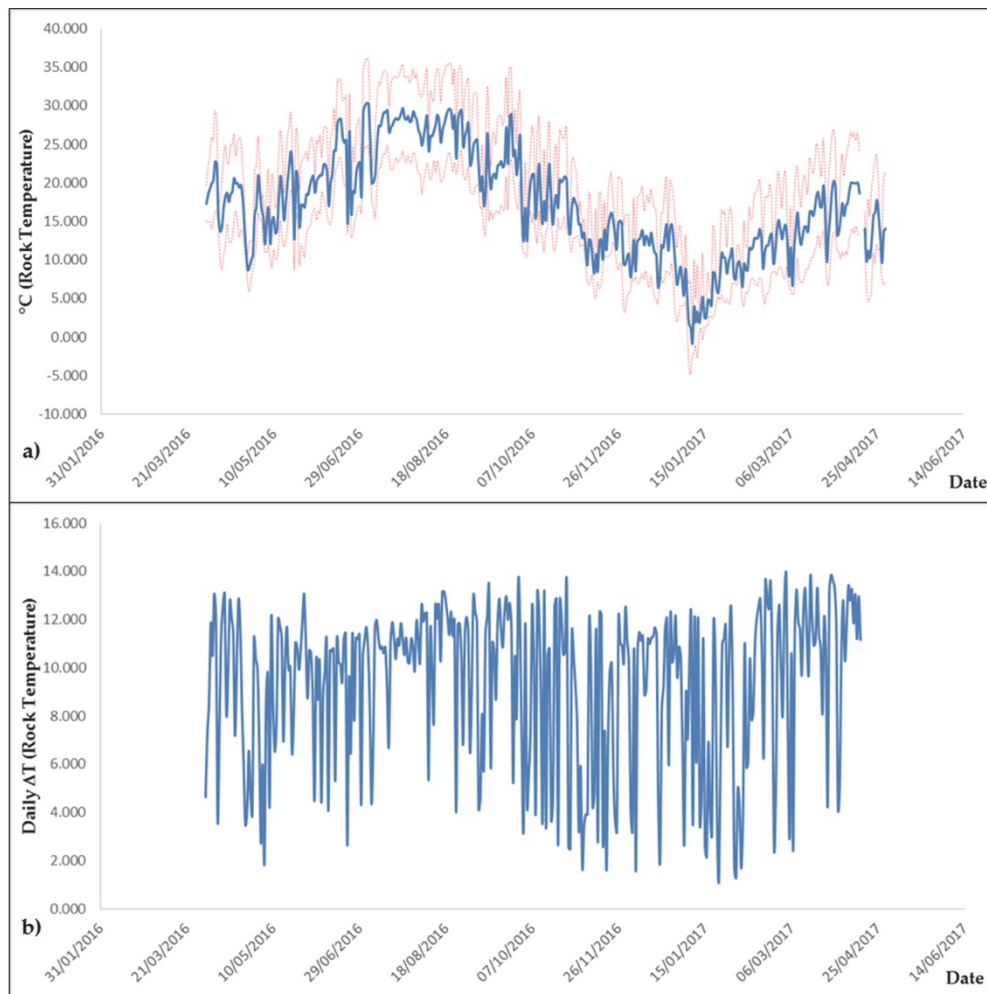


Fig. 33: Time sequence of average daily rock temperature (blue line) with shows maximum and minimum value (red dashed lines; a) and daily rock thermal excursion (b) at Acuto test-site during monitored period.

An important role for rock deformation and in occurrence of rock falls phenomena, can be played by rainfall occurrence. This can be considered as *preparatory factor* if is regular, or can be considered as *trigger factor* in heavy rainfall episodes. The rainfall regime also shows a seasonal trend, with frequent and intense rainfall concentrated in

the autumn and spring months. During the monitoring period, a total of 800 mm of rain was cumulated, with a maximum daily precipitation of 28 mm/d occurred in October 2016 (Fig. 34).

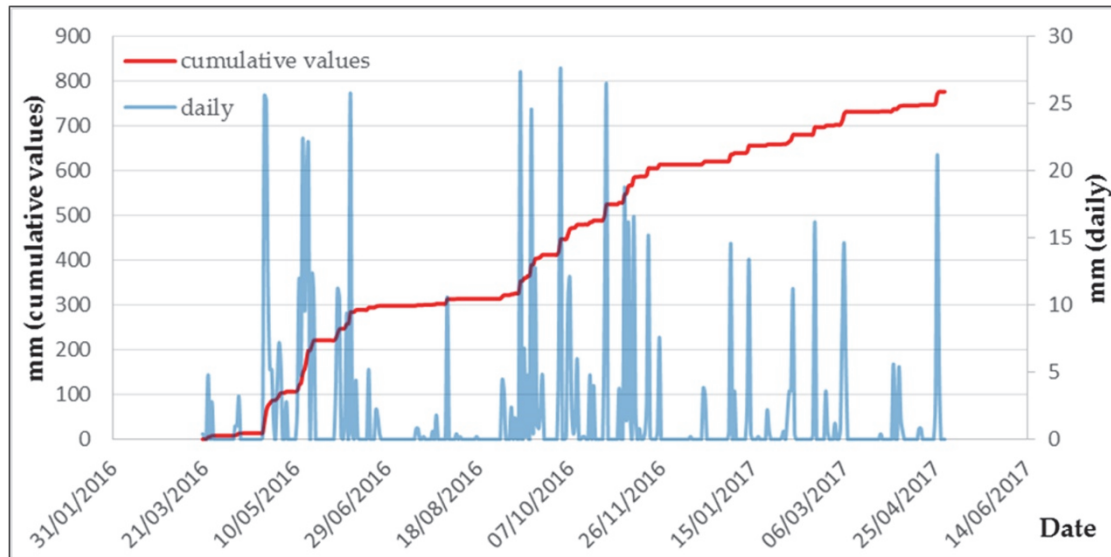


Fig. 34: Rainfall regime in Acuto test-sit during monitoring period. Blue line represent daily rainfall; red line represent cumulative rainfall values over monitoring time.

In addition, windstorms can be occasionally considered as *trigger factor* to joints displacement. Only events with wind direction in an azimuth range from N 10° to N 190° can be taken into account. In fact, the monitored rock wall present an attitude of 100/90. During the monitoring period three strong windstorms occurred, characterized by a wind speed higher than the average value (10 m/s). During these storms, the wind direction had an azimuth compatible with the attitude of the quarry rock wall (Fig. 35).

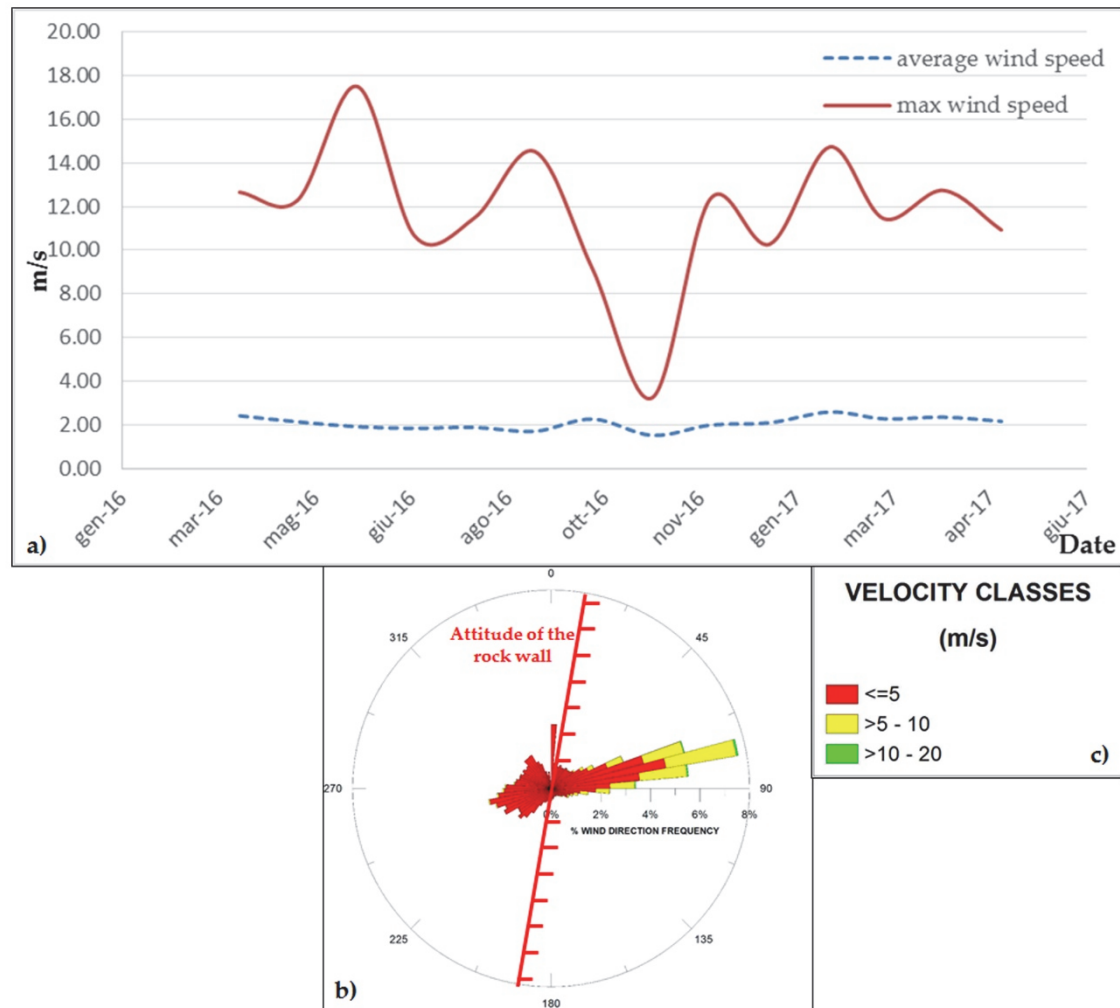


Fig. 35: Average monthly wind speed (red line) with shows relative minimum value (blue dashed line) (a); a rose diagram representing the wind direction in relation to rock wall attitude is also shown (b – c). Only wind that impact against the rock block was considered in OBA analysis.

Analyzing the values of strain sensors (both strain-gauges and extensometers) installed on front side of the block (Fig. 36) and on backside (Fig. 37), notice that a continuous deformational trend is ongoing both on micro fractures (monitored through strain gauges) and on open joints (monitored through extensometer). The sensor, which measured the highest displacement values, is the SG06 installed on the outer edge of the slope in very high release conditions.

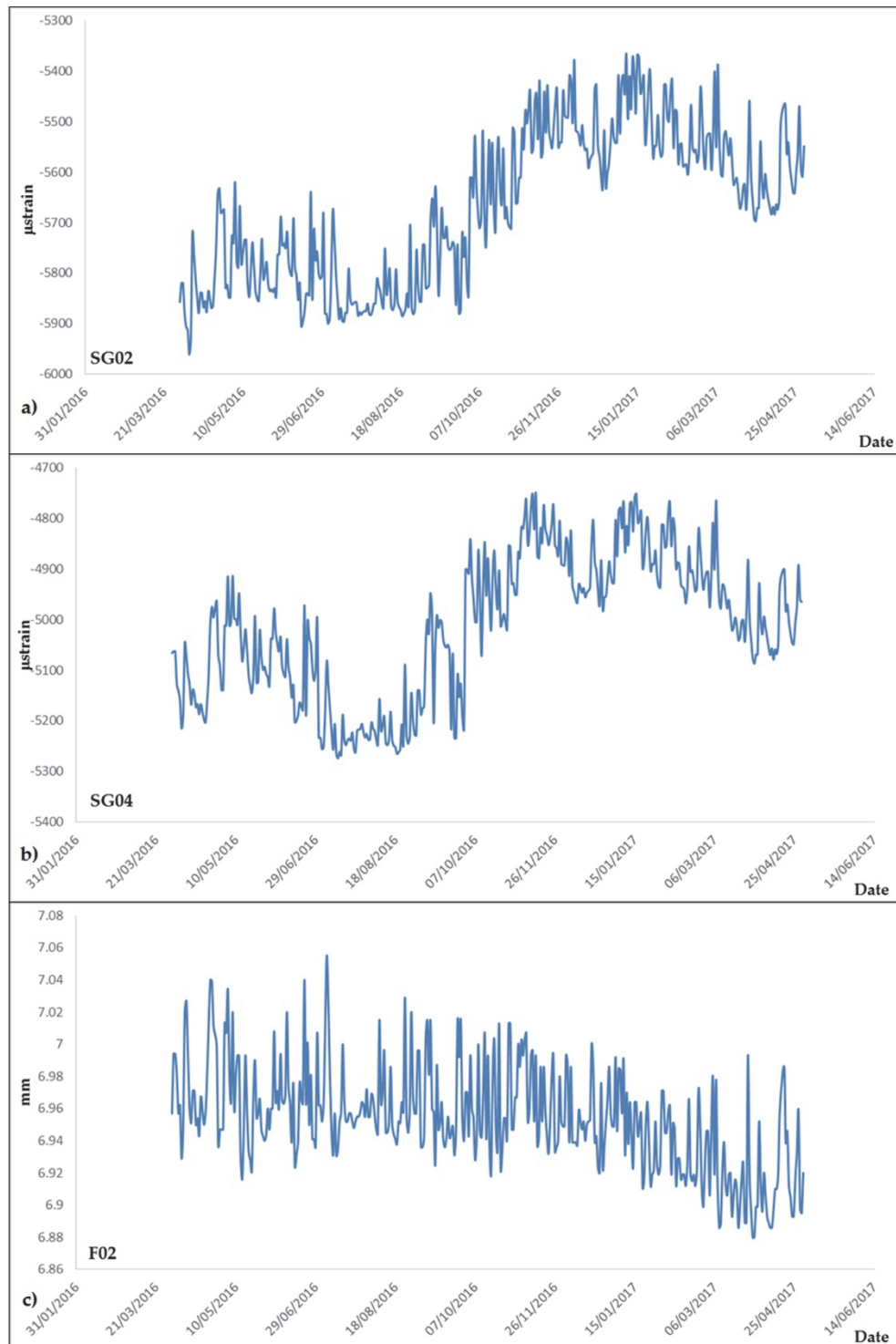


Fig. 36: Time sequence of displacement values recorded by strain sensors installed on front face of the rock block: strain gauges n° 2 (a), strain gauges n° 4 (b) and extensometer n° 2 (c). For see arrangement of these sensors on rock block cf. Fig. 24.

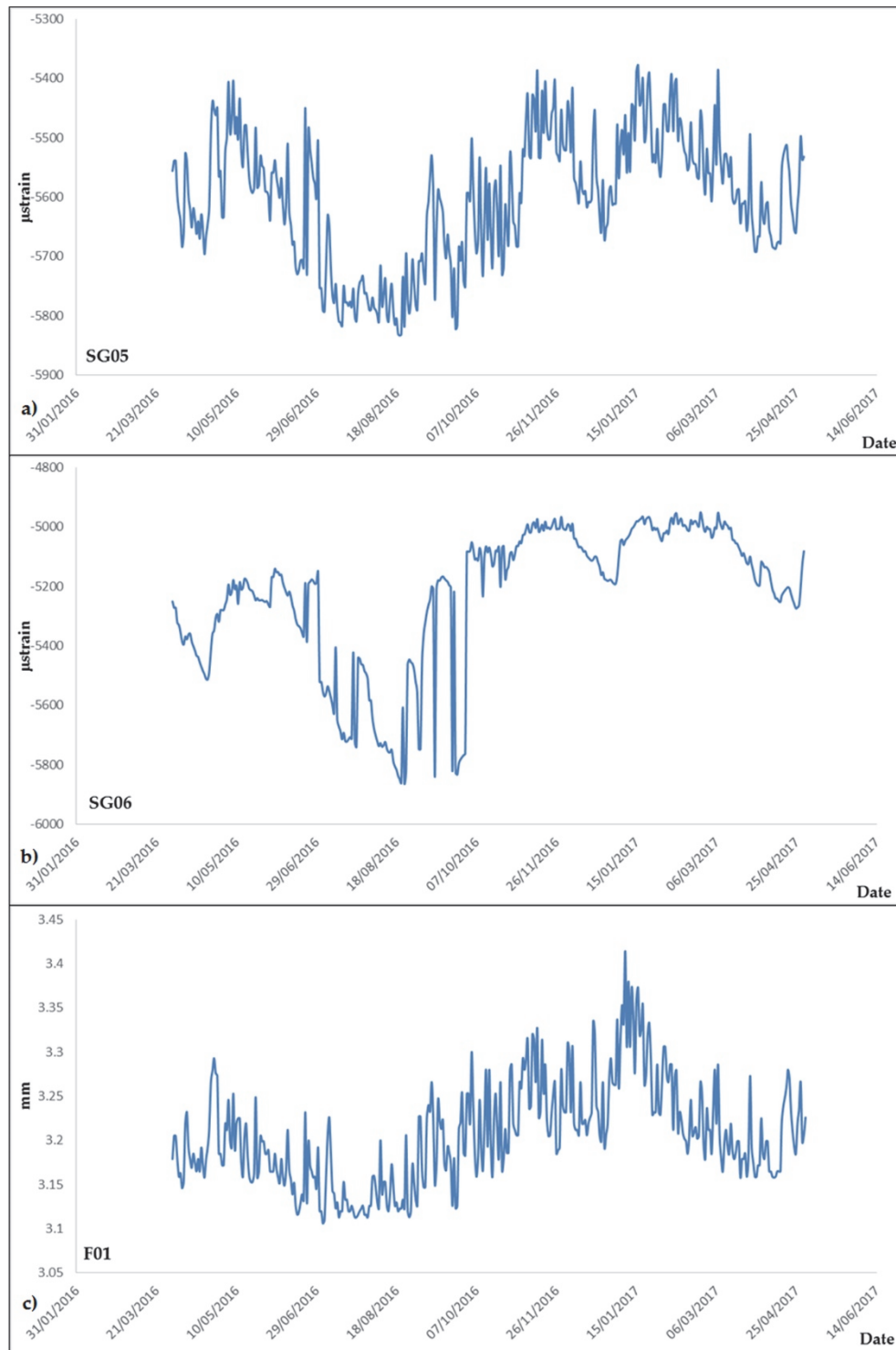


Fig. 37: Time sequence of displacement values recorded by strain sensors installed on backside of the rock block: strain gauges n° 5 (a), strain gauges n° 6 (b) and extensometer n° 1 (c). For see arrangement of these sensors on rock block, cf. Fig. 24.

The displacement trend measured for micro-fractures and joints is strongly related with the rock temperature, which in turn is related to weather conditions and mainly to air temperature. This correlation implies that contraction and expansion of the rock on both side of rock block, is manifest in strain sensors record. The relation between micro-fractures or joints displacement behavior and rock temperature for annual cycle is shown in Fig. 38 and in Fig. 39. An inverse relation between displacement trend and rock temperature is generally achieved for all strain sensors. This kind of behavior is not evident in the extensometer n° 2, installed on horizontal joint of front block face and measuring along vertical direction. In fact, a general trend of closure is evident. Probably along up-down direction, the action of gravity is greater than the effect of temperature, thus filtering the thermal input on the rock deformation.

Similar analysis was carried out for the comparison between the displacement of micro-fractures or joints and the rainfalls. In this case the observation shows that the displacement values increase during rainy seasons. The relation between displacements of micro-fractures or joints displacement and rainfalls over annual period is shown in Fig. 40 and Fig. 41.

The comparison between the annual wind speed values and the displacement trend of micro-fractures or joints, doesn't show a direct relations. Considering only the three windstorm, occurred during monitored period with an azimuth direction compatible with rock wall attitude for generate instabilities events, displacement values do not show significant variation during the episodes or immediately after. Probably, the strong wind events are too impulsive phenomena to give rise appreciable change of displacement trend. A synoptic table reporting the micro-fractures or joints displacement and the wind speed over annual period is shown in Fig. 42 and Fig. 43.

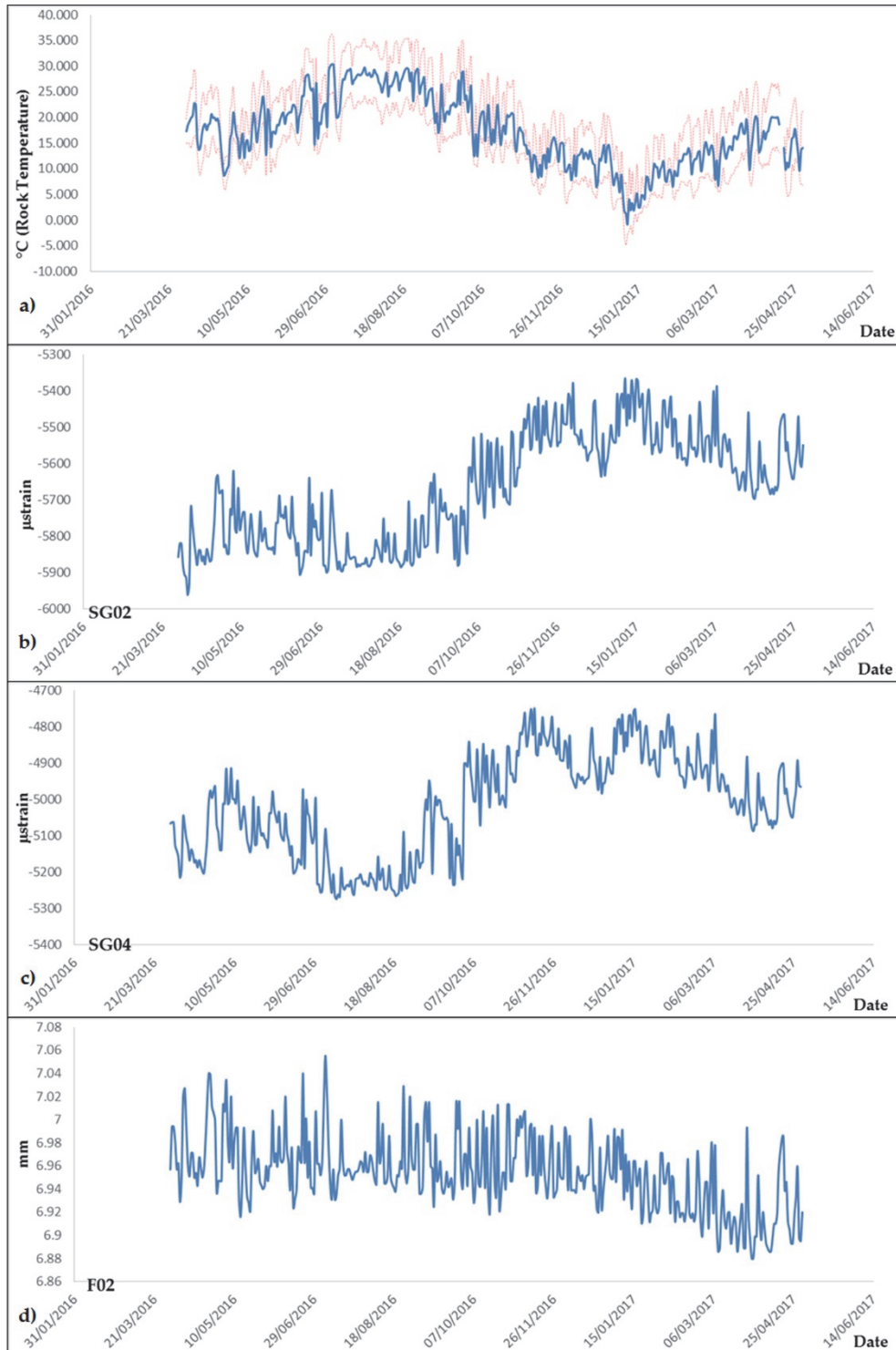


Fig. 38: Synoptic table showing annual cycle of rock temperature (a) and displacement of strain sensors installed on front side of the rock block (b, c, d).

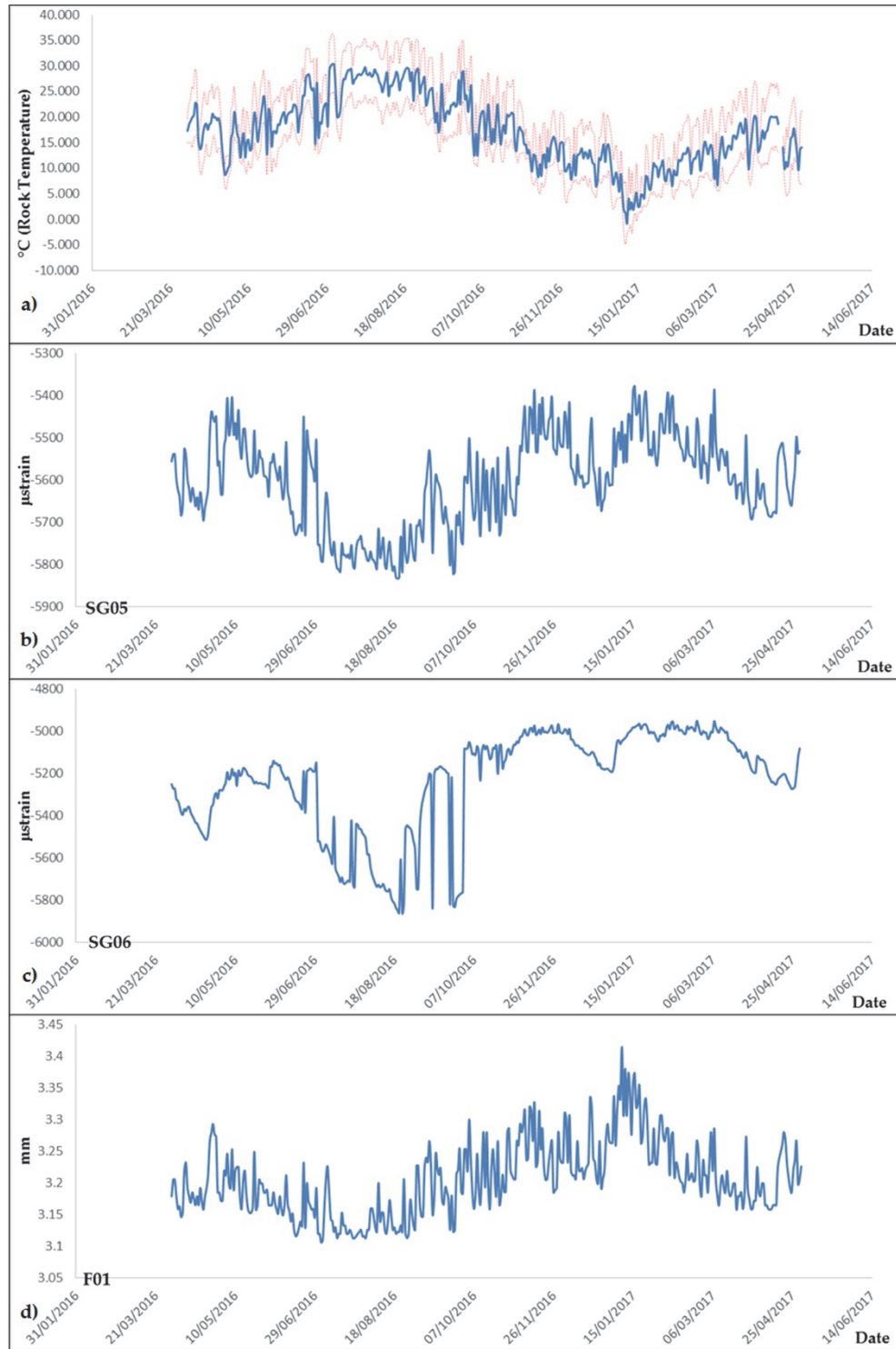


Fig. 39: Synoptic table showing annual cycle of rock temperature (a) and displacement of strain sensors installed on backside of the rock block (b, c, d).

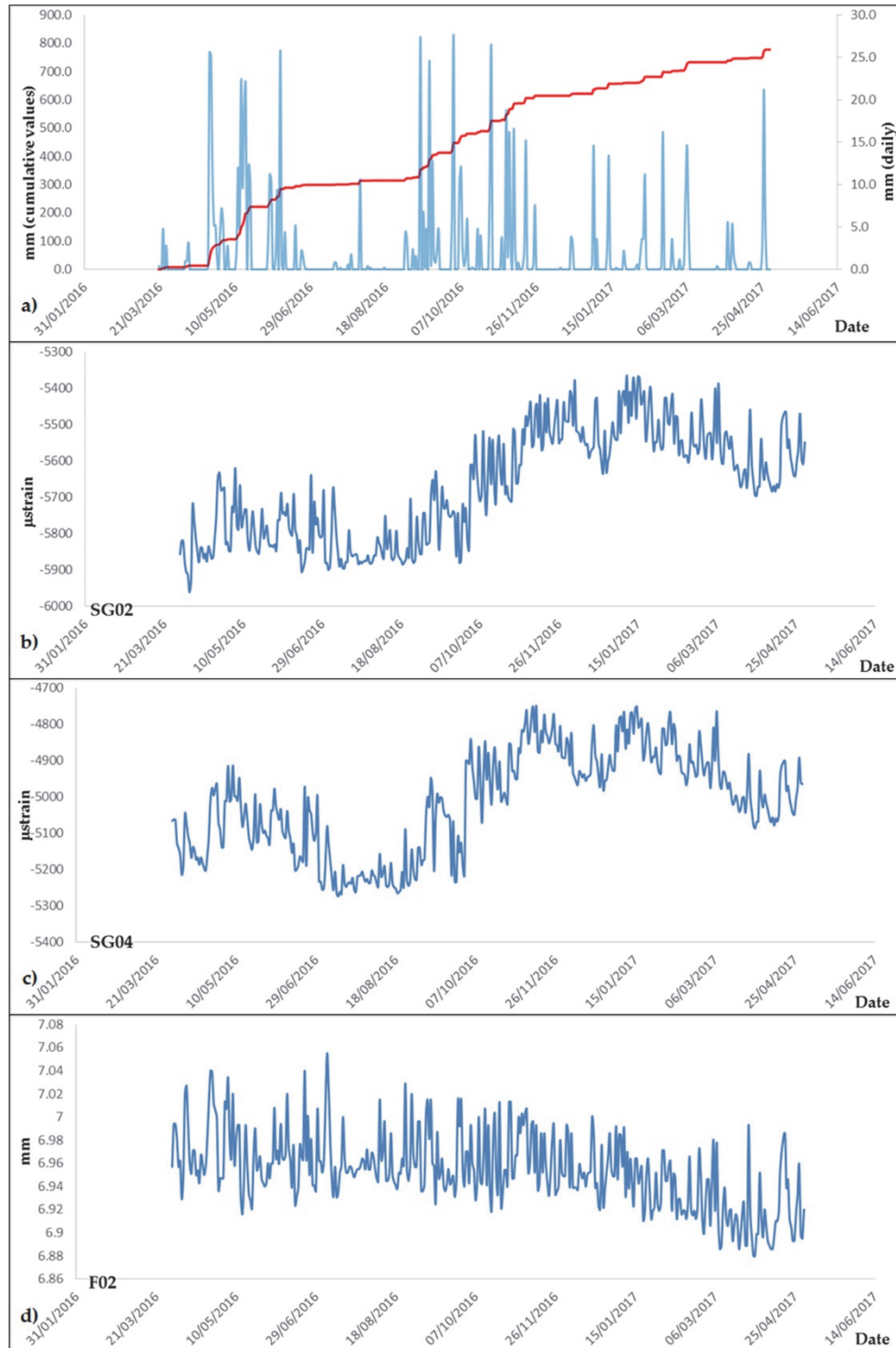


Fig. 40: Synoptic table showing annual rainfall regime (a) in relation to displacement of strain sensors installed on front side of the rock block (b, c, d).

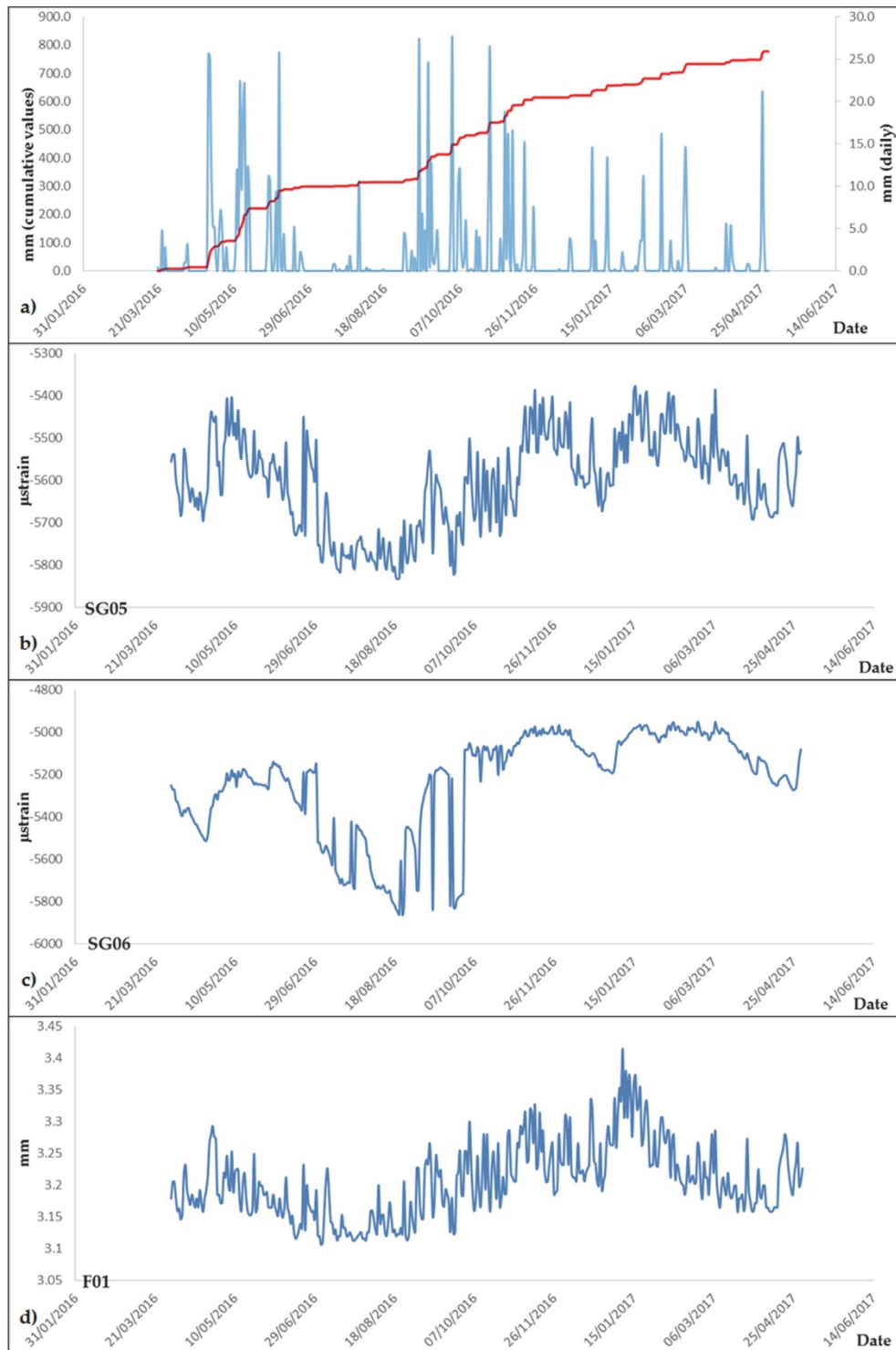


Fig. 41: Synoptic table showing annual rainfall regime (a) in relation to displacement of strain sensors installed on backside of the rock block (b, c, d).

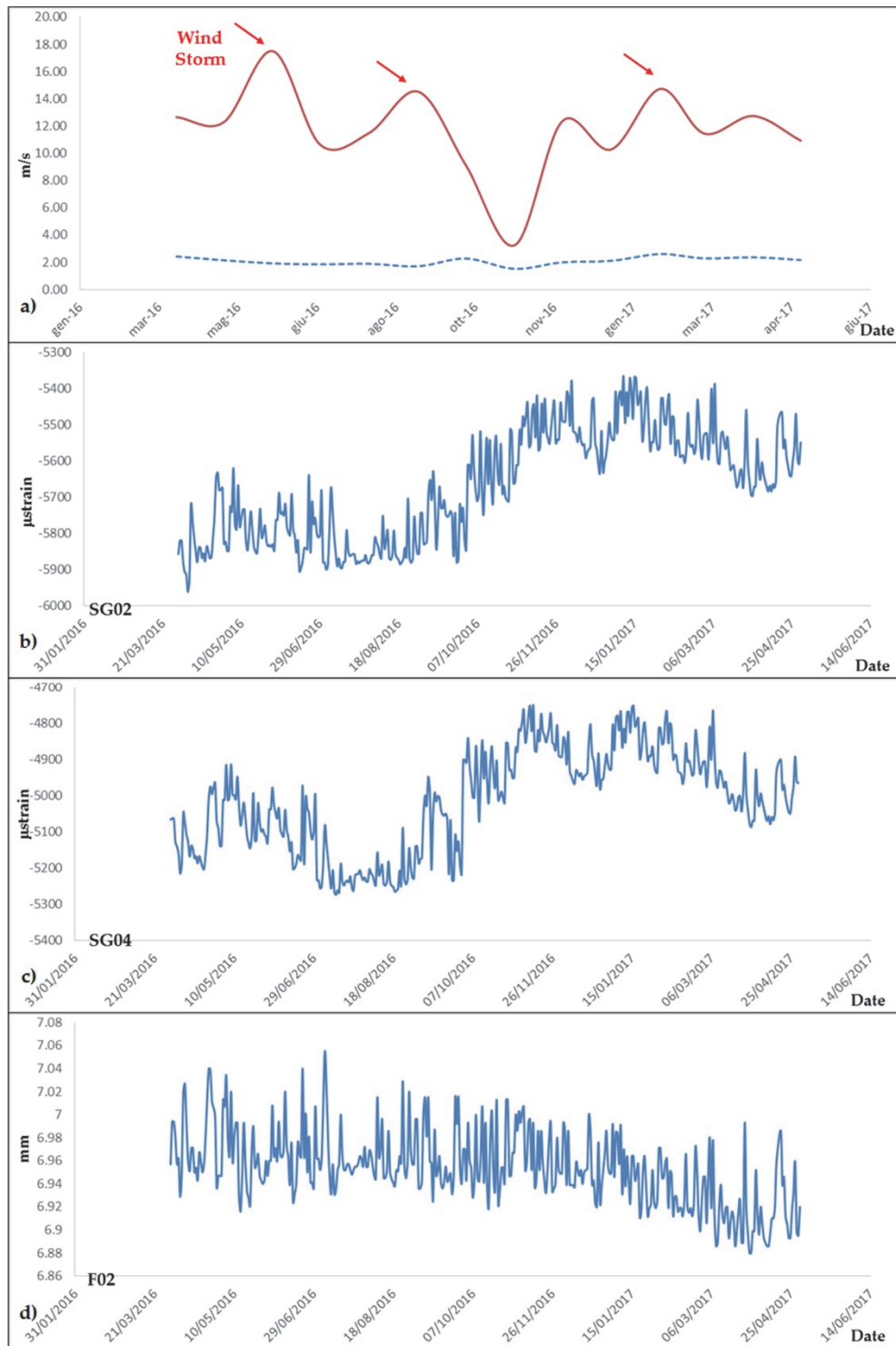


Fig. 42: Synoptic table showing annual average wind regime (a) in relation to displacement of strain sensors installed on front side of the rock block (b, c, d). The storm wind phenomena are shown using red arrows (a).

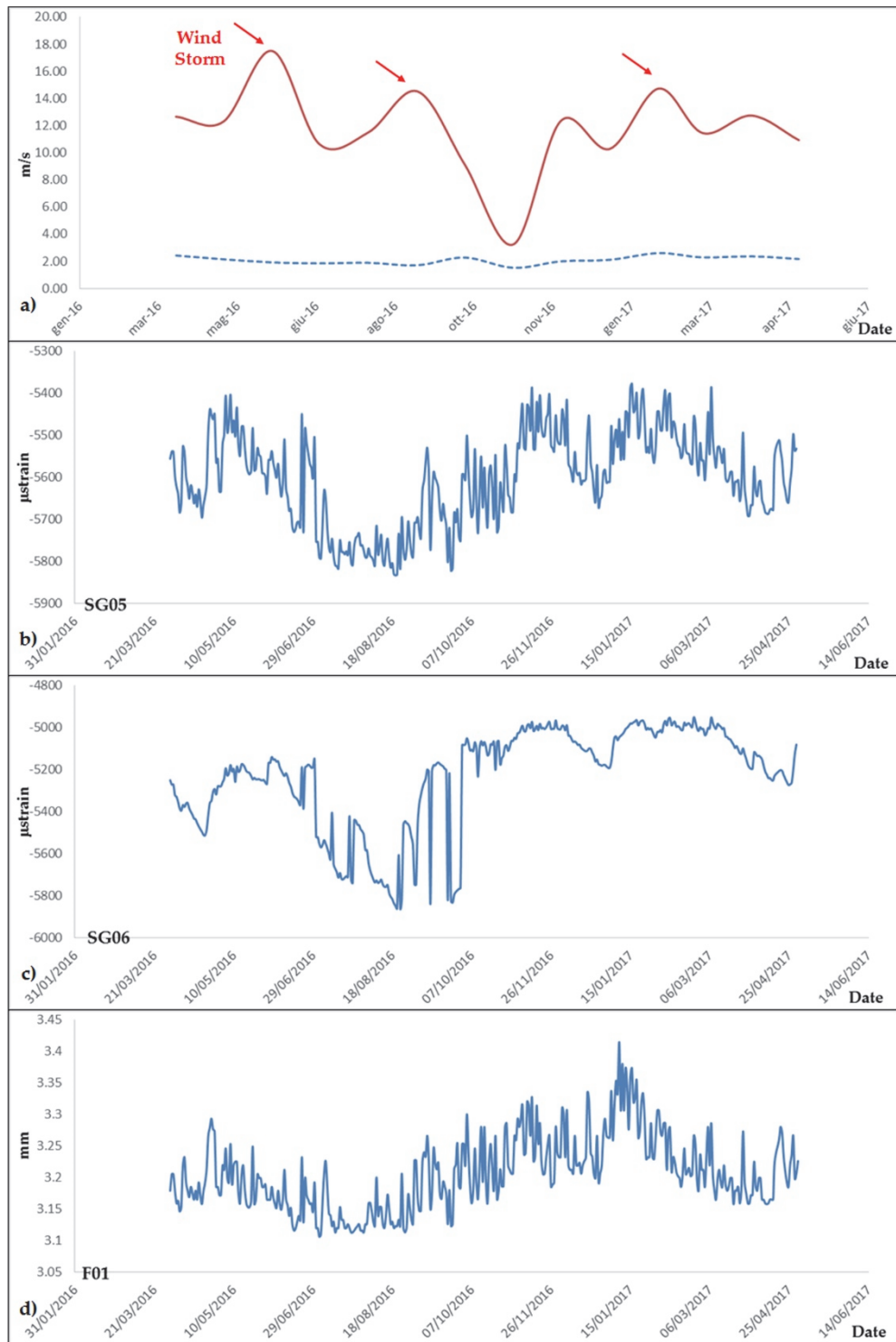


Fig. 43: Synoptic table showing annual average wind regime (a) in relation to displacement of strain sensors installed on backside of the rock block (b, c, d). The storm wind phenomena are shown using red arrows (a).

In the Acuto test-site area is considerable daily thermal oscillations due to direct and intense solar radiation that affect the rock mass. This effect also can influence the long-term behaviour of the rock masses, in addition to daily deformation cycles, operating as thermal fatigue process and acting as a continuously *preparatory factor* for rock failure and for displacement variation on open joints.

In each daily thermal cycle, a heating phase of temperature is followed by related cooling phase. The first phase starting with sunrise time, until midday about and is due to direct solar radiation; the second phase follow the first when the rock block progressively going to shadow. During the heating phase, micro-fractures and joints displacement decrease due to the progressive approach of the edges of the fracture. During the cooling phase, micro-fractures and joints displacement decrease due to the progressive removal of the edges of the fracture. Daily cyclical displacement of micro-fractures and joints, due to solar radiation, reveals an almost thermo-elastic behavior. The heating phases is always shorter than related cooling phase due to effect of direct and strong solar radiation. In fact, during the hours of direct solar radiation, the rock heats up very quickly. The cooling phase is divided in two parts: the first one immediately after the rock goes into the shadows, the second one during the night. In the first part, the rock loses heat quickly and the slope of the line is high. In the last daily part of cooling phase, the rock loses heat more slowly depending on his heat capacity value: the slope of the line is lower than the previous one (Fig. 44). The maximum amplitude of thermal cycles is in correspondence of the more sunny days, especially in the summer months where the effect of solar radiation is stronger and the temperature is higher than other months. In the days when solar radiation is low or in the winter season, the heating phase is temporarily much shorter than the corresponding cooling phase. Also the effect of the aspect seems not negligible since the: sensors that are more exposed to the sun during the day, have a faster heating phase and shows a greater amplitude of related hourly strain rate. The average hourly rates of strain sensors during heating phase and cooling phase are summarized in Fig. 45.

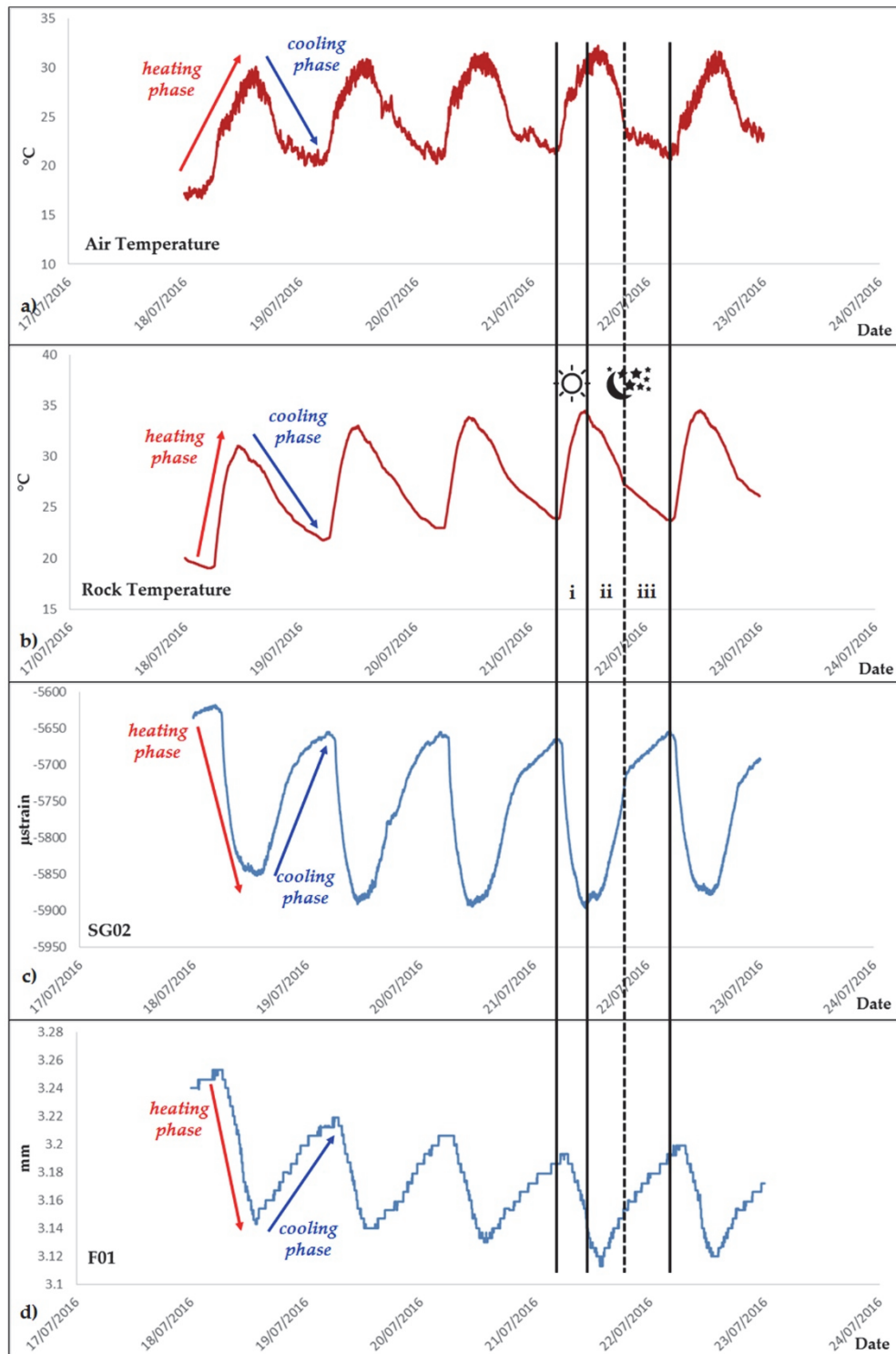


Fig. 44: Example of daily thermal cycles with highlighted the heating phase and follower cooling phase, starting to sunrise hours to nightfall hours for: a) air temperature, b) rock temperature, c) strain gauges installed on micro-fracture, d) extensometer installed on open joint. The features of heating and cooling phase are also shown: heating phase ramp with high slope (i), first part of cooling phase ramp where heat is lost rapidly with high slope, likely heat phase ramp (ii), second part of cooling phase ramp (and last part of daily cycle) where the heat is lost more slowly, function of thermal capacity (iii).

		SG02		SG04		SG05		SG06		F01		F02	
		total μ strain	time (hh.mm)	total μ strain	time (hh.mm)	total μ strain	time (hh.mm)	total μ strain	time (hh.mm)	total mm	time (hh.mm)	total mm	time (hh.mm)
April 2016	cooling phase	177.37	17.07	137.50	16.49	131.47	16.13	49.67	14.42	0.07	18.27	0.06	18.09
	heating phase	173.90	6.58	136.23	7.17	130.30	8.01	49.63	10.44	0.07	7.09	0.06	6.41
May 2016	cooling phase	175.23	16.25	146.74	16.31	129.03	16.01	57.39	15.13	0.07	17.45	0.07	17.52
	heating phase	177.48	7.33	149.03	7.27	132.29	8.43	57.68	8.59	0.07	7.51	0.07	6.58
June 2016	cooling phase	180.43	16.11	154.53	17.26	138.90	15.17	71.53	14.14	0.06	18.02	0.07	18.28
	heating phase	180.70	7.33	154.93	6.50	139.37	8.47	71.70	9.56	0.06	7.26	0.07	6.38
July 2016	cooling phase	216.55	16.18	178.55	16.41	156.61	14.38	92.42	14.02	0.07	17.06	0.08	18.23
	heating phase	217.26	7.33	179.35	7.18	157.52	9.22	96.26	9.58	0.07	7.23	0.08	5.47
August 2016	cooling phase	221.84	16.17	183.39	16.27	171.42	15.15	90.19	14.27	0.10	16.36	0.08	17.57
	heating phase	222.91	7.45	184.03	7.33	172.10	8.35	90.29	10.11	0.10	7.36	0.08	7.03
September 2016	cooling phase	202.47	16.35	176.37	16.45	162.83	15.47	120.63	17.20	0.09	17.51	0.07	17.26
	heating phase	203.33	7.47	176.77	7.36	163.07	7.59	120.73	7.45	0.09	6.54	0.07	7.21
October 2016	cooling phase	165.87	16.20	133.65	16.35	139.81	16.26	61.29	14.21	0.08	20.26	0.06	18.19
	heating phase	165.90	8.22	133.58	7.56	139.87	8.41	61.35	10.34	0.08	7.49	0.06	8.48
November 2016	cooling phase	135.10	17.16	102.70	16.32	121.63	16.41	39.67	15.58	0.07	19.19	0.05	18.32
	heating phase	131.33	7.14	100.67	7.13	116.37	7.45	37.27	9.01	0.07	7.50	0.05	7.31
December 2016	cooling phase	175.29	16.33	139.87	17.30	154.03	16.35	41.58	10.08	0.10	17.59	0.06	16.45
	heating phase	177.52	8.02	141.35	6.20	157.81	7.14	48.00	13.51	0.10	6.40	0.06	7.21
January 2017	cooling phase	142.00	15.40	112.97	16.02	121.13	15.55	46.68	12.13	0.07	16.33	0.05	15.58
	heating phase	143.52	8.50	113.74	8.15	120.61	7.49	42.29	14.24	0.07	9.30	0.05	9.04
February 2017	cooling phase	158.29	17.09	120.50	17.27	128.86	16.47	43.07	14.58	0.07	16.49	0.06	16.23
	heating phase	158.46	7.19	121.00	6.50	129.57	7.50	41.71	10.59	0.07	8.39	0.06	8.44
March 2017	cooling phase	198.39	16.24	156.81	16.22	153.97	16.09	47.10	13.23	0.27	17.49	0.10	17.21
	heating phase	201.55	7.27	160.65	7.22	157.81	7.59	52.71	10.56	0.27	7.05	0.10	7.41
April 2017	cooling phase	217.71	16.50	176.18	16.56	162.18	16.35	59.07	16.27	0.40	18.30	0.14	16.23
	heating phase	216.07	12.04	172.79	12.24	157.29	14.02	54.57	15.55	0.40	13.05	0.14	13.18

Fig. 45: Average monthly displacement rate calculated during heating phase and cooling phase, for the strain sensors (strain gauges and extensometers) installed both on front face of rock block and on backside. The time represent the duration (presented as hh.mm) of the heating and cooling ramps.

After each daily thermal cycle, which is supposed to have an almost thermo-elastic behavior, the rock mass accumulates a small rate of daily net deformation. This deformation was calculated for each daily cycle using a compiled Unix script, which obtains the value of daily net contribution to the strain (ϵ_p) as such as the difference between the length of the heating ramp and the length of the subsequent cooling ramp of the same daily cycle (Fig. 46).

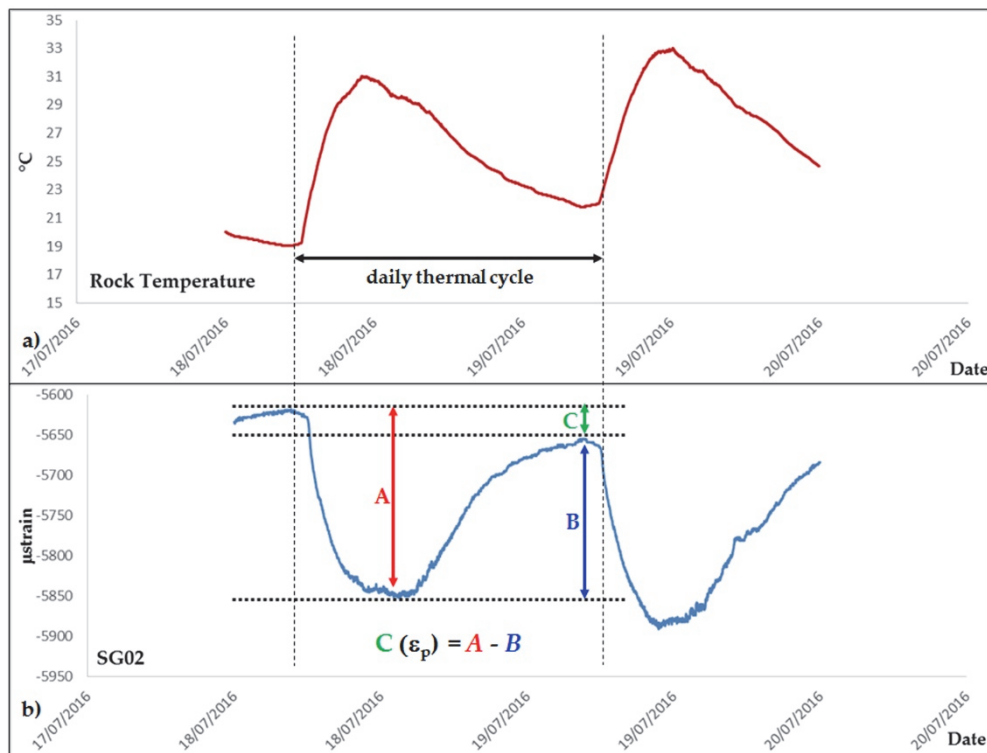


Fig. 46: Example detail of a daily thermal cycle recording by rock thermometer (a) and of a front side strain gauges (b). The formula for calculating daily net deformation is also shown.

The preliminary OBA analysis carried out in order to obtain the daily net deformation, show that the maximum amplitude of this value and the higher frequency of peaks are concentrated in spring and autumn seasons. During these periods, the days are characterized by a higher thermal excursion that heavily influences the amplitude of the daily net response of the rock mass deformation. During summer and winter seasons, the thermal excursion is lower and the rock mass tends to a more elastic behavior (Fig. 47 and Fig. 48).

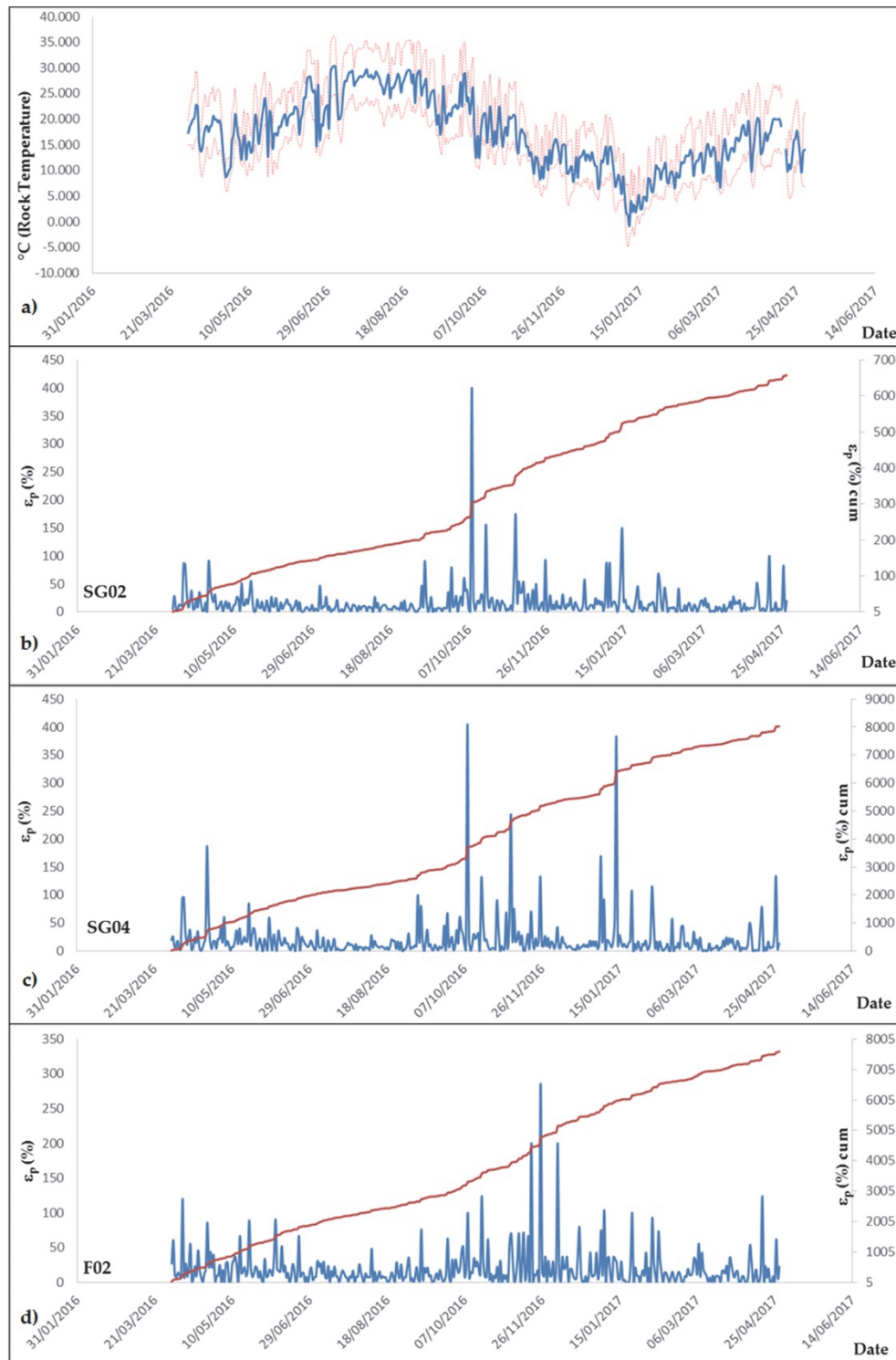


Fig. 47: Synoptic table showing cycle of rock temperature (a) and daily net contribution to the strain computed from the records of the sensors installed on the front side of the rock block (b, c, d). The main amplitude and the high number of daily net deformation peaks are concentrated in the periods with higher thermal excursion.

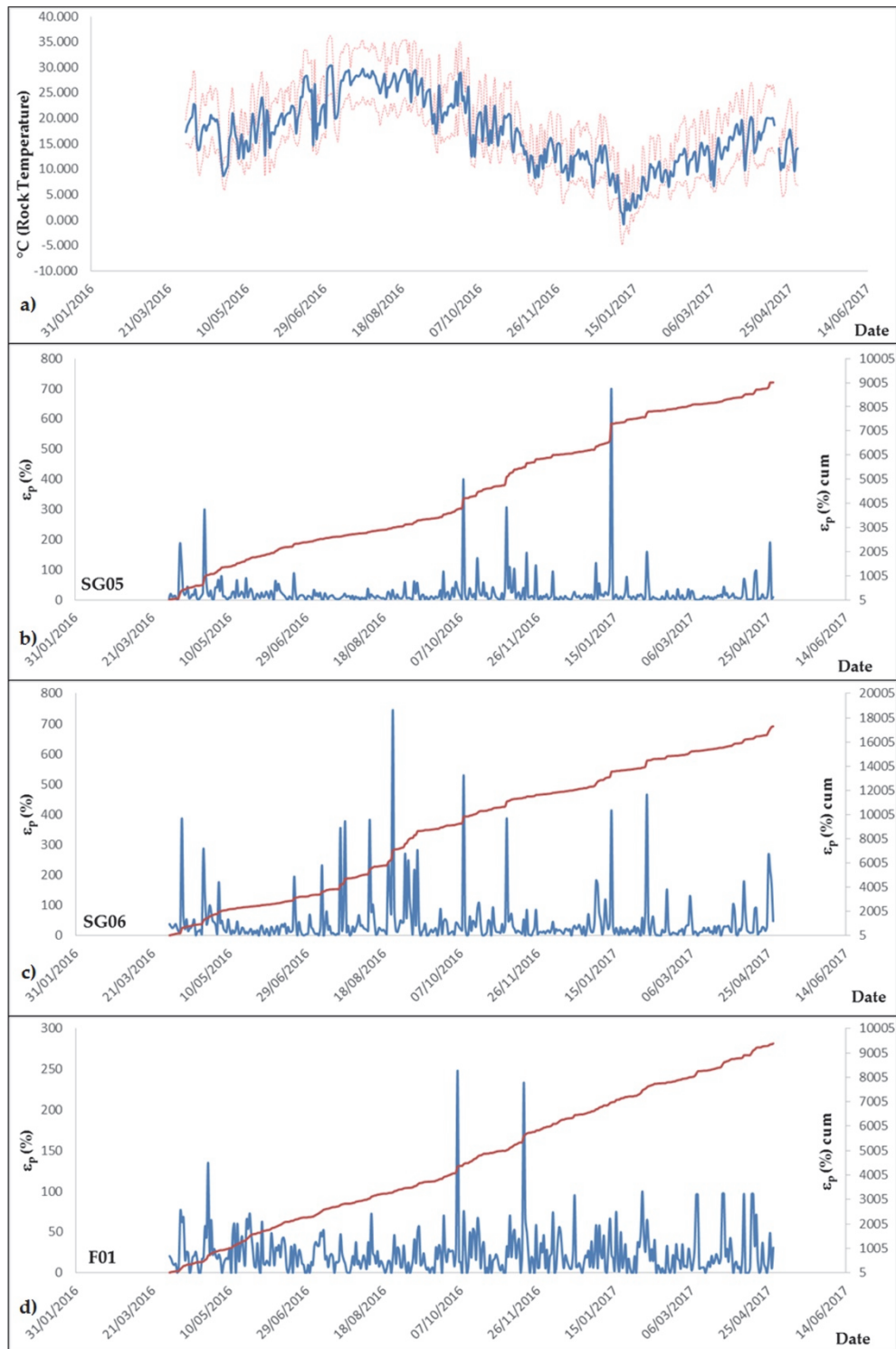


Fig. 48: Synoptic table showing cycle of rock temperature (a) and daily net contribution to the strain computed from the records of the sensors installed on the backside of the rock block (b, c, d). The main amplitude and the high number of daily net deformation peaks are concentrated in the periods with higher thermal excursion.

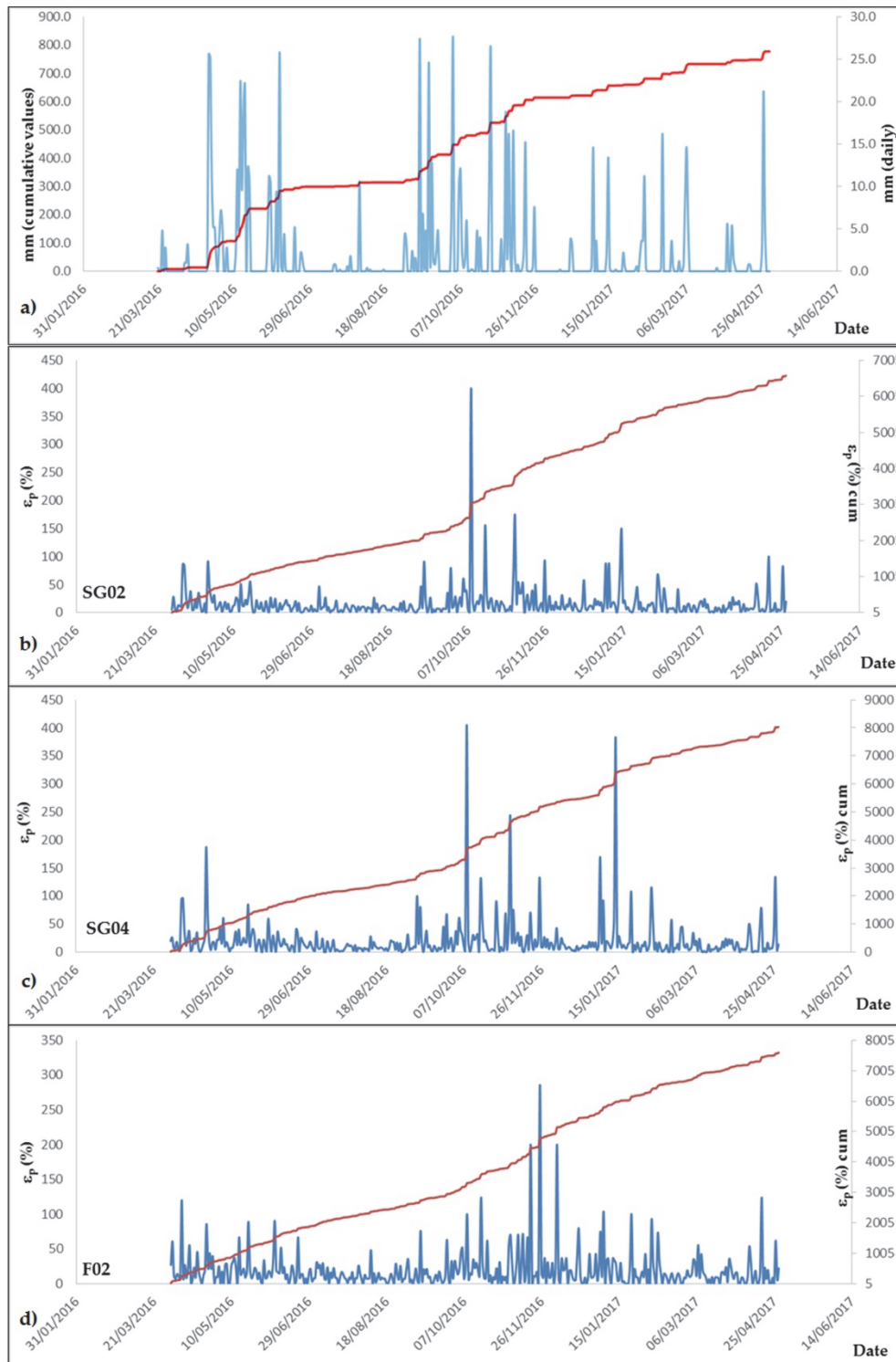


Fig. 49: Synoptic table showing rainfall regime (a) in relation to daily net contribution to the strain computed from the records of the sensors installed on front side of the rock block (b, c, d). In periods characterized by increased rainfall, there is also an increase in the daily net deformation of the monitored block.

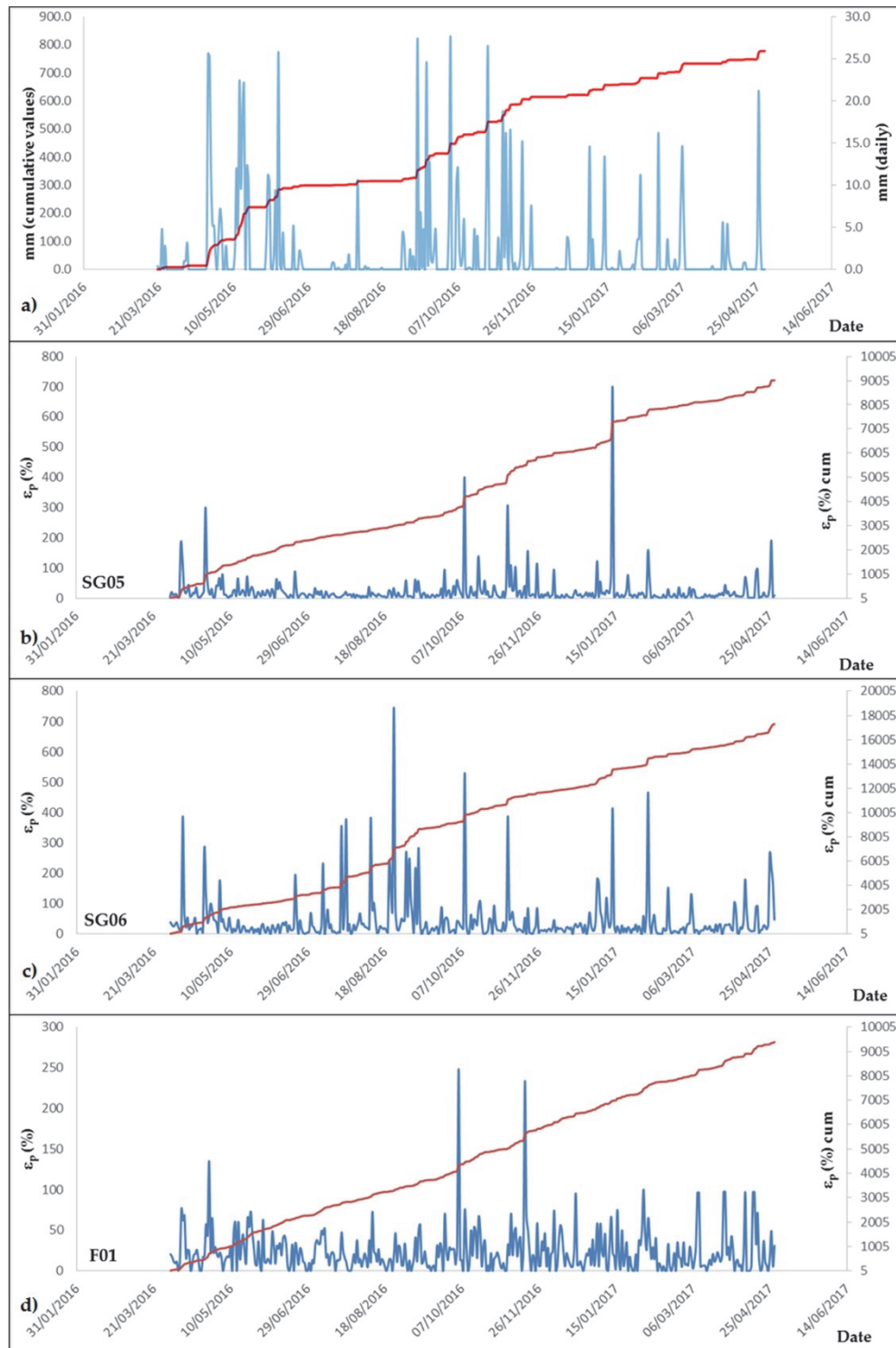


Fig. 50: Synoptic table showing rainfall regime (a) in relation to daily net contribution to the strain computed from the records of the sensors installed on backside of the rock block (b, c, d). In periods characterized by increased rainfall, there is also an increase in the daily net deformation of the monitored block.

Even in correspondence of the most significant rainfall episodes, an increase in the daily net contribution to strain of the rock mass can be observed (Fig. 49 and Fig. 50). In fact, the rainfall cumulative intensity sharply increases in autumn and spring seasons. The concomitant increase of rock deformation, especially regarding the peaks, maybe also due to intense and frequently heavy seasonal rainfall. No relations were found between storm wind phenomena and an increase of rock deformation behavior.

The daily net deformations are the result of at least two different factors: inelastic deformations cumulated at repeated daily cycles and attributable to thermo-mechanical interactions, and secondarily to long-term time dependent deformations ascribable to creep phenomena (for this issue, see 5.3).

A laboratory physical characterisation of thermal parameters (i.e. thermal conductivity and linear thermal expansion) was carried out on rock samples according to international standards for testing materials. The lab-tests were performed by external laboratory in the framework of dedicated research starting project. The obtained thermal parameters allowed the calculation of heat flow associated with conduction, according to Fourier's law. For future developments, the main goal of these laboratory analysis is to perform a stress-strain numerical modelling aiming at establishing cause-to-effect relations between thermal forcing and induced elastic and inelastic deformations (i.e. thermal fatigue), with the purpose of assessing predisposing conditions for slope instability after daily and seasonal thermal changes.

The analysis of the data collected during the activities of the Phase A in Acuto test-site, and carried out following the OBA approach, allowed to understand some cause-to-effect relations among possible destabilizing actions and related strains when the rock block is exposed to several environmental conditions. More in particular, the following was determined:

- a) the recognition of some *predisposition factors* (as climate of Acuto area, characterized by sharp temperature contrasts and by an high precipitation

- rate in autumn and spring seasons) and of some *preparatory factors* (as daily and seasonal rock temperature oscillations and regular rainfall regime);
- b) the recognition of continuous forcing, as temperature, and discontinuous forcing, as rainfall and wind;
 - c) the recognition of daily and seasonal deformational trend of rock mass, due to the action of *preparatory factors*;
 - d) the understanding of daily elastic thermomechanical behavior of rock mass due to temperature and the definition and characterization of heating phase and of cooling phase for daily and seasonal time periods;
 - e) the observation of inelastic strain cumulated in the rock mass at each thermal cycle, inducing a stationary seasonal trend.


It follows that the OBA approach has allowed to detect the main *preparatory factors* that influence the rock mass deformation. These destabilizing actions act on various time-scales. Some of them have daily or seasonal cycle (like as the temperature) that affect the rock mass deformation in the same cyclic way; others of them act continuously over time (like as creep processes) and affect the rock mass deformation in a long-period time window. The OBA approach has also allowed defining a very robust cause-to-effect relation between the temperature and the strain of the exposed rock mass.

To have reliable results from applying the OBA approach, the choice of devices that compose the multi-parametric monitoring system and their disposition on the rock mass result to be very important and based on reconstructed geological model. The redundancy of monitoring devices is an important aspect in terms to have a greater number of data series to improve and validate the detected cause-to-effect relations. In fact, if there is the same cause-effect relationship between time-series recorded by the same kind of devices (that analyze the same natural process), the result seems to be strengthened.

As it regards the Phase B of the experiment, this was carried out from 18th July to 21th July 2016, by using a dynamic forcing device and detecting strain effects, induced by vibrations in the rock; this forcing can be regarded as representative for such train traffic on railways.

At this aim, a vibrodyne was located on a concrete base at the foot of the instrumented rock block and was operated to induce frequencies in a range between 5 Hz and 25 Hz with incremental step of 5 Hz (Fig. 51). After each shaking sequence, the experiment was interrupted for at least one hour, in order to restore undisturbed vibrational conditions on the rock wall. The vibrodyne is an electro-mechanical excitation device, which is able to produce sine waves at fixed frequency and amplitude, to induce stress-strain effects under controlled conditions.

As above mentioned, during the Phase B the monitoring system was implemented with the installation of six mono-axial Kinematics FBA11 accelerometers, cable-connected with a datalogger Kinematics K2. The datalogger was provided with an internal tri-axial accelerometer station and was set with a sampling frequency of 250 Hz.



N° of excitation	Frequency (Hz)	Time duration (s)
1	5	2400
2	10	1500
3	15	1020
4	20	780
5	20	1560
6	25	360

Fig. 51: Picture of Vibrodyne used at Acuto test-site (on the left). Table reported the dynamic excitation carried out in experimental activities, complete of frequency (Hz) and duration (second) of each vibration.

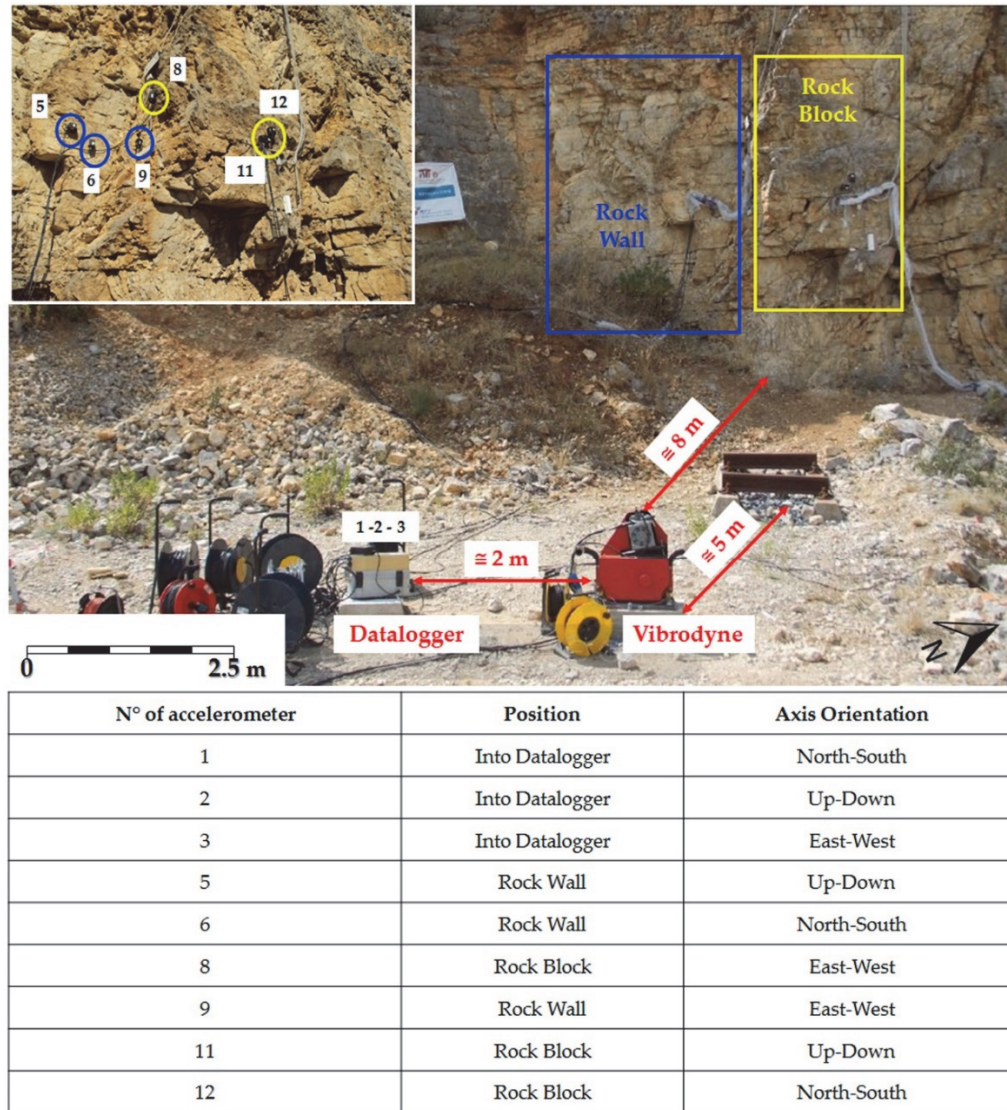


Fig. 52: Experimental activities at Acuto test-site performed on July 2016. The two concrete bases on which was installed the Vibrodyne and the accelerometric datalogger (K2 Kinematics) are shown. The arrangement of the mono-axial accelerometric sensors is shown in the dedicated frame.

Two concrete platforms (about 50x50 cm) spaced 2 m among them, were built about 8 m far from the rock block and 5 m far from the railway target, to fix the vibrodyne and the accelerometric datalogger. Since the concrete bases were jointed to the underneath bedrock, the vibration produced by the vibrodyne can be considered as completely transmitted to the rock mass wall. The FBA11 accelerometers were installed partly on the quarry wall and partly on the prominent block. Such distribution was chosen to record the different induced effects by the Vibrodyne to output different responses between protruded rock block and rock wall behind (Fig. 52).

Spectral analysis was performed by Geopsy open-source software (www.geopsy.com) in order to compare the records obtained close to the vibrodyne with the ones obtained on the rock block during the excitation sequences. The Standard Spectral Ratio – SSR obtained on the block (assumed as receiver site) respect to the wall (assumed as reference site) for the same component of the ground motion, outputs that in case of both 15 and 20 Hz dynamic inputs, a seismic amplification exists on the block at 25 Hz (Fig. 53).

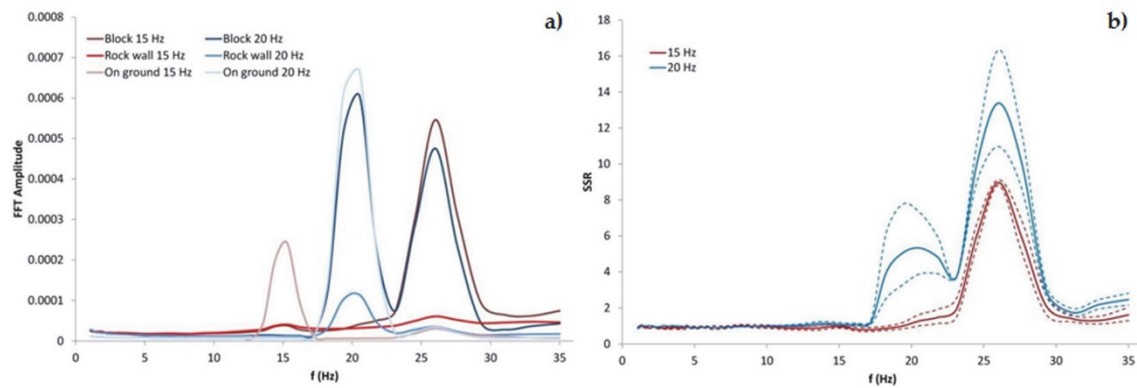


Fig. 53: Fast Fourier Transform (FFT – a) and rock block/rock wall Standard Spectral Ratio (SSR – b). The rock block dynamic amplification response at 20 Hz is visible (blue line – b). Dashed lines indicate standard deviation values.

A time-frequency analysis was also performed. Based on the spectrograms of the recorded signals, acquired close to Vibrodyne, on rock block and on rock wall, at the lowest generated frequencies (5 and 10 Hz) no energy was received by the rock block and consequently no significant induced vibration was detected. On the contrary, starting from the 15 Hz excitation frequency, a very low energy response was detected at the rock block. More in particular, at 20 Hz excitation frequency a dynamic response of the rock block is possible to see at same frequency, such as a rock block resonance frequency (Fig. 54).

The 25 Hz and 40-50 Hz frequencies are unfortunately caused by the power unit supply used to energize the vibrodyne, so the data derived from the 25 Hz shaking test are of difficult interpretation.

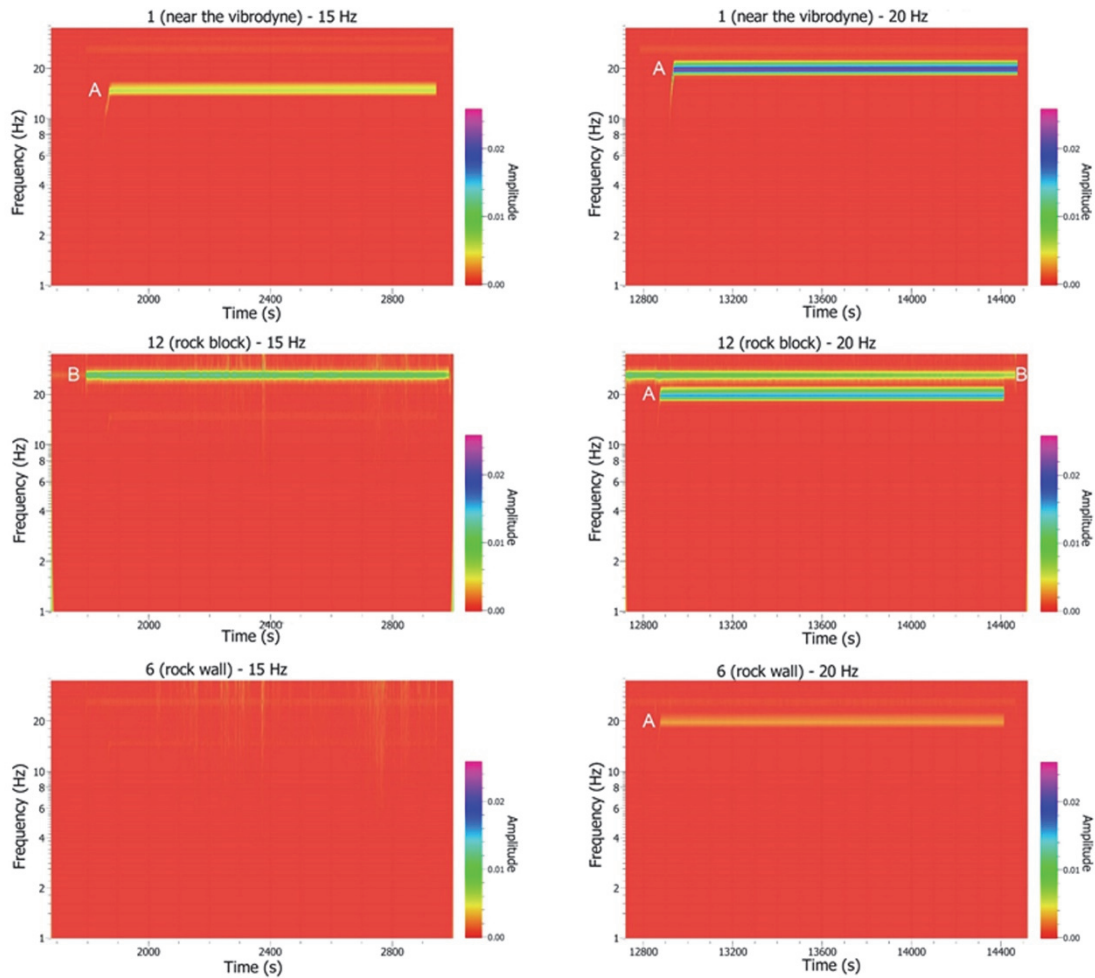


Fig. 54: Time-frequency analyses obtained for the 15 Hz (left side) and 20 Hz (right side) shaking tests: close to Vibrodyne (up), on the rock block (in the middle), on the rock wall behind (down). Markers on spectrograms indicate frequencies due to vibrodyne excitation (A) and to power unit supply (B). For the 20 Hz excitation, is possible to see the resonance of the monitored rock block.

The same results was also highlighted thanks to Spectral analysis. In case of 20 Hz dynamic input, the FFT amplitude shows a rock block response at the same frequency band (Fig. 55).

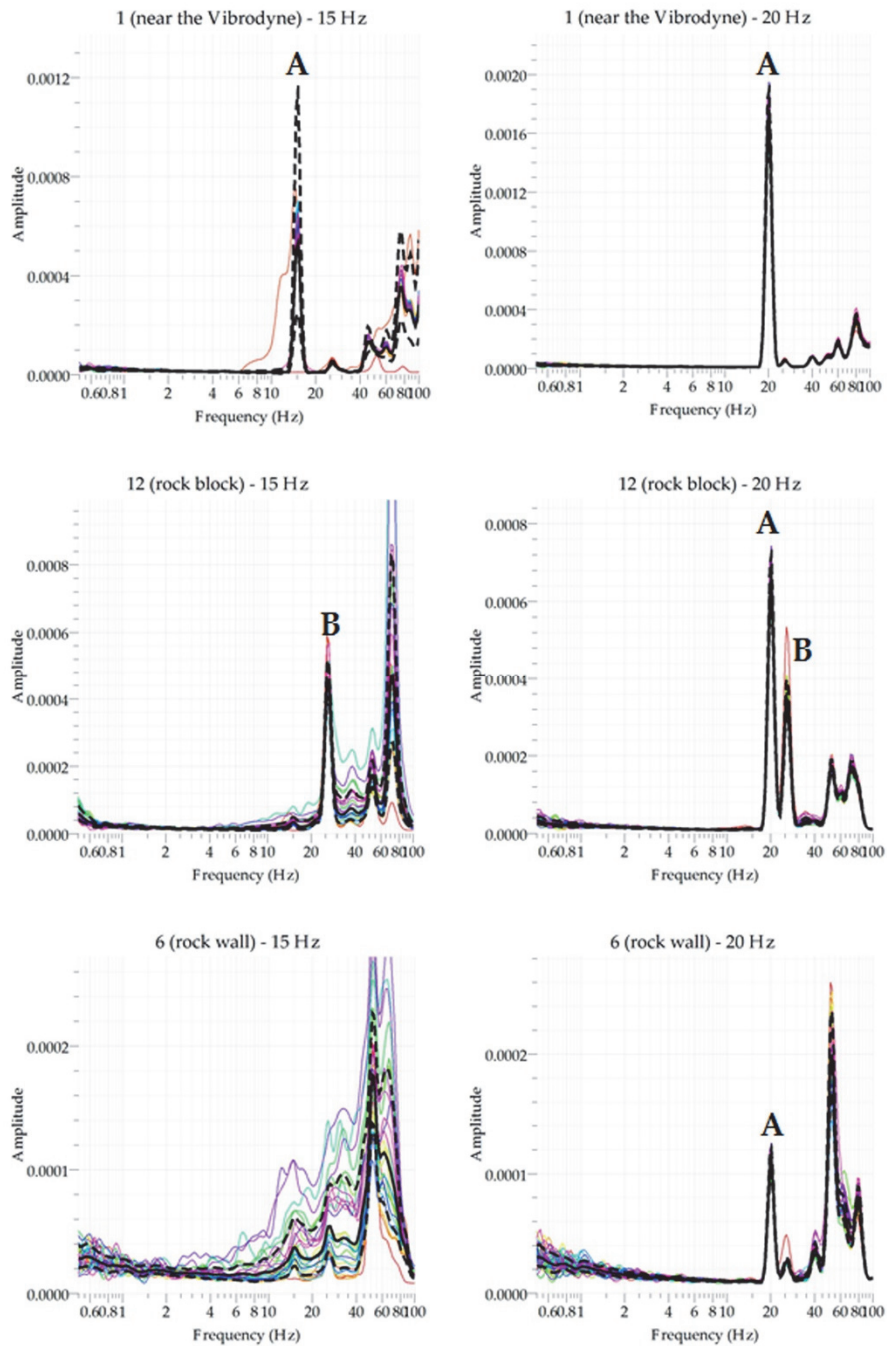


Fig. 55: Spectral analysis obtained for the 15 Hz (left side) and 20 Hz (right side) shaking tests: close to Vibrodyne (up), on the rock block (in the middle), on the rock wall behind (down). Markers on spectrograms indicate frequencies due to vibrodyne excitation (A) and to power unit supply (B). For the 20 Hz excitation, is possible to see the resonance of the monitored rock block.

The resultant 3D displacement induced over time by the rock block vibration was computed through a costumised Octave (open-source software). More in particular, were calculated the azimuth value and the tilt value of the three monitored point (close

to Vibrodyne, the rock wall and the rock block), with an accuracy of a tenth of a micron. The deformative response of the rock block to induced excitations at different frequencies, imposed through the Vibrodyne, was analyzed (Curi, 2017).

The 3D displacements result up to three times higher in the rock block respect to the back wall during the 20 Hz dynamic input. With regard to low frequency excitations (from 5 Hz to 15 Hz), no significant displacement has been measured both on rock block and on rock wall (Fig. 56).

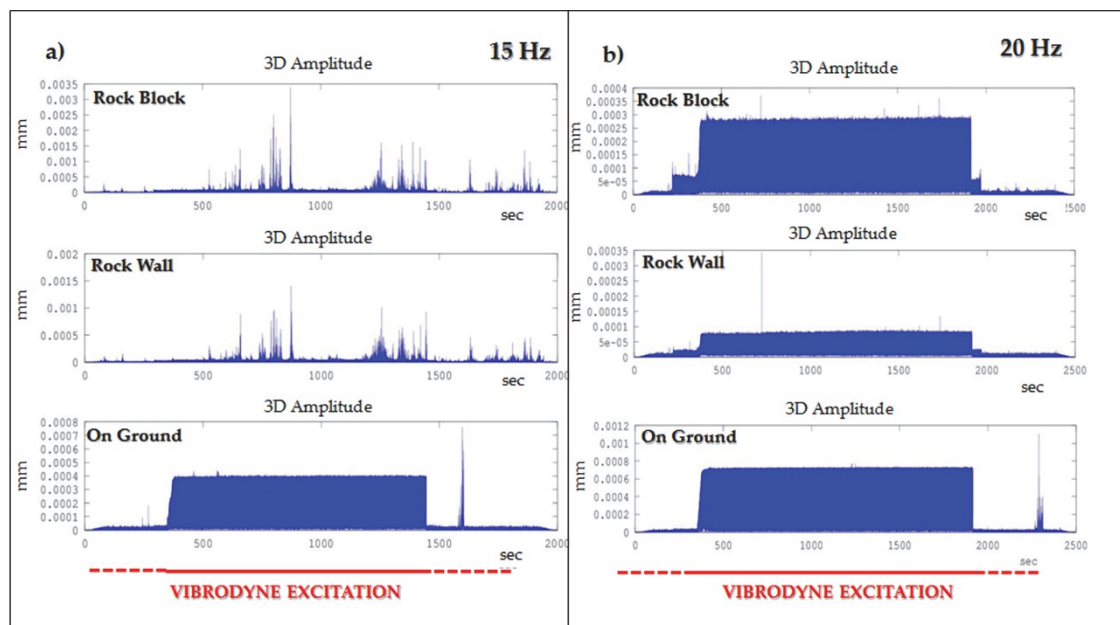


Fig. 56: Value of 3D displacement, computed in the case of 15 Hz dynamic input (a) and 20 Hz dynamic input (b) at the 3 measurement points: rock block (top graph), rock wall (middle graph) and bedrock close to Vibrodyne (bottom graph). Modified from (Curi, 2017).

Analysing azimuth and tilt values during the dynamic excitations, notice that the displacement of rock block and rock wall suffer a marked polarization with respect to the free oscillation state. During the shaking test at 20 Hz (Fig. 57), the azimuth values assumes a value of 160° for the rock block and 190° for the rock wall. The tilt assumes a value of 0° for both rock block and for rock wall. Then the rock block vibrates, it is

polarized about 30° respect to rock wall, demonstrating its release condition from the rock wall behind. After the dynamic excitations, the azimuth and tilt polarized values return to the initial state, so indicate that the induced displacements by shaking tests remained in the elastic field without causing anelastic deformation in the rock block. Furthermore, the direction of the polarization suffer by rock wall is orthogonal to the direction attitude of the wall itself. This assumes that polarization is due to the action of surface waves (with particular respect to Rayleigh waves), which tend to polarize in the direction of maximum anisotropy of the physical system.

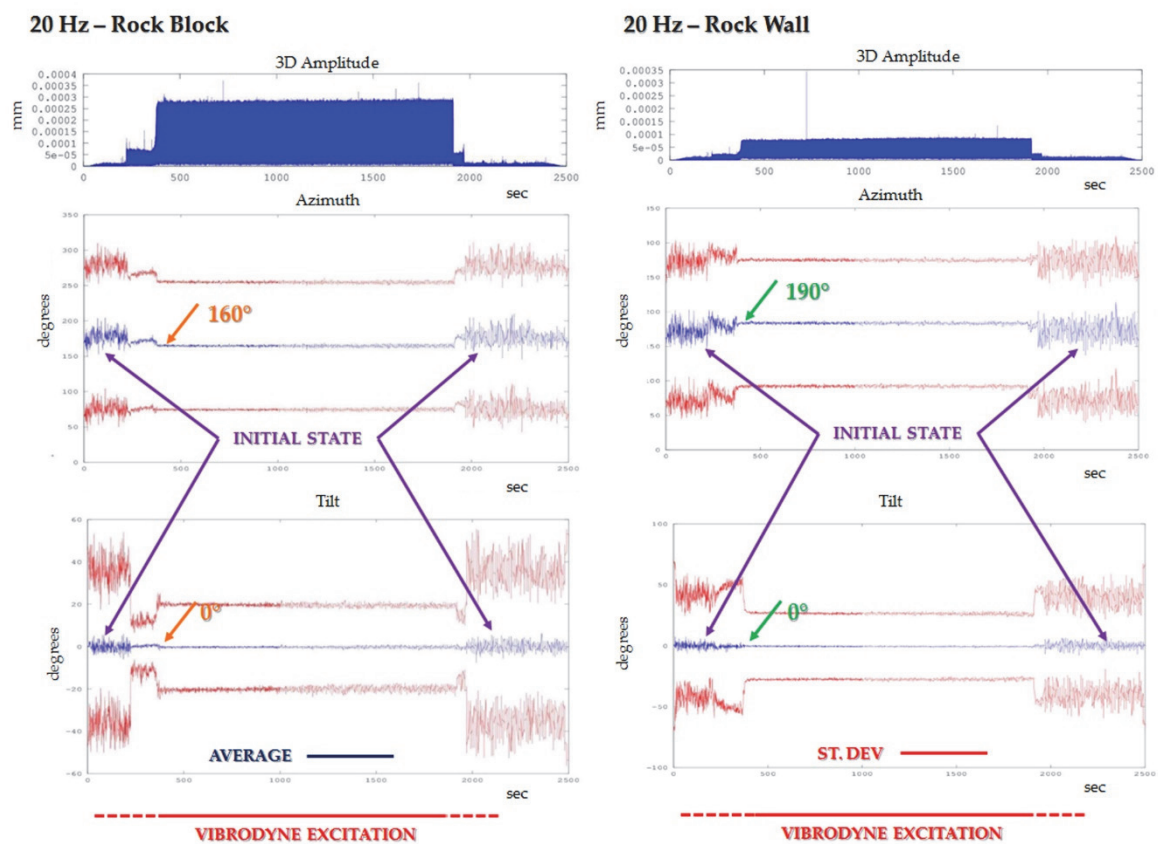


Fig. 57: Azimuth (middle graph) and Tilt (bottom graph) values of the rock block and of the rock wall, calculated during 20 Hz excitation. It's possible to see the polarization behaviour of both rock block and rock wall. Modified from (Curi, 2017).

With regard to low frequency excitations (from 5 Hz to 15 Hz), no significant polarization behaviour has been observed both on rock block and on the rock wall (Fig. 58).

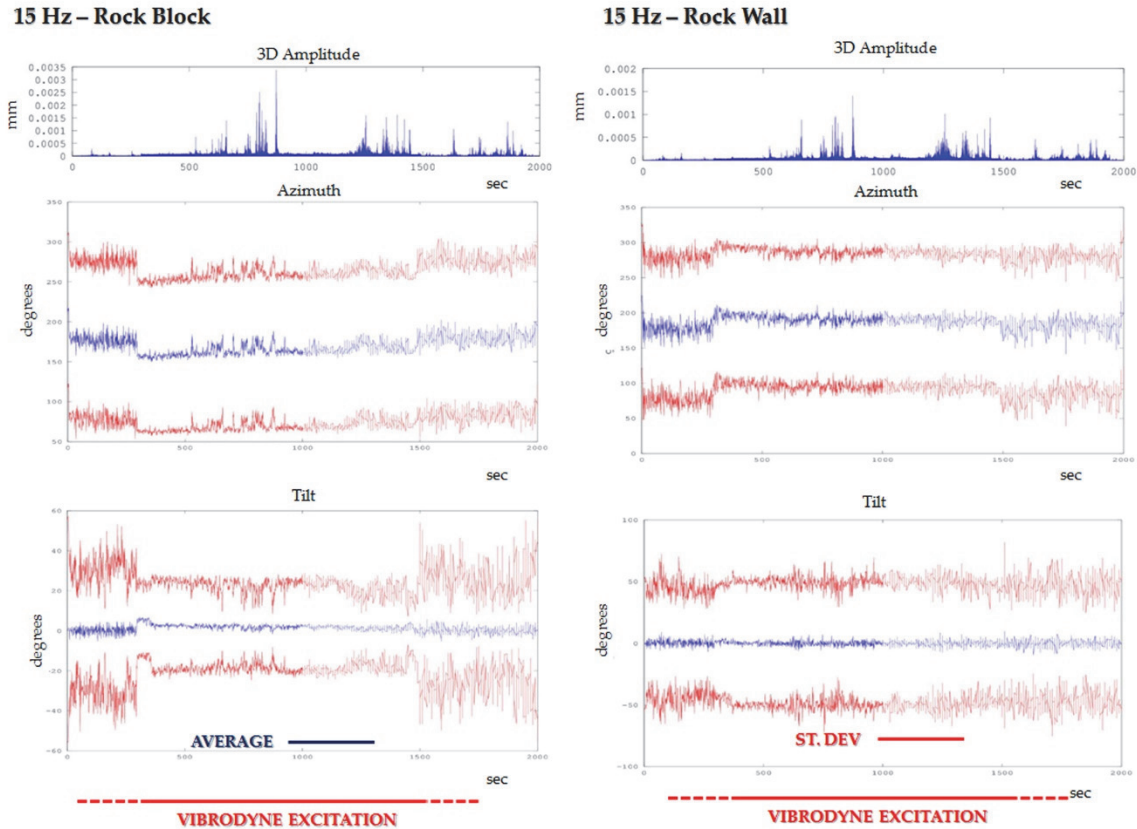


Fig. 58: Azimuth (middle graph) and Tilt (bottom graph) values of the rock block and of the rock wall, calculated during 15 Hz excitation. No significant polarization values were observed. Modified from (Curi, 2017).

During the dynamic experiments of the Phase B, the rock wall and the rock block was also monitored by using a terrestrial Interferometer that worked in RAR and SAR mode. The data acquired in RAR mode, allows a preliminary estimate of the displacements recorded on the rock wall at several distance from radar and during each Vibrodyne excitation. Only data acquired during the shaking tests were considered for the displacement analysis and that falls within the pixel corresponding at distance between the radar and the monitored rock block (about 18 m). Appropriate displacements, in the order of $1 \cdot 10^{-5}$ m, were recorded only during 15 Hz excitation.

Otherwise, during other stress frequencies, no displacements have been detected using interferometric technique. The same results were also confirmed by the FFT amplitude analysis performed on interferometric data, recording during each excitation frequencies. Only on the 15 Hz spectrum is possible to see a slight amplitude peak (Fig. 59).

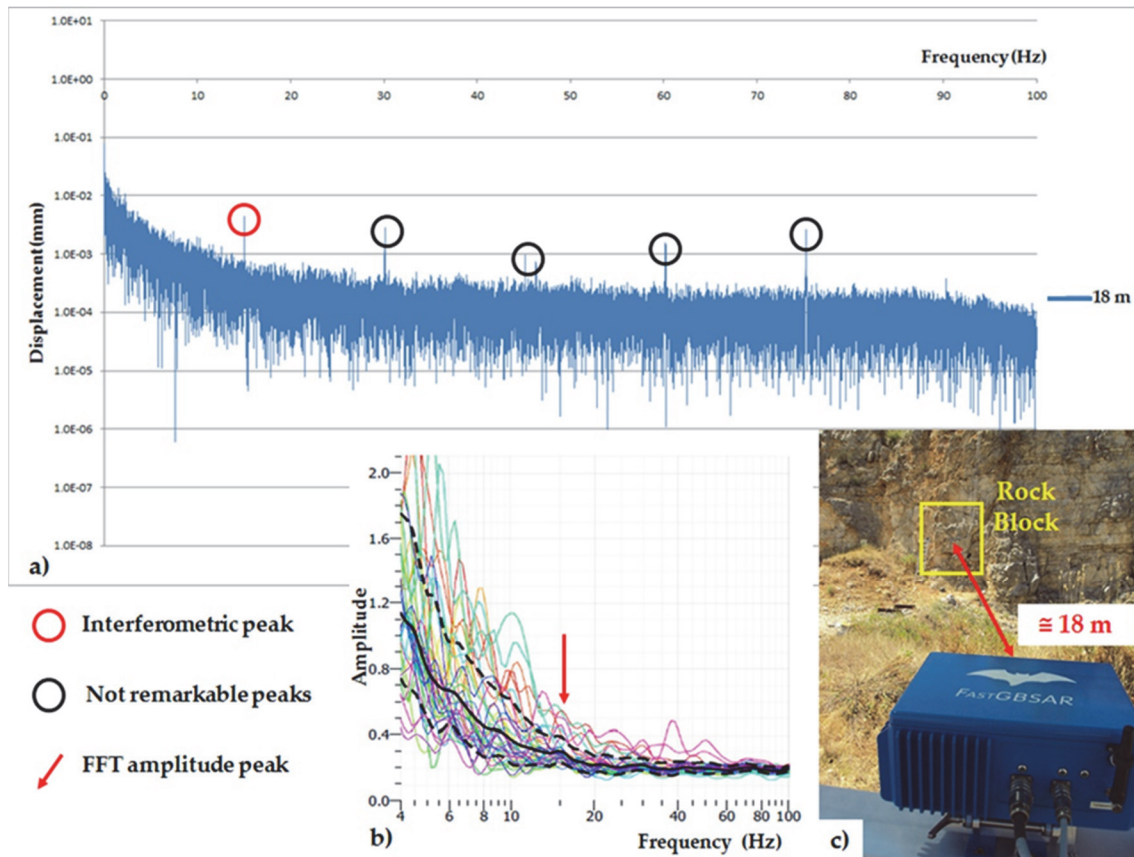


Fig. 59: Displacement peak from interferometric record, during 15 Hz shaking test (a). Peaks in black are multiples of the main peak at 15 Hz. The analysis was performed from pixel detected at 18 m from radar: the same distance between the rock block and the interferometer (c). The peak at 15 Hz is also slight visible on the FFT spectrum, carried out on radar time-histories (b).

The analysis of the data collected during the activities of the Phase B in Acuto test-site, and carried out following the OBA approach, has allowed to understand the behaviour of the monitored rock block when it is exposed to induced vibrations. More in particular, the following was determined:

- a) the resonance of the rock block at 20 Hz input signal. No resonance effects were seen for other induced frequency (5 Hz, 10 Hz, 15 Hz, 25 Hz);
- b) the polarization of vibrational motion during the maximum of the Vibrodyne excitation, consistent with the direction of maximum anisotropy of the physical system (air-rock interface);
- c) the complete reversibility of the induced displacement, due to inelastic behaviour of the rock mass.

Therefore, the OBA approach applied to data from Phase B has allowed to recognize the induced vibrations as possible *trigger factors* (*sensu* Gunzburger et al., 2005) for rockfalls from very fractured rock wall and rock slope. In fact, due to the activation of an external dynamic input, the rock block assumed a different and amplified mobility compared to the rock wall behind and respect to the presence and the kind (in terms of his duration and frequency) of external vibrational source. The dynamic input assumes an important role in conditioning the kinetic behaviour of the rock block, being able to facilitate its failure conditions and the consecutive detachment by the rock wall. Possible sources of induced vibrations can be the rail traffic at the foot slope, in a configuration similar to the one in the Acuto test site with the railway target.

As it regards the second site-test, the gravitational deformation process that affect the Peschiera Spring slope and related drainage plant, data from multi-parametric monitoring system installed inside the drainage tunnels were analyzed following, in a first attempt, an OBA approach in order to point out objective cause-to-effect relation among several monitored parameters. As presented in Chapter 4.2, the entire slope of the Peschiera Spring is mainly involved in a multi-stage mass rock creep process (Chigira, 1992), acting on a time-scale of several tens of years, that continuously evolves from rock mass spreading (Hutchinson, 1988) to rock block mass deformation (Martino et al., 2004). Single portions of the slope, released and bounded by trenches or

inherited tectonic lineaments, are also involved in deformation processes due to internal hydrodynamic forcing acting on seasonal time-scales (Fiorucci et al., 2016; Maffei et al., 2005). Finally, a deformative response of small portions of the slope (i.e. down to single rock block-scales) is present, due to external forcing related to regional earthquakes or teleseismic events (Lenti et al., 2015). Compared to Acuto test-site, the multi-parametric monitoring system installed at Peschiera Spring slope test-site allows to investigate natural processes that act on larger space- and time-scales (up to entire-slope scale evolving on a long period).

The multi-parametric monitoring system installed inside the drainage plant, continuously provide, since 2007, data from stress-strain devices, seismic and micro-seismic devices and from hydrological sensors. The existence of a long-term and multi-device dataset, allows to search cause-to-effect relations between destabilizing factors and related strains over long time, considering different time-scale at various space. The focus is mainly on data from accelerometric networks and from SNS array (micro-accelerometric innovative network) which has greatly increased system resolution, allowing to detect more microseismic events with weak energy and magnitude. These events are the tangible expression of the ongoing deformation of the slope. The data of accelerometric network are available until November 2015; the discharge values are available until September 2015; the data of permanent SNS array are available starting from February 2015; the data of stress-strain devices are available throughout the completely monitoring period, but several device was out of order.

Until November 2015, the accelerometric network recorded 2311 events, consisting of 1031 earthquakes (originate outside the slope) and 1280 microseismic events (originate inside the slope) due to 262 failures and 1018 collapses and related to the active deformation processes (Fig. 60).

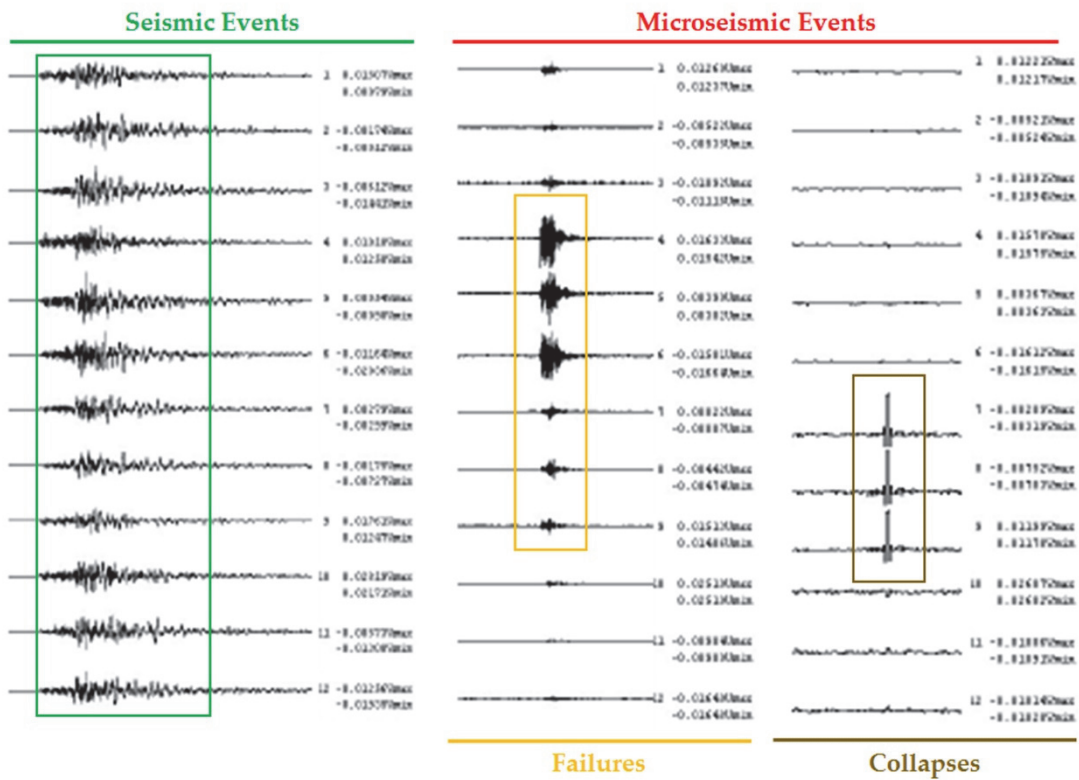


Fig. 60: Examples of events recorded from accelerometric network during monitoring period and automatic recognize using the procedure described in 4.2.2.

Since January 2014, a relevant increase in the time frequency of microseismic events (attributable to hypogeous collapses) was observed respect to the previous 7 years. In fact, from January 2014 to September 2015 the accelerometric network recorded 689 collapses, grouped in 46 crises. These crises are characterized by the rapid succession of events that follow one another at intervals varying between few minutes and 1.5 hours. The PGA and the AI of the vertical component of the signals (PGA_v and AI_v respectively) are generally higher than the ones related to the horizontal components. The recorded events are characterized by an average PGA_v of 10^{-3} g, with maximum of 10^{-2} g, and an average AI_v of 10^{-8} g² s, ranging a maximum of 10^{-6} g² s.

The recurrence of collapses could be influenced by variation of groundwater level within the slope. A relevant change of the cumulative trend of recorded collapses occurs indeed in correspondence of the maximum daily total discharge that affects the

stress field within the karstified rock mass, recorded during the completely monitoring period (2008–2015). A similar behaviour is being observed in the last recorded data, since July 2015 (Fig. 61).

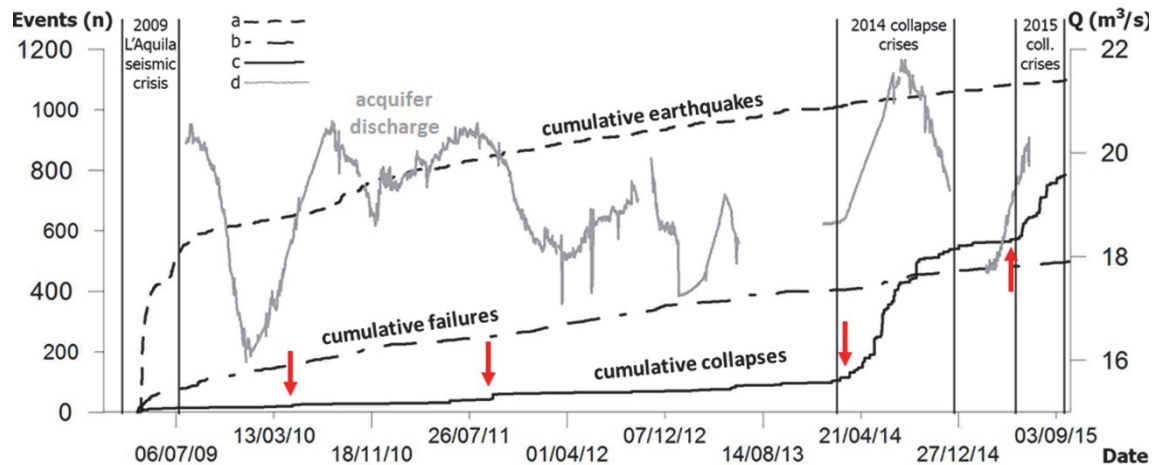


Fig. 61: Cumulative numbers of (a) earthquakes, (b) failures and (c) collapses recorded by the accelerometric network; (d) the daily total discharge (data are not available where line is interrupted) is also shown. The red arrows shows incremental steps of recorded collapses in correspondence of discharge variation (modified from Fiorucci et al., 2016).

The physical parameters of the collapses also could be influenced by variation of groundwater level within the slope. A relevant increase of the Arias Intensity value of the recorded collapses crises occurs indeed during the period in which the groundwater level, and thus the totally aquifer discharge, increase or decrease.

No objective cause-to-effect relation was found between variation of groundwater level within the slope and data from stress-strain devices, as well as between occurrence of microseismic events that are originated within the slope and displacement values. In fact, no relevant change of the strain trend occurs indeed in correspondence of the maximum daily total discharge or during collapses crises (Fig. 62).

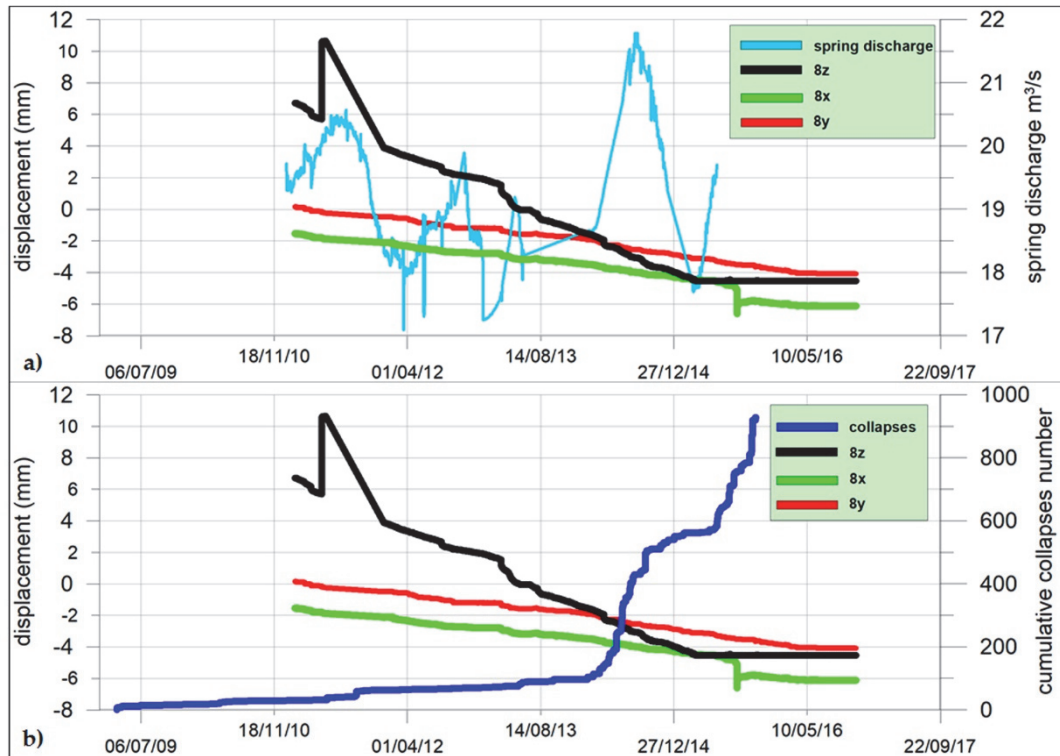


Fig. 62: Total daily discharge in relation to triaxle extensometer record of ongoing deformation processes (a) and cumulative numbers of collapses in relation to same displacement record (b): no relation was detected.

Starting from 2015, the multi-parametric monitoring installed within the slope was implemented with a permanent SNS array. The SNS nanoseismic array results to be a reliable tool for improving the detection of underground instabilities as it is contributing to identify sequences of very low-energy microseismic events that cannot be recorded by the traditional accelerometric network and that could be precursory signals of larger scale deformational events. The SNS array also is able to record regional earthquakes, local earthquakes and teleseismic events (originated outside the slope) and slope microseismic events (Fig. 63).

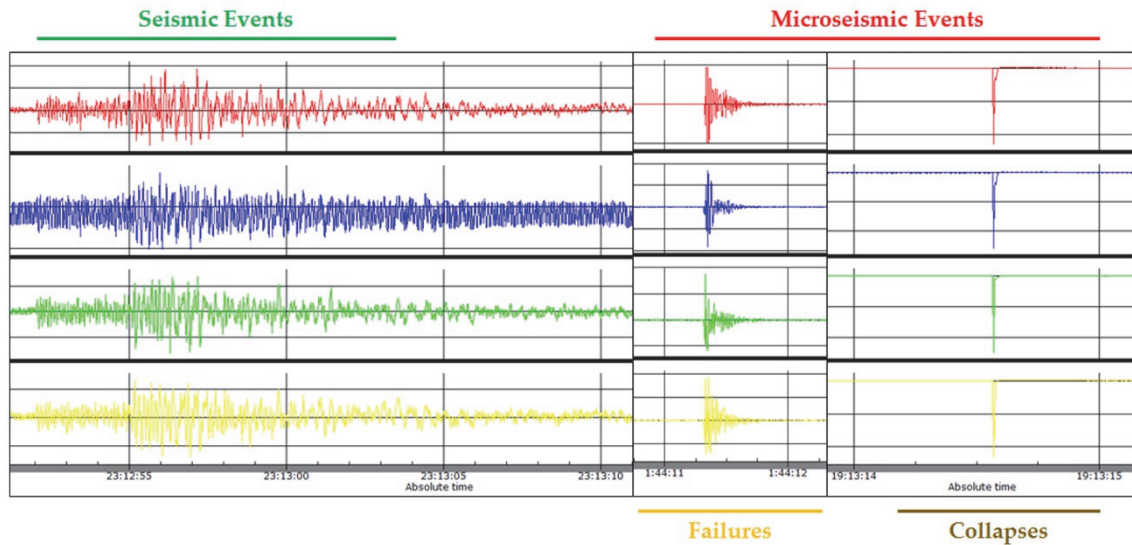


Fig. 63: Examples of seismic and microseismic events recorded from SNS array during monitoring period.

The total number of collapses recorded by the permanent SNS during the 14 collapse crises observed in 2015 is up to 8 times higher respect to the number of collapses recorded by the accelerometric network in the same period. Only during 2015 the accelerometric network and the SNS array worked coupled, with SNS array set in continuous mode.

Also in 2015, the time distribution of recorded collapses versus the daily total discharge measured at the Peschiera Springs highlights that the main collapse crises occur when a highest rate of discharge variation is observed, i.e. in correspondence with the yearly raising up and drowning down phases. During 2015, these phases, respectively, occurred in June–July 2015, when the SNS array recorded 482 collapses and the accelerometric network 118 ones, and in September 2015, when the SNS array recorded 168 collapses and the accelerometric network 26 ones (Fig. 64).

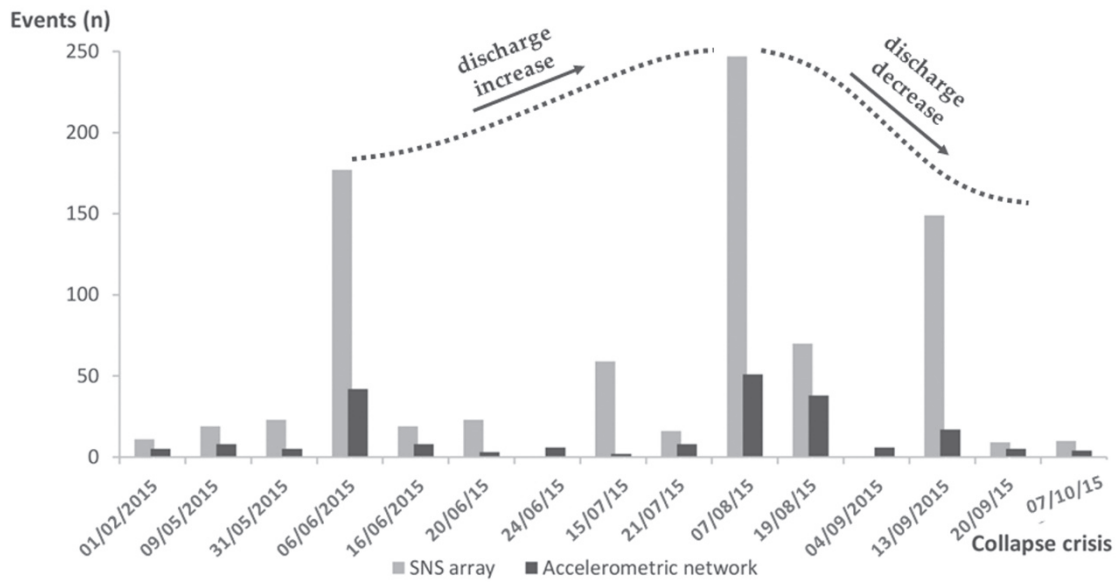


Fig. 64: Frequency histogram showing the collapses recorded by the accelerometric network and the permanent SNS array during the 14 collapse crises occurred in 2015. The discharge trend is also shown (modified from Fiorucci et al., 2016).

The SNS enlarged the sensibility field of the monitoring system down to 10^{-5} m s^{-2} for the PGA_h (average values between the two horizontal components) and to $10^{-11} \text{ m s}^{-1}$ for the AI_h (average values between the two horizontal components). The collected data confirm that the accelerometric network is more reliable for detecting higher-energy events, whereas the SNS array shows a good response to detect also events characterized by low- to very low-energy (Fig. 65). These could be precursory signals and expression of gravitational slope deformation, being so very useful for the infrastructure management.

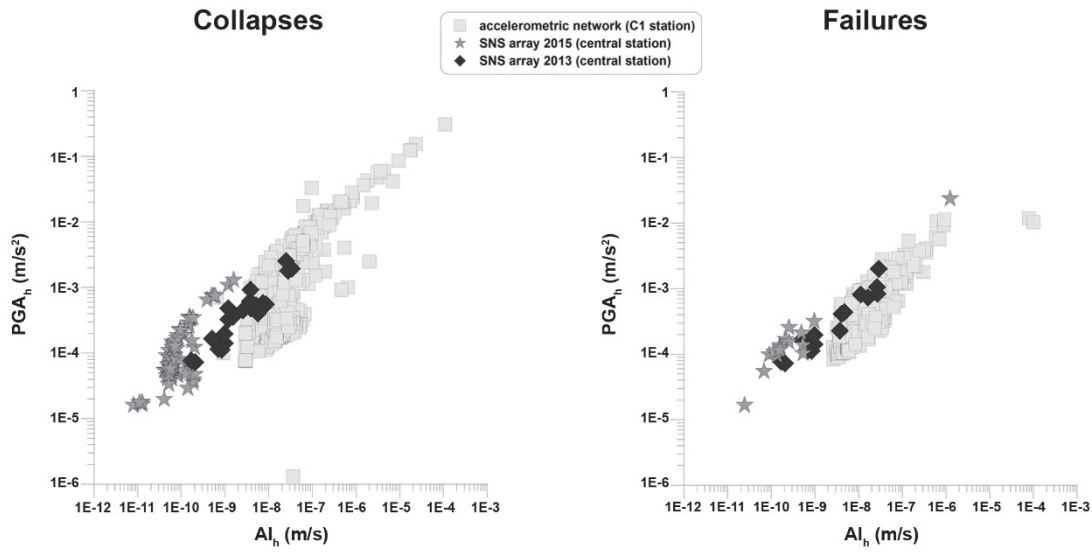


Fig. 65: PGA_h versus AI_h for the seismic events recorded by the accelerometric network, the 2013 temporary SNS array (see 4.2.2) and the permanent SNS array. The localization of the C1 station and of SNS array are shows in Fig. 27; (from Fiorucci et al., 2016).

During 2016 the SNS permanent array was working and recorded data in trigger mode, while the accelerometric network was out of order. Until October 2016, 149 collapses grouped into 18 crises were recorded. The cause-to-effect relation between the fluctuation of total daily discharge and the occurrence of collapses crises is confirmed. In fact, 8 collapses crises occurred in June and July 2016 during the raising up phases, while 5 collapses crises occurred in September and October 2016 during the drowning down phases. The discharge data of 2016 are unavailable, but a trend similar to that of previous years was considered. The recorded events are characterized by an average PGA_v of 10^{-4} g, with maximum of 10^{-3} g, and an average AI_v of 10^{-9} g² s, ranging from a maximum of 10^{-7} g² s to a minimum of 10^{-10} g² s. On average, the 2014 collapses are placed in the low field of PGA_v vs AI_v , thus confirming the higher resolution of SNS array than the accelerometric network (Fig. 66).

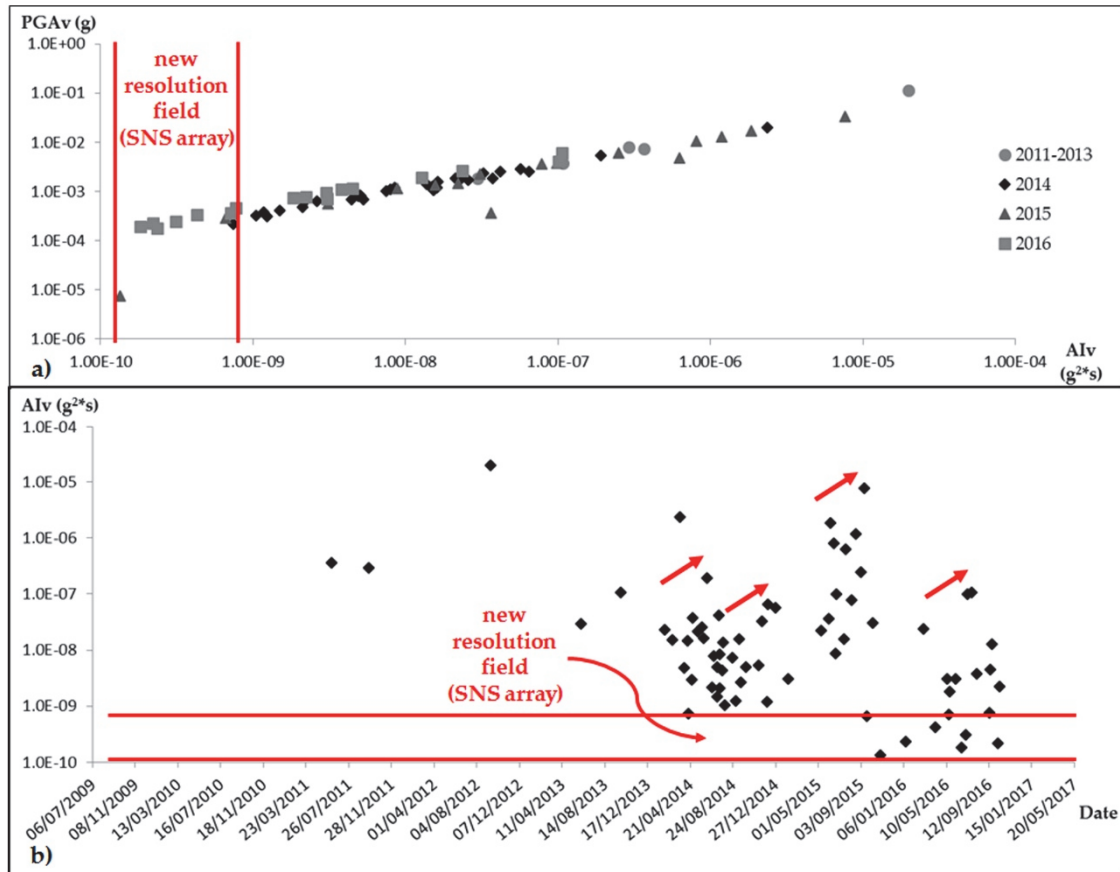


Fig. 66: a) PGAV vs AIV obtained for the most energetic collapse recorded by the accelerometric network (2011-2015) and by the SNS array (2016) for each collapse crisis: the higher resolution of SNS array compared to accelerometric network is shown; b) AIV vs time of the most energetic collapses for each crisis: red arrows indicate the increase of AIV values and of frequency of collapse crises in correspondence of discharge fluctuation (increase or decrease).

Analysing the multi-parametric monitoring system data, has been seen that earthquake induced phenomena inside the slope can be always excluded, given the absence of earthquake sequences before or during the collapse crises. This confirms that the gravitational dynamic generates deformational and paroxysmal events, which can occur independently of external factors or actions. The microseismic events are the expression of the ongoing gravitational deformation process and are located in correspondence of the main geomorphological features surveyed on the slope (see 4.2.1). Especially the collapses crises are influenced by variation of the groundwater level in recharge or in discharge phases and affecting a saturated mass volume where

tensile stresses can be enucleated due to the interaction between effective stresses and ground water flow (Fig. 67). The data from geotechnical devices do not show an objective relation with other parameters, but a steady deformation rate of 1 mm/year are highlighted.

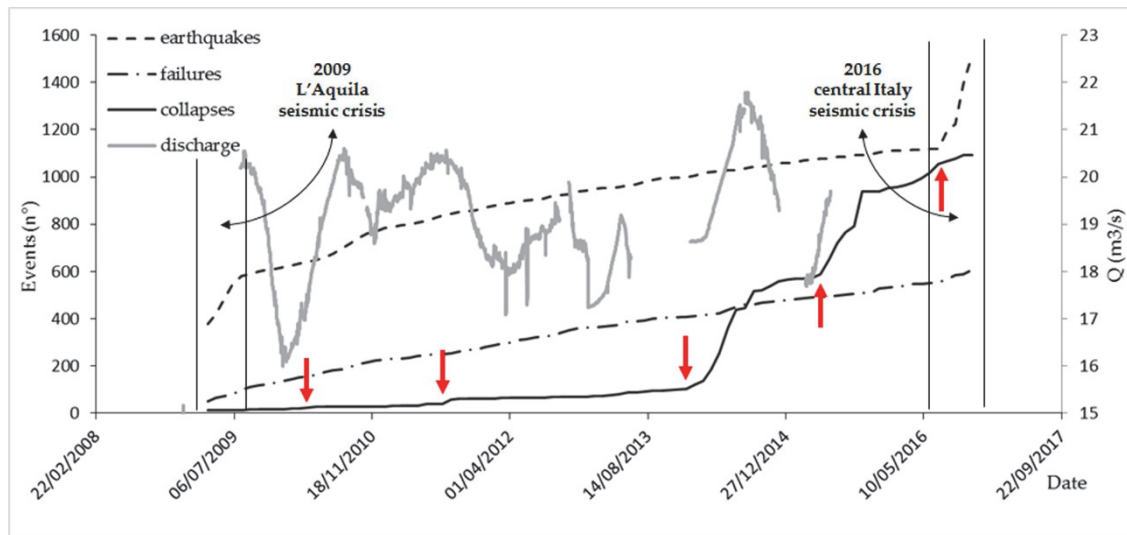


Fig. 67: Seismic and microseismic events recorded by both accelerometric and nanoseismometric networks, until 2016. It is worth noting that the two seismic crises (2009 and 2016) do not change the trend of failures and collapses. The collapses trend it is rather influenced by groundwater level variation.

In the last years, the multi-parametric monitoring system have allowed to recognize the microseismic events, related to gravitational process that affect the slope. Thanks to data analysis following OBA approach, the times when deformation was incipient were identified. Based on these results, a Control Index for infrastructure management and safety was provided and it is summarized in the next Chapter.

The OBA data analysis approach, applied to Peschiera Spring slope gravitational deformation processes, has allowed trying to understand the behaviour of the monitored entire slope and of deformational process that affect it, defining some cause-to-effect relations. More in particular, the following was determined:

- a) recognize and detect several kinds of seismic and microseismic events, that are the expression of the ongoing deformational processes;

- b) define the influence of groundwater level variation, increase during the spring season and decrease during the autumn season, on the occurrence of the collapse crises;
- c) understand the independence between groundwater level variation and strain effects monitored inside the drainage tunnels, as well as between collapse crises or failure events and displacement records;
- d) the implementation of accelerometric network with a SNS array, has allowed to increase the resolution of monitoring system, regarding the ability to detect more weak microseismic event. The OBA analysis on these recorded data allow to detect precursors signals of the strongest events.

More in particular, the cause-to-effect relations analyzed applying the OBA approach has allowed to strengthened a multi-level deformation model (already known and present in the literature) that involve entire rock mass slope and acting on three different time-scale:

- a) a short-time processes due to external transient actions, like as regional earthquakes or teleseism;
- b) a middle-time processes due to seasonal dynamic of the aquifer and related to groundwater variation phases;
- c) a long-time processes due to time-dependent creep phenomena.

5.2. SBA approach analysis

A statistic-based analysis, following SBA approach, was performed on data from Acuto test-site multi-parametric monitoring system. Cross-correlation function was defined between time series of the rate of air temperature and rock temperature. In fact, the exposure of the sun simultaneously acts on both. The analyses carried out on these series, always show a very high cross-correlation values (i.e. measured by the Cross-Correlation Function - CCF). The rate series of the air temperature always anticipates the rate series of rock temperatures of about 10 minutes (Fig. 68). The cross-

correlation function was carried out also comparing the rate series of rock temperature and the rates series of cumulative rainfall and wind speed, in order to verify if these two destabilizing factors can influence the temperature of rock wall, thus changing the thermal deformation response in heating or cooling phases of daily or seasonal thermal cycles. The results of statistical analysis show a slight influence of rainfalls on the rock temperature, returning a very low CCF values (Fig. 69). No statistically cross-correlation was found between rate series of wind speed and rate series of rock temperature (Fig. 70).

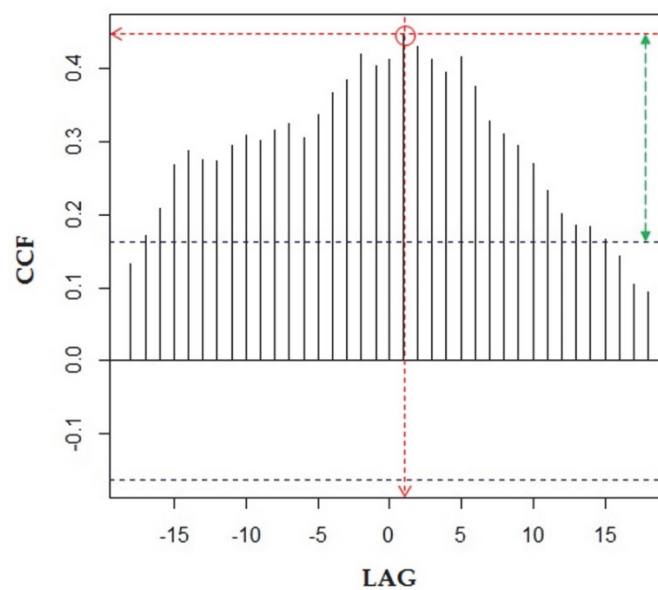


Fig. 68: Correlogram indicating an example of cross-correlation between rock temperature (α) and air temperature (β) at Acuto. The air temperature always anticipate the rock temperature. The green arrow indicates the statistical significance of the result.

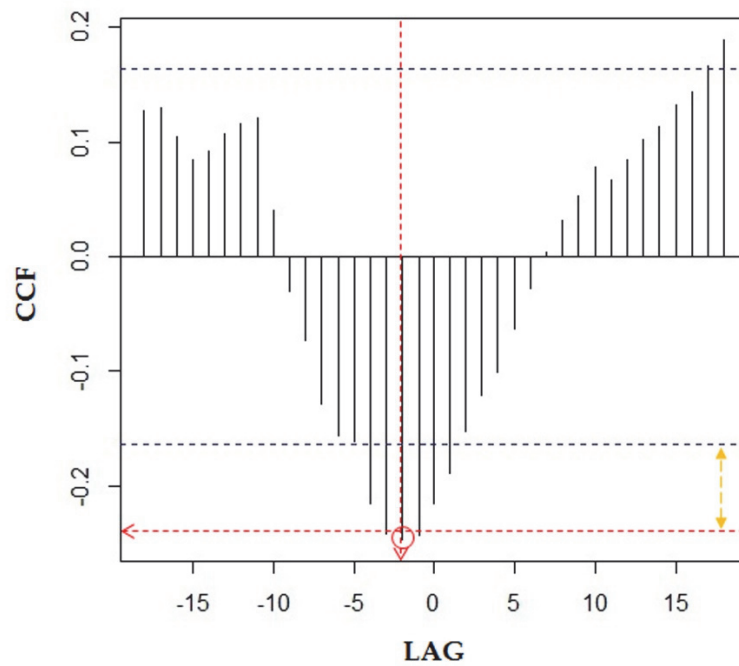


Fig. 69: Correlogram indicating an example of cross-correlation between rainfall (α) and rock temperature (β) at Acuto. The rainfall anticipate the rock temperature but with a very low CCF value. The yellow arrow indicates the short statistical significance of the result.

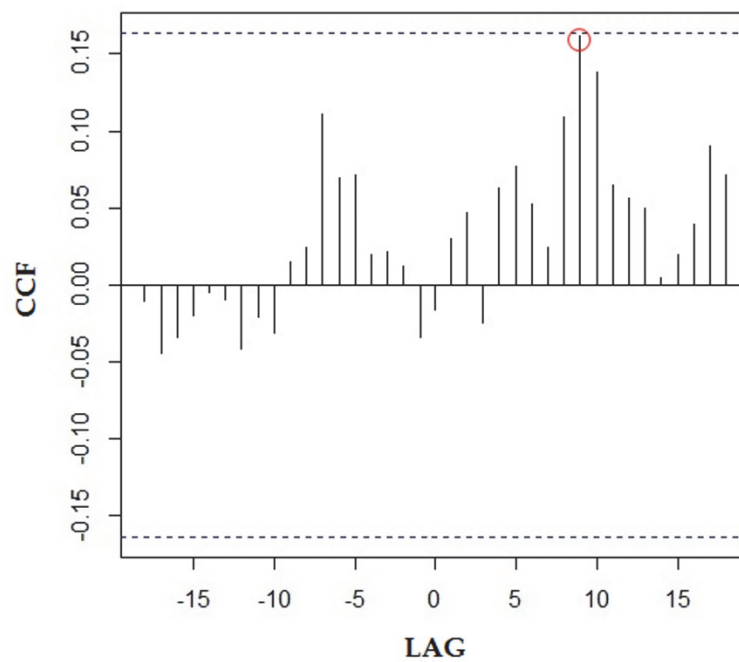


Fig. 70: Correlogram indicating an example of cross-correlation between wind speed (α) and rock temperature (β) at Acuto. No peak of cross correlation is evident on the graph and the results remain below the statistical significance threshold.

Statistical analysis were performed on the whole monitoring period during which several meteorological conditions (i.e. strong or low rock temperature, intense or absence rainfalls, strong wind speed) were detected, representing potential destabilizing actions for the stability of monitored rock block. Following the SBA, cross-correlations were carried out among rate series of each considered forcing action, assumed as *preparatory factors*, and rate series of joints or micro-fractures strain. The obtained results show that rainfall (Fig. 71) and wind speed (Fig. 72) are always poorly or very poorly cross-correlated with the rock mass strain. On the contrary, the rock temperature reveals a very good cross correlation with the rock mass strain, i.e. demonstrating a significant influence on the rock mass deformation. In this case, no significant lag between thermal action and recorded effect was observed. This means that the high rock temperature can be regarded as main destabilizing action to rock block stability, which can cause a response of the jointed rock-mass in a short- to very-short (into 10-minutes) time window (Fig. 73).

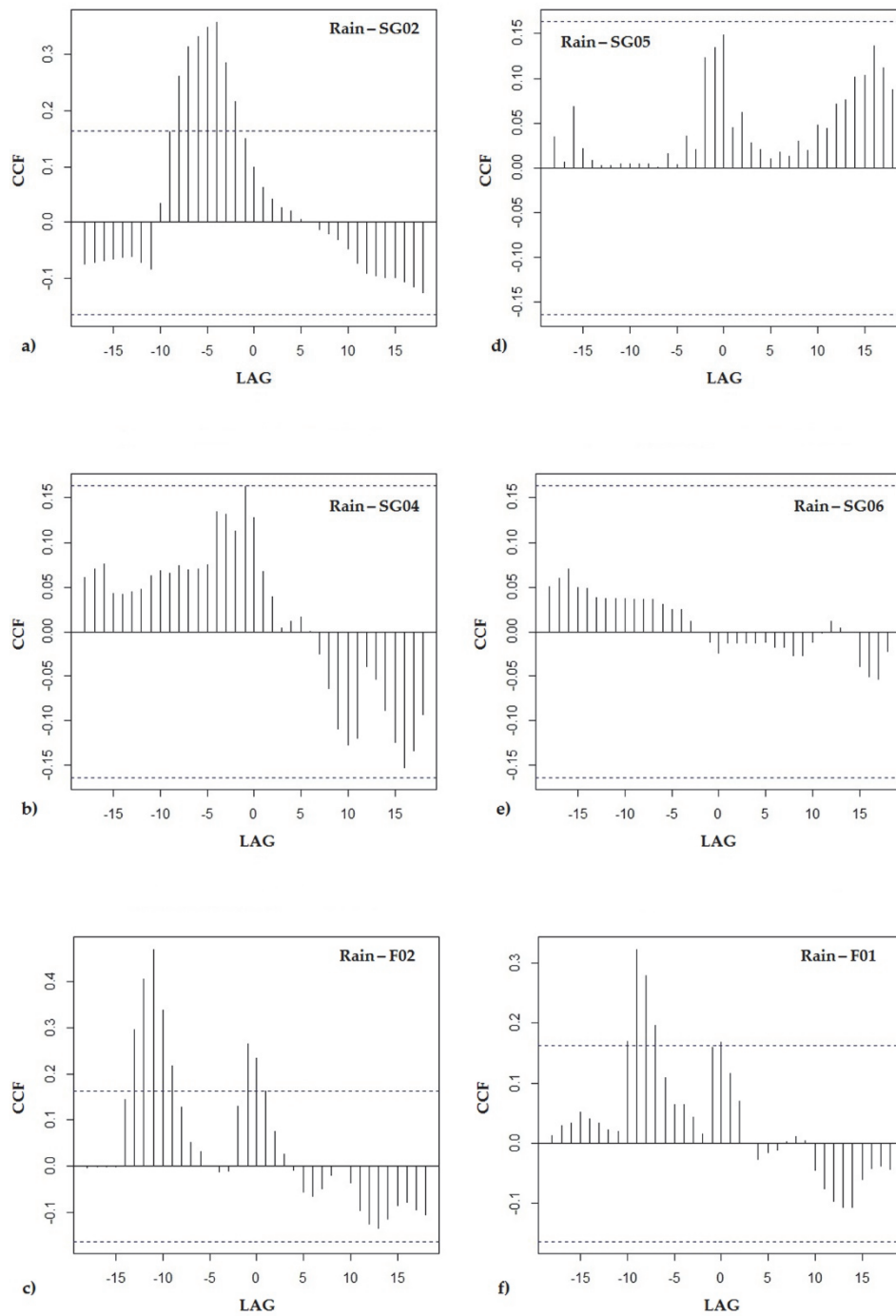


Fig. 71: Correlograms indicating examples of cross-correlation between rainfall (α) and rate series of strain sensors (β) for devices installed on front side of rock block (a-b-c) and for devices installed on backside of rock block (d-e-f). A peak of CCF value is presented only on correlograms of extensometers, so attesting a general poorly cross-correlation among rainfall and strain rate of the monitored rock block.

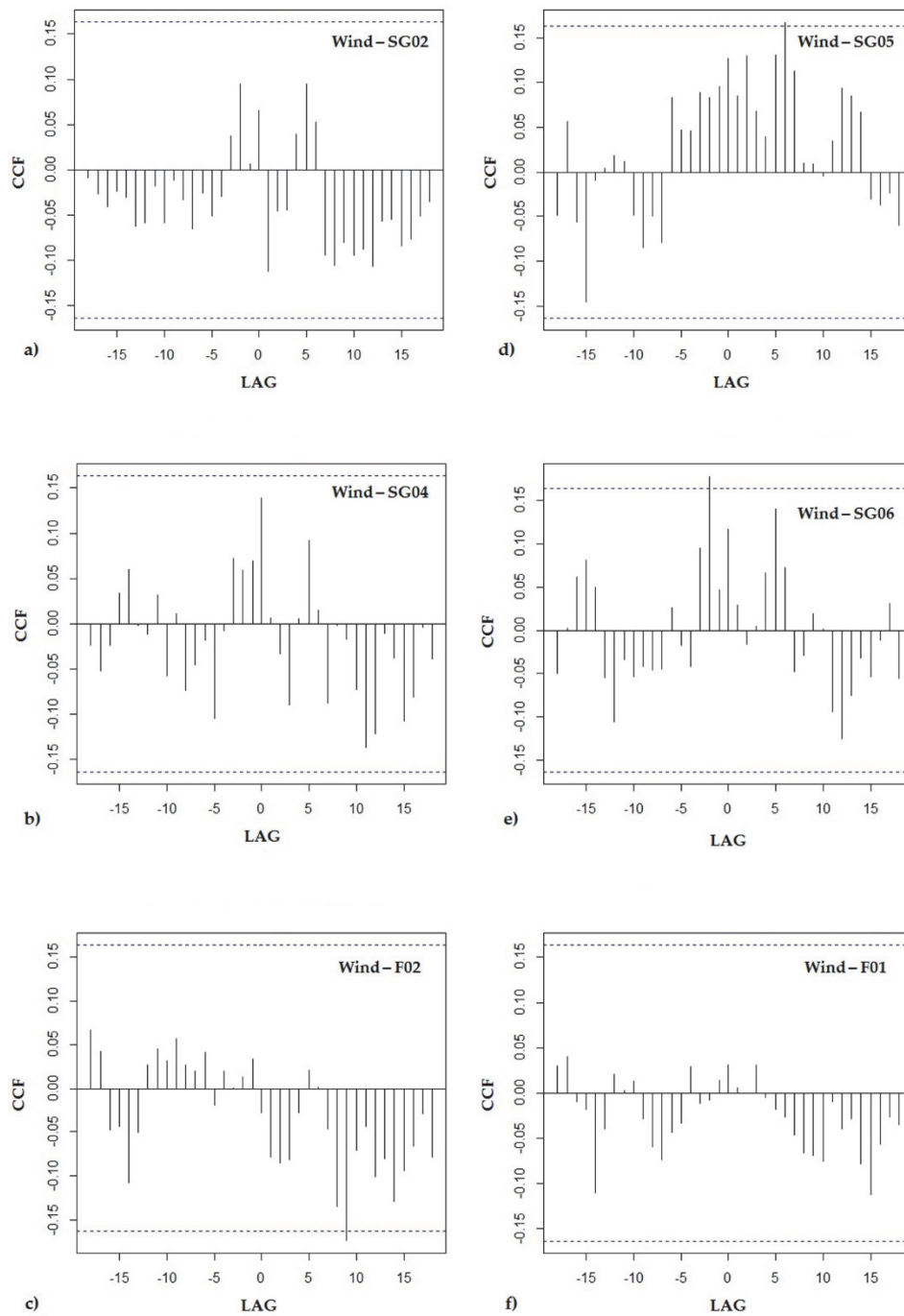


Fig. 72: Correlograms indicating examples of cross-correlation between rainfall (α) and rate series of strain sensors (β) for devices installed on front side of rock block (a-b-c) and for devices installed on backside of rock block (d-e-f). For all sensors considered, the two rate series are always non-cross-correlated in all time period.

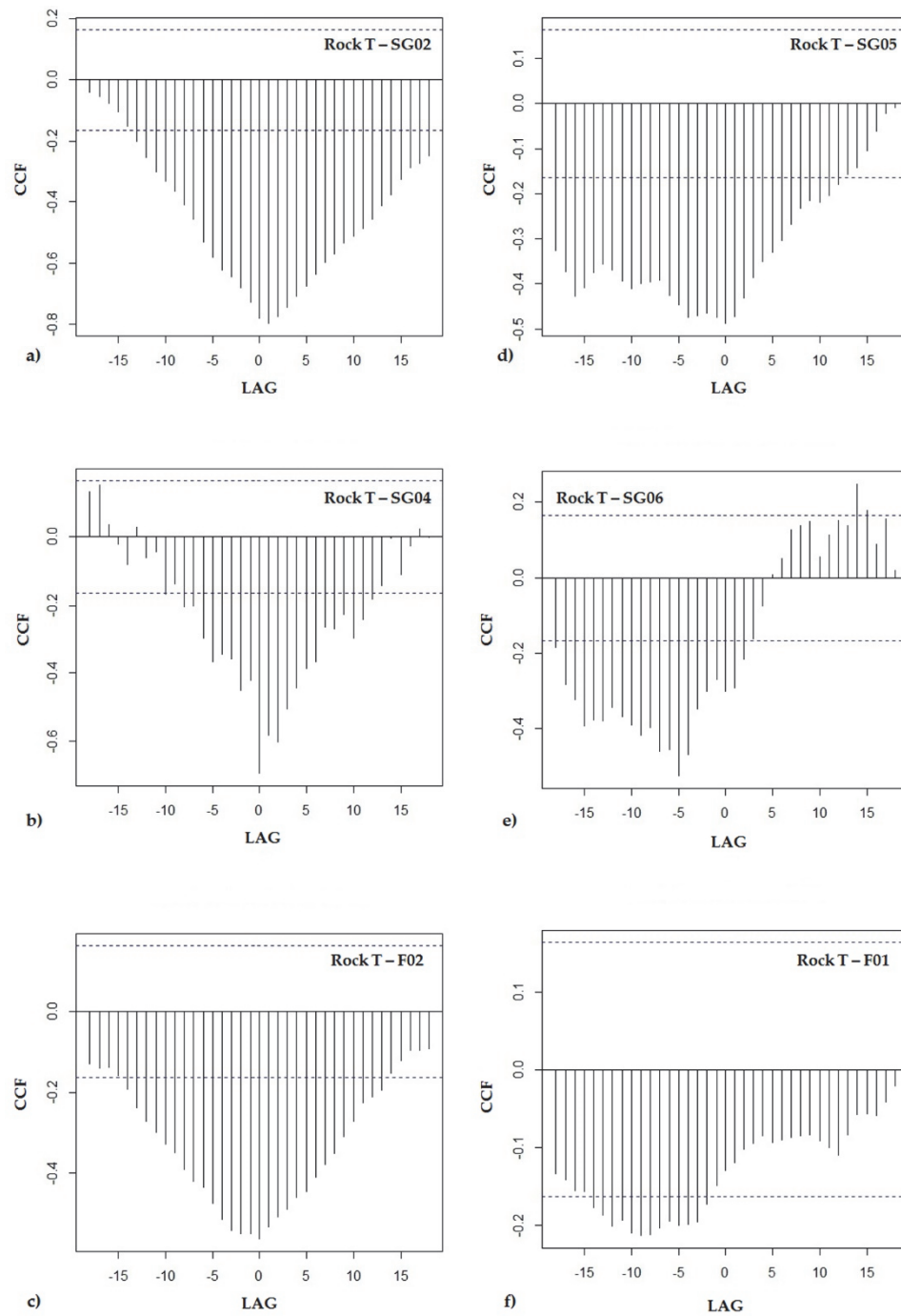


Fig. 73: Correlograms indicating examples of cross-correlation between rock temperature (α) and rate series of strain sensors (β) for devices installed on front side of rock block (a-b-c) and for devices installed on backside of rock block (d-e-f). For all sensors considered, the two rate series are always cross-correlated with an high CCF and a low LAG.

The obtained results reveal that the temperature is the factor that most influences the deformative response of the rock wall and, in particular, of the monitored rock block. In fact, all strain devices return rate series that are always cross-correlated with rate series of rock temperature. The CCF value is always high and above the threshold of statistical significance. In particular, this value varies in a range from -0.3 in winter season, when the thermal input on rock mass is low, to -0.8 in summer season, when the thermal input on rock mass is higher. The strain gauges show a CCF value always higher than that of the extensometers, during all seasons, because are characterized by a higher sensitivity and resolution allowing them to follow the micrometric deformation. Finally, the effect of the aspect also affect the goodness of cross-correlation function: strain sensors exposed for more time at sunlight presented higher CCF value and lower LAG value than strain devices exposed for more time at shadow.

The analysis of the data collected during the activities in Acuto test-site, and carried out following the SBA approach, has allowed verifying the statistically significant cross-correlations existing among the various rate series of destabilizing factors and induced deformations. More in particular, the following was determined:

- a) high cross-correlation between air temperature and rock temperature: the first one always influence the second one with a LAG of about 10 minutes and with a very high CCF (cross-correlation function);
- b) very poor cross-correlation between rainfall and rock temperature as well as wind speed and rock temperature, even in the case of particularly intense phenomena: the peak of CCF is below the threshold of statistical significance;
- c) a significant cross-correlation among rate series of rock temperature and rate series of all strain devices (both strain-gauges and extensometers), so indicating as the temperature is the most active force on the deformative response of the rock mass, and in particular of the rock block;
- d) the time LAG in which a rate series influences the others and with what significance (expressed by the cross-correlation coefficient: CCF).

For the Peschiera Spring slope test-site, a seismic noise trend analysis was carried out on continuously micro-seismic record. An automatic procedure for calculating the variation of trend in seismic noise rate has been preliminary experimented in order to point out the correlation between the trend of noise value and the occurrence of microseismic events (failures and collapses crises) that are originated within the slope. These are the expression of ongoing deformational process that affect the slope, as remarked in 5.1.

The main aim of this experiment was to investigate the content of the seismic noise recorded by SNS array, installed inside the drainage plant, in order to determinate if variation of seismic noise rate can be a way to follow to monitor entire slope deformation. This can be alternative strategies for infrastructure management and for provide a correct control index in the definition of alert levels in an early warning system.

At this aim, continuous seismic records were analyzed in time domains. The SNS array has been recorded in continuous mode throughout 2015, with 600 Hz sampling step. This allowed to record seismic noise and collapses crises occurred in the same period. More in particular, the period in which the experiment was carried out starts from 5th February 2015 and ends 3rd August 2015. Over this time, 131 collapses were occurred, grouped in 8 main collapses crises, summarized in Fig. 74. In the same time, also 20 failures have been recorded.

crisis ID	from	to	time lenght (d)	n° collapses	n° collapses/h	Ev max ($g^2 \cdot s$)	PGAv max (g)
CC040	09/05/2015	09/05/2015	1	8	0.33	2.22E-08	1.48E-03
CC041	31/05/2015	31/05/2015	1	5	0.21	3.64E-08	3.60E-04
CC042	06/06/2015	11/06/2015	6	42	0.29	1.85E-06	1.71E-02
CC043	16/06/2015	17/06/2015	2	8	0.17	8.07E-07	1.07E-02
CC044	20/06/2015	20/06/2015	1	3	0.13	8.82E-09	1.17E-03
CC045	24/06/2015	24/06/2015	1	6	0.25	9.85E-08	3.76E-03
CC046	15/07/2015	15/07/2015	1	8	0.33	1.57E-08	1.32E-03
CC047	21/07/2015	25/07/2015	5	51	0.43	6.31E-07	4.75E-03

Fig. 74: Table summarizing the main physical features of the collapses crises occurred in the time period in which seismic noise analysis was carried out.

In order to represent most of the information contained in the seismic noise signal in a compact form, the averaged smoothed periodogram (Jenkins and Watts, 1968) and the base noise level (Vila et al., 2006) were computed for six different frequency bands and in each hour of record. At this aim, an automatic computing procedure was predisposed and a UNIX - Fortran77 – Matlab - SAC (*Seismic Analysis Code*) script was compiled.

In the pre-processing step, the accelerometric files acquired by SNS array with 600 Hz sampling rate and having a time length of two hours each, are input. Each two-hour files are merged to return a 24-hour file, with the right sampling rate. These files are the input files for the processing script. Each file is straightened, in order to eliminate the instrumental drifts, and filtered, using a band pass filter, in several frequency bands. For each filtered file, the average seismic noise level and the seismic base noise level were computed on 20-second time window. This data is further averaged, to obtained values of average seismic noise level and of seismic base noise level computed on 1-hour time window (Fig. 75).

The frequency bands used for this experiment are six: i) one very low (0.1 – 1.5 Hz), ii) one low (1.5 – 5 Hz), iii) one medium (5 – 10 Hz), iv) one medium-high (10 – 50 Hz), v) one high (50 – 100 Hz), vi) one very high (100 – 250 Hz). These frequency bands were chosen pondering the frequencies that the various categories of microseismic events may “enlighten” on the spectrogram and, therefore, changing in relation to occurrence of collapses crises or failures. The characteristic frequencies of the microseismic events were obtained analyzing the data recorded by the SNS array with the supersonogram, i.e. a specific spectrogram with an autoadjustment function of noise variation and a color scale that shows the frequencies with higher energy (Sick et al., 2014). In particular, a collapse enlighten on the upper part of the supersonogram, which indicates that the signal is characterized by a very high frequency content, that cover a band ranging from about 50 Hz up to 190 Hz about. Failures events enlightening the intermediate and lower part of the supersonogram, indicates that

these events are characterized by a frequency content corresponding to an average bandwidth, and cover a specific band ranging from 5 Hz up to 80 Hz about.

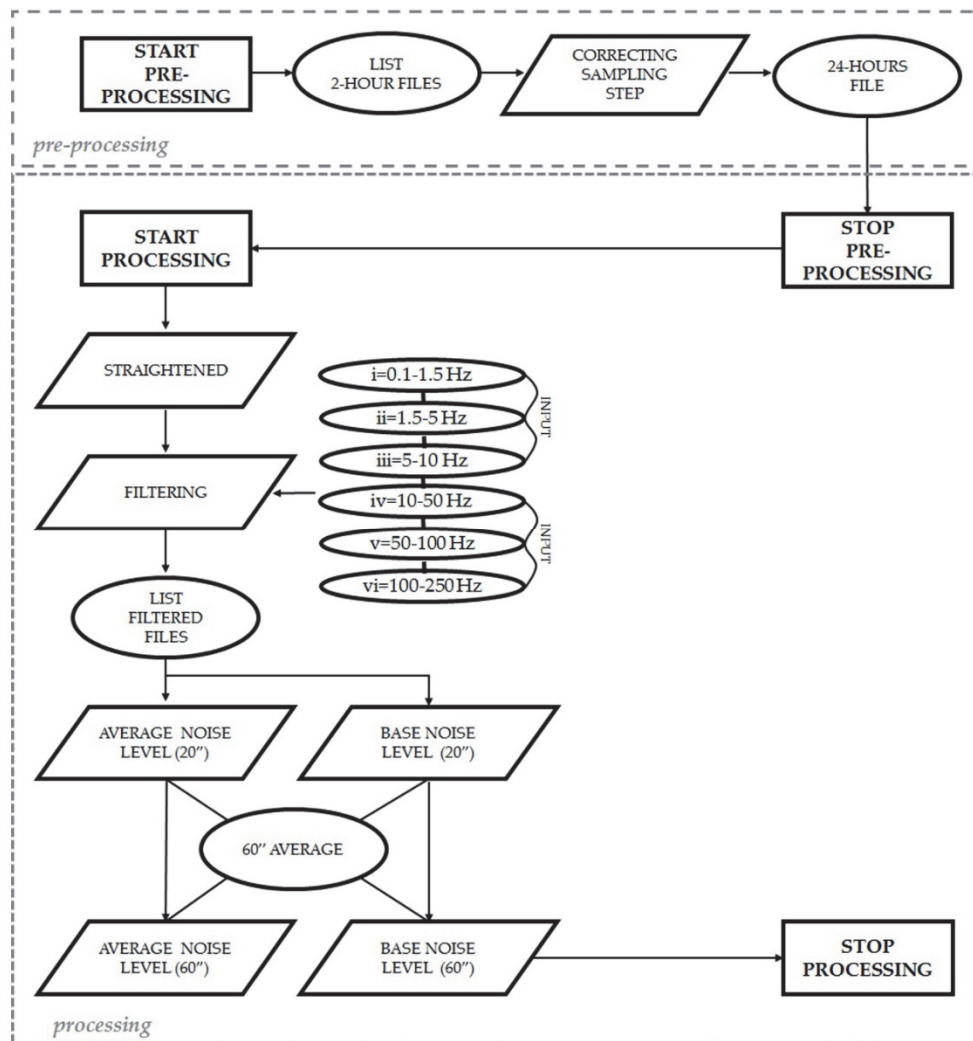


Fig. 75: Flow chart illustrating the tools of the script compiled for seismic noise analysis, starting from SNS array records of Peshiera Spring slope.

The seismic noise analysis was carried out on 13 continuous recording traces, with a few minutes intervals due to manual data download. The lack of data of March and of the end of June is due to out of order of the SNS array for technical problem.

Results computed for SNS central station show a significant reduction of average noise level for the three upper frequency bands (10 – 50 Hz; 50 – 100 Hz; 100 – 250 Hz) in correspondence of the main collapse crises, starting from 6th June 2015 and end to 25th July 2015. These frequency bands are the same characteristics bands energized by

collapse events. The results also show a gradual decrease of the average periodogram amplitude, from 10 – 50 Hz frequency band to 100 – 250 Hz frequency band (Fig. 76). A similar evidence is also in the base level of the seismic noise, computed in the same time interval and for the same frequency bands. The intensity of the values has fallen between 10 – 50 Hz frequency band to 100 – 250 Hz frequency band (Fig. 77).

Results computed for SNS central station at lower frequencies (0.1 – 1.5 Hz; 1.5 – 5 Hz; 5 – 10 Hz) do not show a decrease of average noise level during the main collapse crises. In these lower frequencies, the energy content remains unchanged. The frequency band from 5 Hz to 10 Hz, has a higher amplitude value than the others do two lower frequency band (Fig. 78). Similar trend is also found in seismic base noise level, computed in the same time and for the same frequency bands: during the occurrence of the main collapse crises, the trend of base noise level do not shows variations. The base noise level of the lower frequency remains with a constant linear trend during all monitored period. A very lower frequency band (0.1 – 1.5 Hz) shows a higher amplitude of base noise level than the others ones (Fig. 79).

Correlating the groundwater level with the seismic noise rate, it is possible notice that the rise up of the groundwater level within the karstified slope, from April to June 2015, do not change both average noise level and base noise level values.

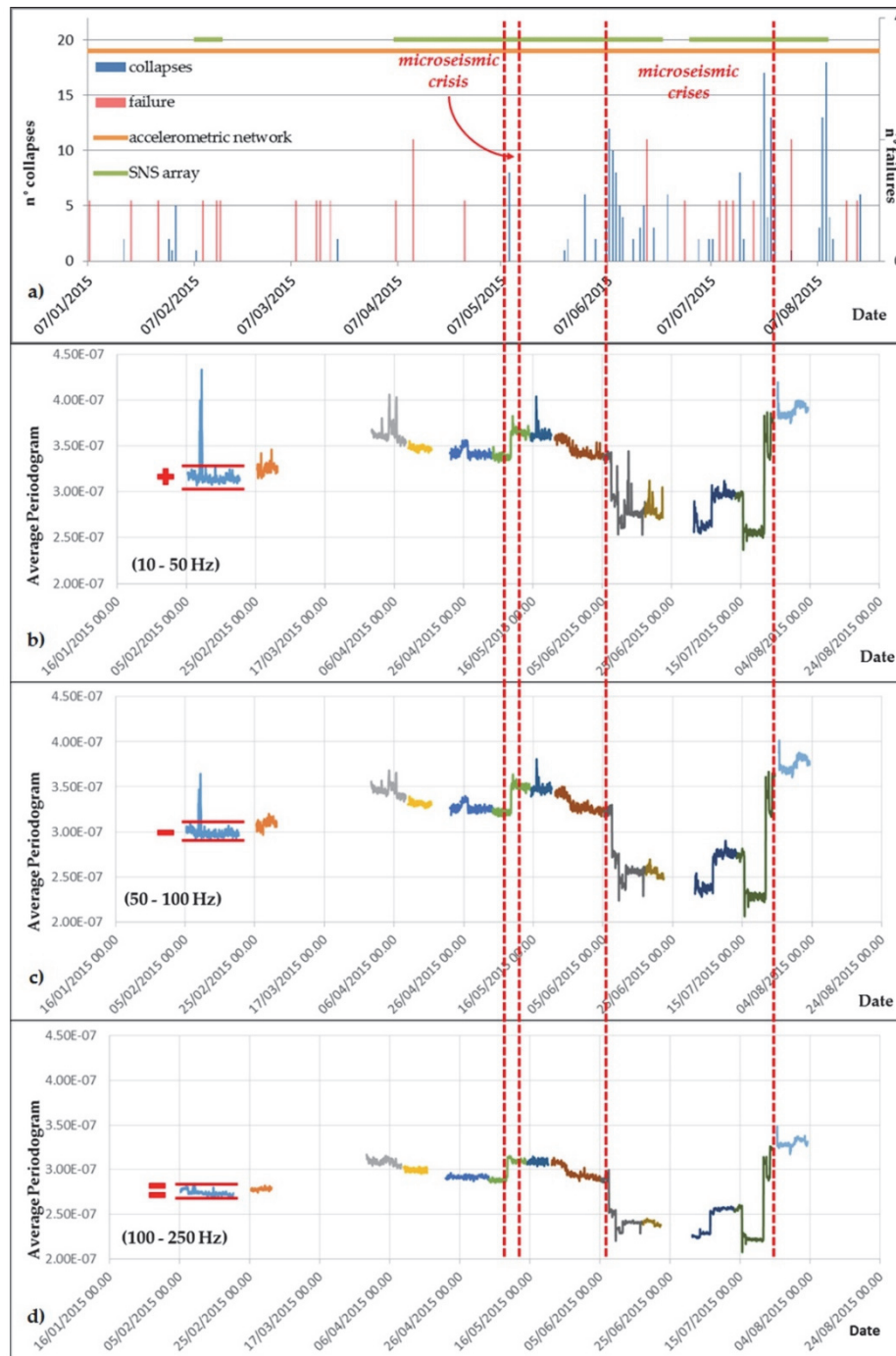


Fig. 76: Average noise level analysis conducted for frequency bands ranging from 10 Hz to 250 Hz. The decrease of average periodogram values, perfect matching with occurrence of collapse crises. Singular collapse crisis can induce variation. The amplitude of the averaged periodogram decrease as frequency increase (red plus and red minus on figure).

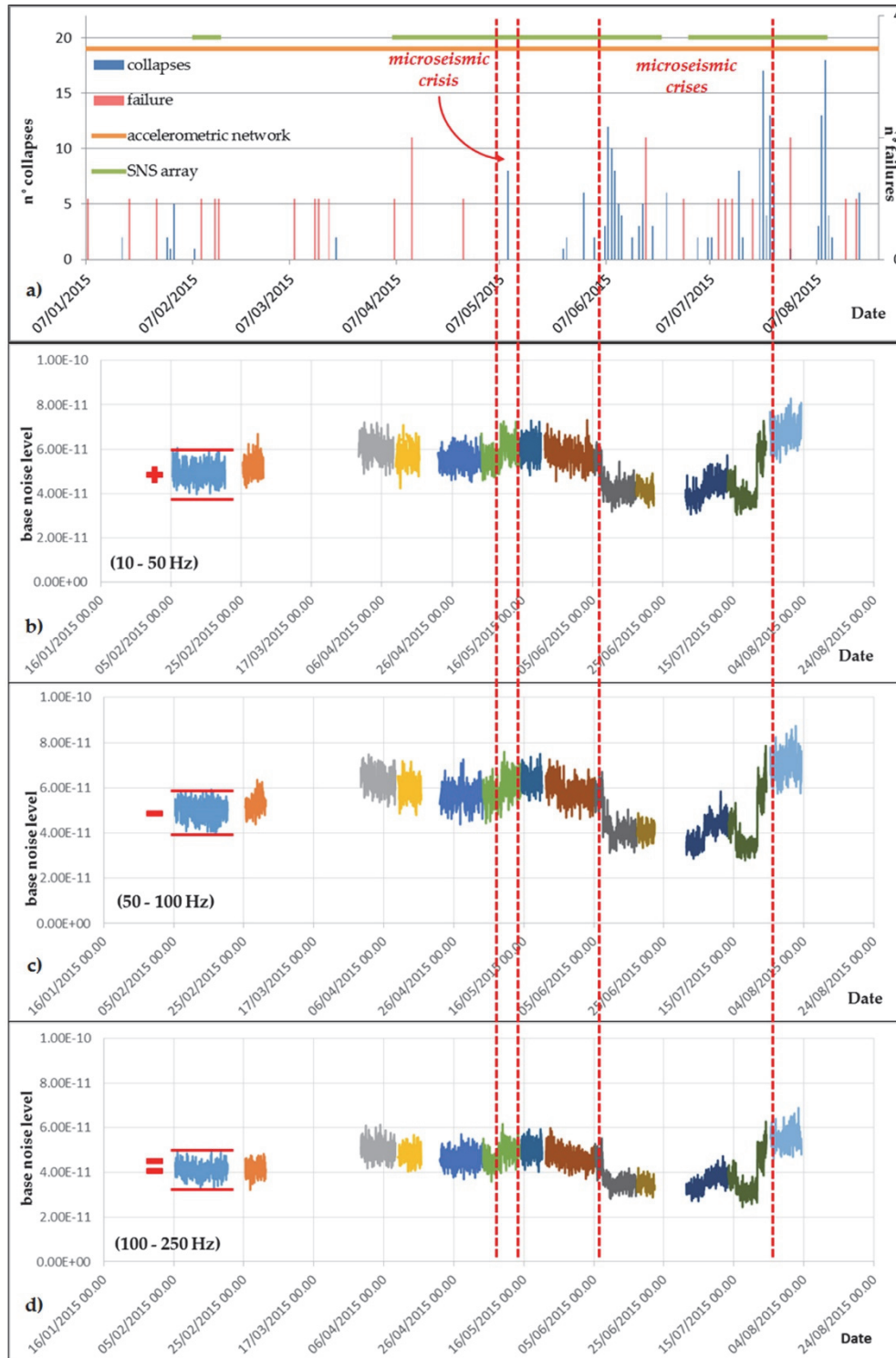


Fig. 77: Base noise level analysis conducted for frequency bands ranging from 10 Hz to 250 Hz. The decrease of base noise level, perfect matching with occurrence of collapse crises. Singular collapse crisis can induce variation. The amplitude of the base noise level decrease as frequency increase (red plus and red minus on figure).



Fig. 78: Average noise level analysis conducted for frequency bands ranging from 0.1 Hz to 10 Hz. Differently from what occurs at higher frequencies, during the collapse crises the average periodogram values remain unchanged. The amplitude of the averaged periodogram increase as frequency increase.

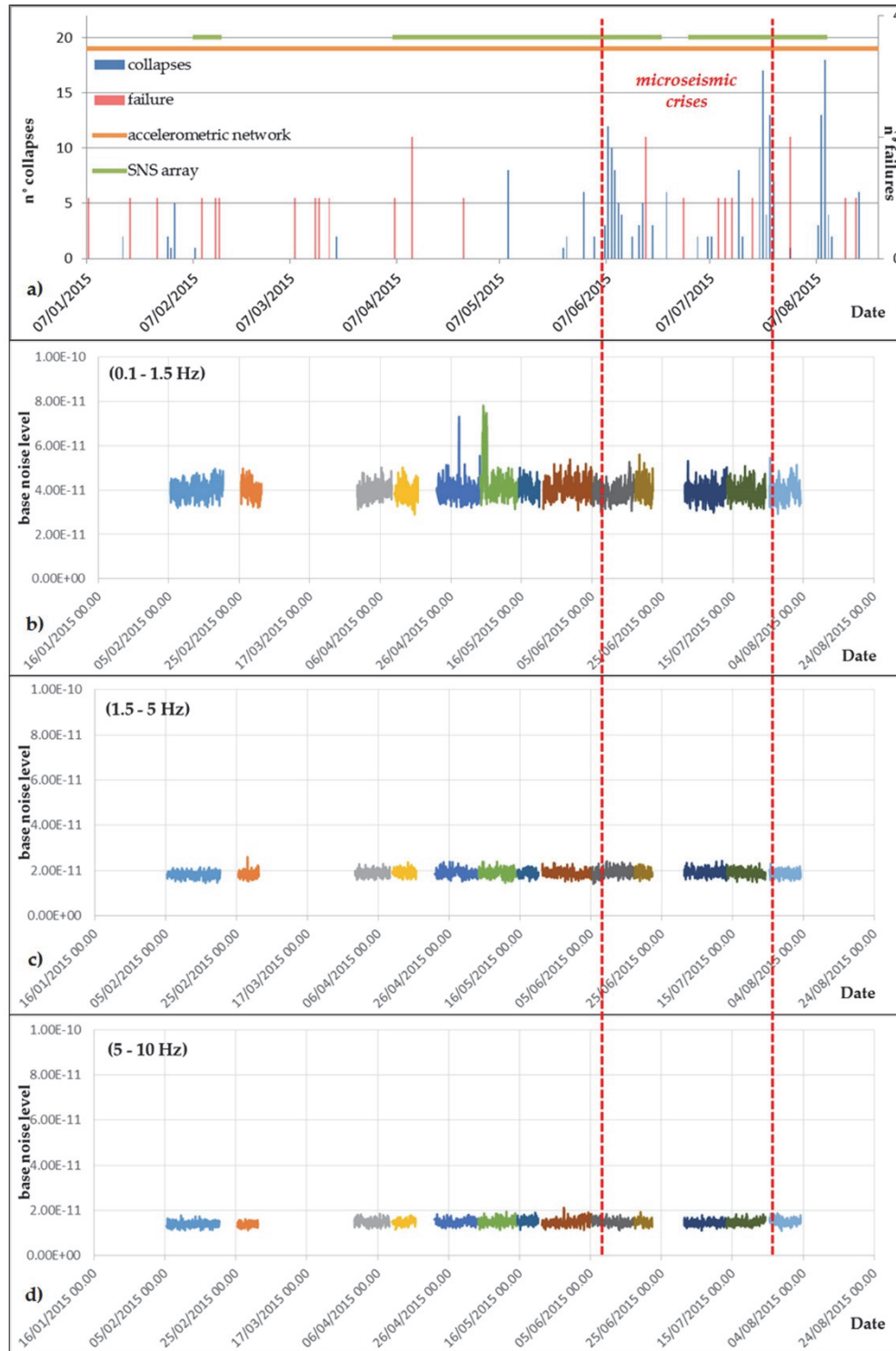


Fig. 79: Base noise level analysis conducted for frequency bands ranging from 0.1 Hz to 10 Hz. Differently from what occurs at higher frequencies, during the collapse crises the base noise level remain unchanged with constant trend. The amplitude of the base noise level decrease as frequency increase.

Preliminary statistical significant cross-correlation analysis was performed on these data and has allowed to establish the LAG between seismic noise rate variation and occurrence of the first collapse of each collapse crisis. In fact, the seismic noise rate variation anticipates the first collapse of about an hour and a half. This LAG is the same for each occurrence of collapse crisis: both if seismic noise decrease and if seismic noise increase (Fig. 80).

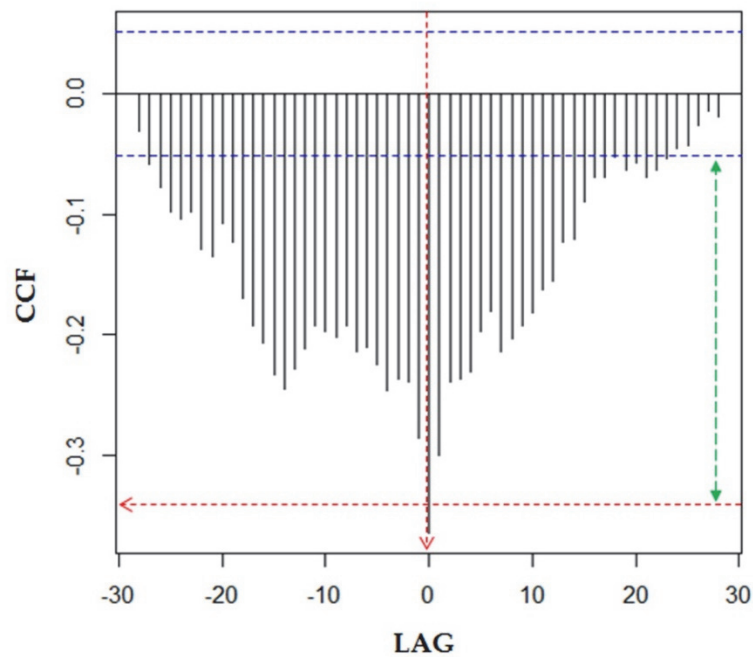


Fig. 80: Example of correlogram indicating the cross-correlation between seismic noise rate (α) and collapse crises frequency (β).

The seismic noise rate variation always anticipate the occurrence of collapse crises. As example, during the collapses crisis number ID 42 (see Fig. 74) the first collapses was occurred at 13:35 of 7th June 2015 while the decrease of seismic noise rate starting from 12:00 of 7th June 2015 (Fig. 81).

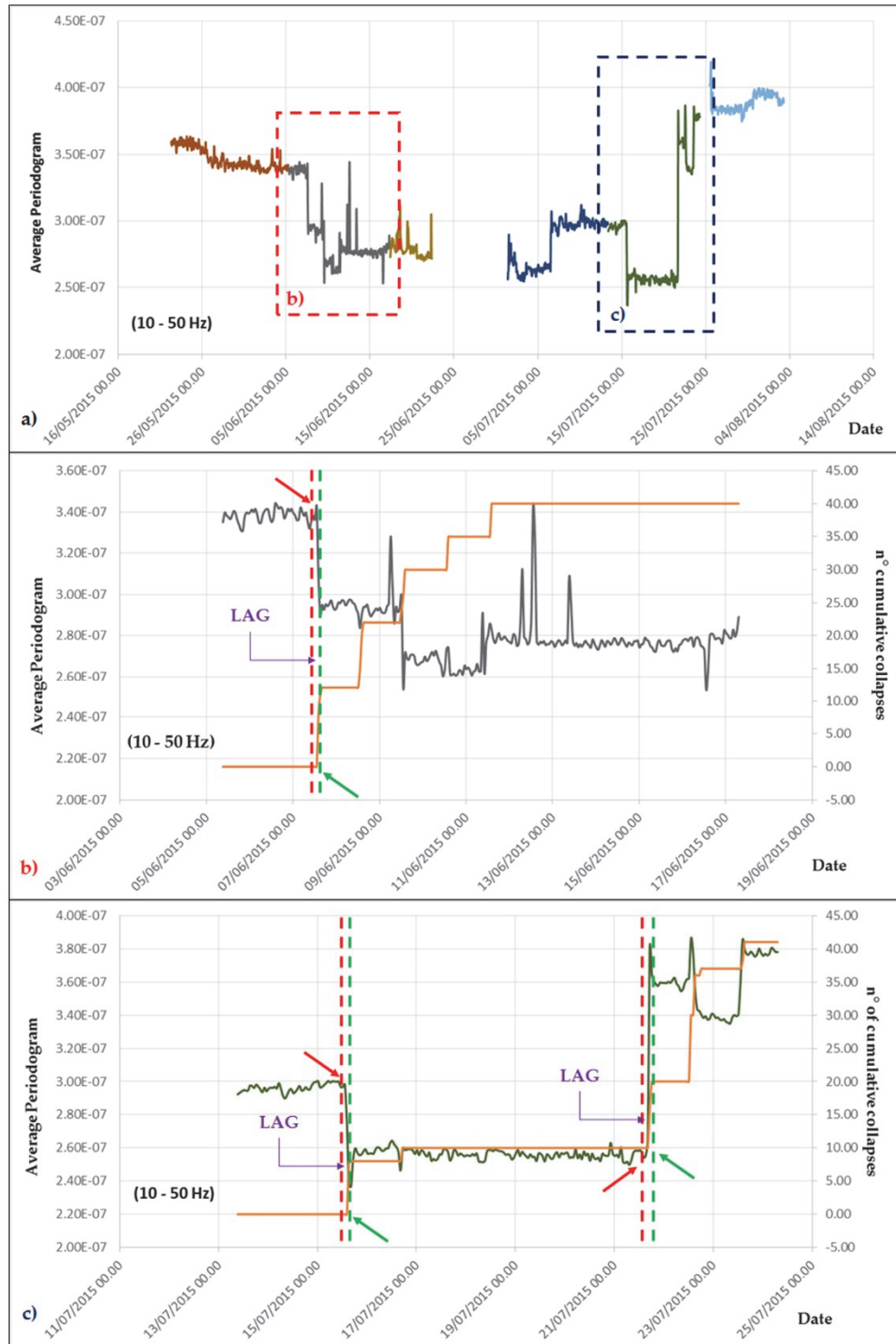


Fig. 81: Comparison between variation of seismic noise rate and occurrence of collapse crises that indicate the activity of the ongoing deformational processes that affect Peschiera Spring slope. Start of decrease or increase of seismic noise values (red arrows) always anticipate the occurrence of microseismic crises (green arrows). The LAG interval time is also shown and corresponds at value of one hour and a half.

The SBA approach applied to seismic noise analysis, has allowed understand the seismic noise behaviour of the monitored entire slope, correlated with the ongoing deformational process that affect the Peschiera Spring slope. In fact, the occurrence of the main collapse crises causes the decreasing of the average periodogram and the base noise level at specific frequency bands, from 10 Hz to 250 Hz, that are the same of the microseismic events. The SBA approach not highlighted correlation between groundwater level variations and changes in seismic noise rate.

5.3. SEA approach analysis

Very preliminary analysis were carried out following SEA approach on data from monitoring system installed on both test-sites.

As it regards the Acuto test-site, during the monitored period the instrumented joints and micro-fractures do not show significant deviations by their natural deformation trend; furthermore, do not show an incipient variation in the rheological behavior (Fig. 82).

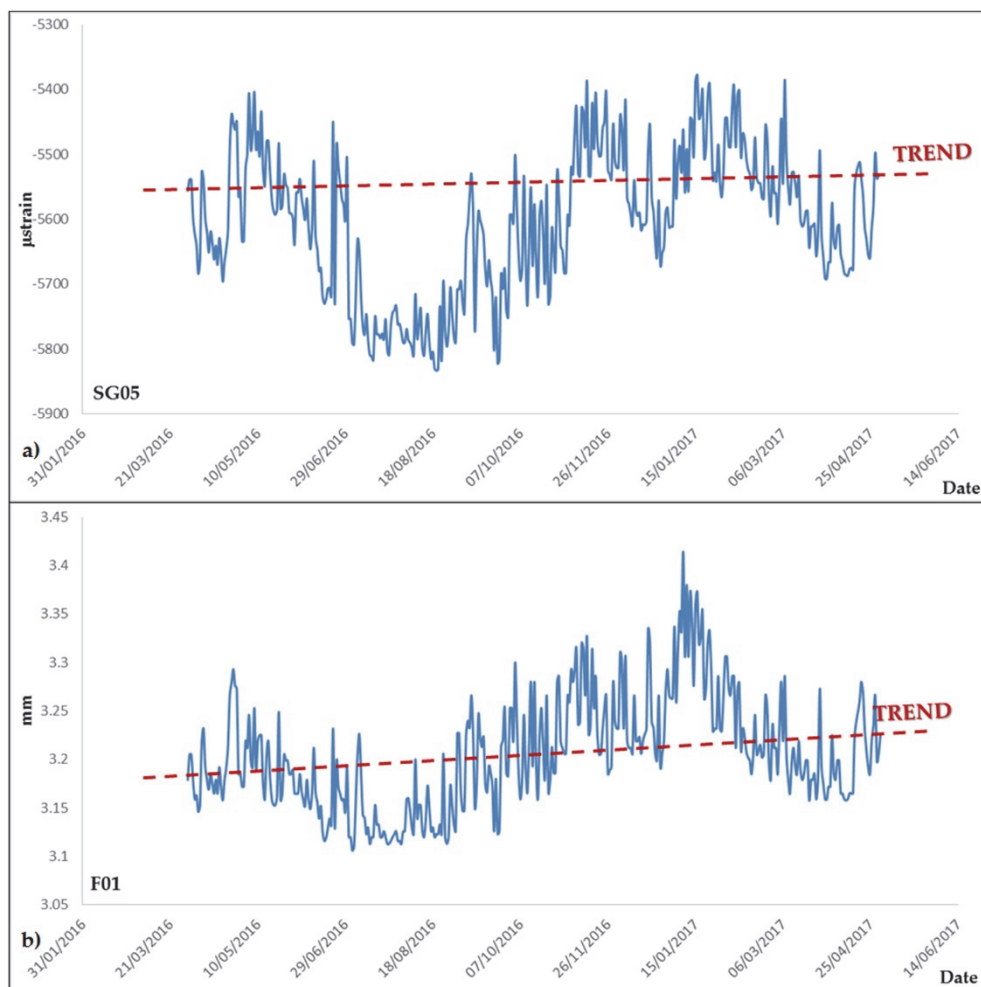


Fig. 82: Example of deformative trend on two different kinds of strain sensors installed on Acuto rock block: a) strain gauge on micro-fracture and b) extensometer on open joint. The constant trend suggest that the Acuto rock block deformation fall on second stage of creep curve.

Considering the cumulative value of the inelastic joints deformation in a long-period time-window, the process seems to be attributed to steady creep phenomena acting on the rock mass. Decreasing the considered time-window, it could be notice that rock mass deformation is driven by elasto-plastic effect due to repetition of thermal-cycles, which are cumulated in the joints deformation. Considering a long-period time-window the process seems to be a rheological effect of a Newtonian behavior deformation (at constant load), but the short period time-window reveals that the strain is, indeed, the result of continuous repetition of load-unload thermal cycles on rock mass and on joints. These kind of effects can act as thermal fatigue processes on rock mass over a long-period time window, leading it towards prone-to-failure conditions (Fig. 83).

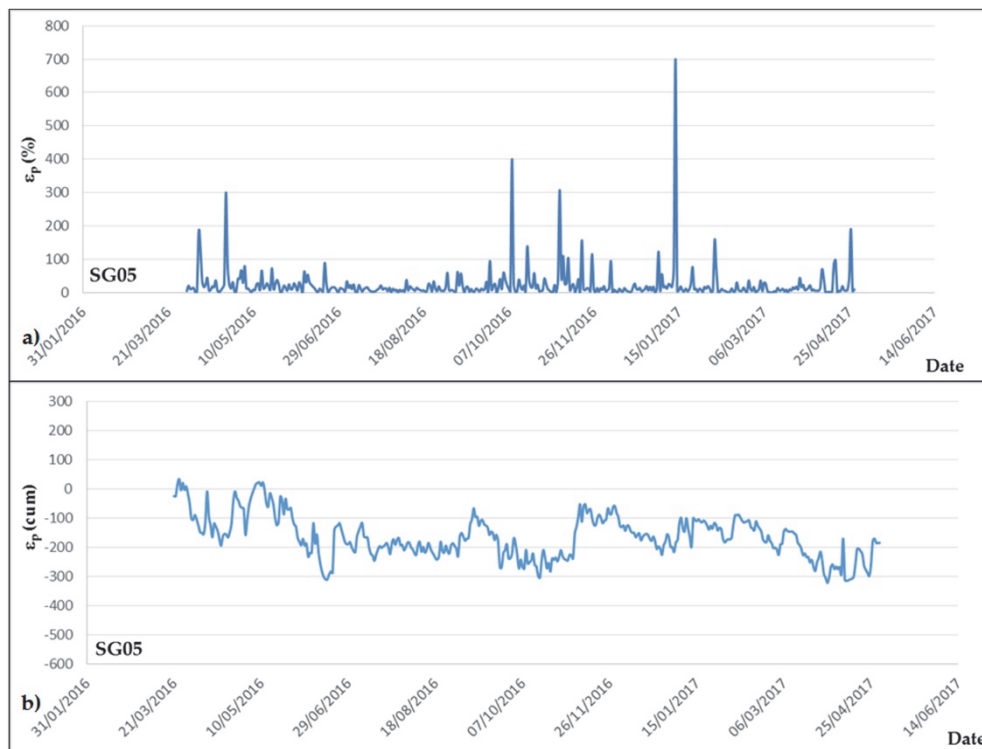


Fig. 83: Inelastic daily contribution to the strain (a; for the computed procedure see Fig. 46) and cumulative deformative trend due to repetition of load/unload cycles on the rock mass (b). The trend showing an increase of the micro-fracture opening.

Regarding the data from Peschiera Spring slope test-site, previously studies have highlighted the dynamic of the ongoing deformation process that affect entire slope (Casini et al., 2006; Maffei et al., 2005; Martino et al., 2004). In fact, the data from geological and geomorphological surveys allowed reconstructing the dynamics and kinematics of the processes acting on the various portions of the slope and referring them to different evolutionary stages present on three different slope sectors (see 4.2.1).

The results from multi-parametric monitoring system indicate the multi-level evolutionary process of slope system and describe that the stress-strain conditions in the slope imply the involvement of portions of the rock mass in a rock mass creep deformation (Chigira, 1992). Considering a very long-period time-window, in the last ten years the deformative process is driven by a steady creep phenomena with regular decrease of slope of the curve. This behavior is attributable to mass rock creep deformation processes and not present any relations with external or internal destabilizing factors (Fig. 84). Furthermore, no cyclic deformation process has been identified. Therefore, instead of Acuto test-site, the long-period deformative process that involve the Peschiera Spring slope is completely attributable to steady creep phenomena because there are not cyclical processes downstream of which inelastic deformations are cumulated.

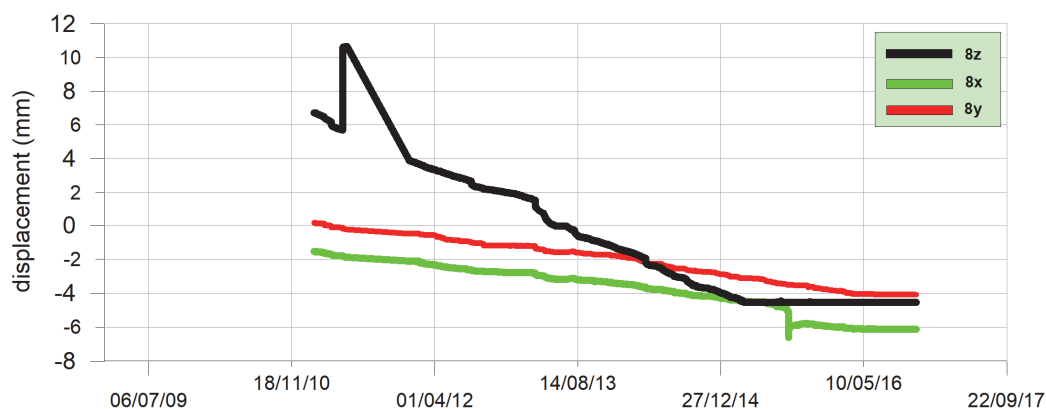


Fig. 84: Example of deformational trend of Peschiera Spring slope from triaxial extensometer installed on western sector where lateral spreading affected entire slope sector. The trend show the constant slope of the curve.

On this long-period rock mass behavior, deformations with seasonal recurrence and episodes related to transient and external processes are modulated. More in particular, middle-time evolutionary processes are recognized due to hydrogeological factors, as groundwater level excursion. These kind of processes are the only ones showing seasonal cycles (cf. Fig. 67).

In addition, also short-time evolutionary processes are detected in Peschiera Spring slope deformation due to occurrence of external factors, like as some types of near-field and far-field earthquakes. More in particular these kind of events can induce displacements along joints due to specific physical properties of the seismic signals associated with the energy content, the distribution of relative energy and peak of ground acceleration related to the ground motion components and, finally, the spectral amplitude distribution in the frequency domain. The deformations are induced in the parallel direction respect to the dip of the slope and the landslide dimensions are associated with the characteristic periods that control the landslide response in relation to the spectral content of the ground motion (Lenti et al., 2015). In other words, some particularly regional earthquakes and teleseisms may give rise to resonance effects that involve the entire slope, inducing an almost instantaneous deformative response along monitored joints. The earthquake-induced displacements are significant because they have the same order of magnitude (i.e. 1 mm/year) as the average annual cumulative displacement based on a decade of measurements within the slope. Similarly to what was seen for the first test-site, the regional earthquakes and teleseisms act the same way as vibrodyne device but involving different dimensional scales. In fact, in the first test-site, the vibrodyne induce resonance effects in a rock block, instead, in the second test-site, external vibrational events induce resonance effects involving entire slope (cf. Fig. 1).

The SEA analysis applied to long-period monitored time-series represent the starting point for assigning different risk exposures to the buildings and infrastructures that interact with the ongoing deformation processes, leading to define a “multi-level” and “multi-time” concept of the geological risk.

6. Discussion

The proposed approaches for data analysis from multi-parametric monitoring systems have been tested in this research aiming at determining their feasibility in the following three features:

- the ability to detect precursor signals of landslide phenomena;
- the ability to analyse and determine cause-to-effect relations among *preparatory factors* and related strain effects;
- the ability to provide an early-warning in order to manage the safety of strategic infrastructure.

These approaches have to be suitable to detect any possible destabilizing factors in rock slope stability in order to reduce the “advice-time” that should be necessary to transmit an alarm signal for early-warning in case of exposed infrastructure, thus managing the related risk. They have been applied to two different landslide phenomena, acting on different dimensional scales (rock-block scale and entire slope scale). In both cases returns encouraging results.

The OBA approach allowed to establish some main cause-to-effect relations among several predisposing factors to slope instabilities and their related strain effects, acting on different time- and dimensional- scales. Focusing on environmental factors, the OBA approach have seen how the temperature and, secondly, the rainfall are the principal destabilizing factors to deformational processes acting on (exposed) rock block scale. Often, these kind of factors present a cyclical behaviour on daily time-window, like as the temperature, or on seasonal time-window, like as the rainfall, which are reflected in a cyclical trend of strain that can cumulate inelastic deformation on joints or on rock mass. This plastic behaviour can due to thermo-mechanical effects and/or to creep-effects: the OBA approach does not allow separating the two aliquot and assessing which of the two is predominant over the other. With the use of the OBA approach, it was possible to understand the dynamic behaviour of a rock mass, in a rock-block scale, when it is exposed to induced vibrations. Considering a larger

dimensional scale of the deformative processes (i.e. entire slope scale), a very important cause-to-effect relation was found between the occurrence of microseismic crises that are originated inside slope and the variation of groundwater level, showing as the hydrogeological factors influence the deformative response of the rock slope in a middle-period time-window. The OBA approach was useful also for detect cause-to-effect relations acting on a very short-period time-window. This is the case of the interaction between vibrational events originated outside of the slope and his related deformative response. Starting from a well-designed multi-parametric monitoring system is possible to detect precursory signals of a greater rock failure phenomenon. Data analysis following OBA approach, allows to recognize precursor events. A lesson learned on these kind of processes comes from the second test-site. In fact, in some cases a significant sequence of precursors that anticipates of some tens of minutes the strongest collapse (expression of ongoing deformational processes that afflict entire slope), were observed. The functionality of OBA approach for detecting cause-to-effect relations, considering different dimensional scale and different time window, is summarized in Fig. 85.

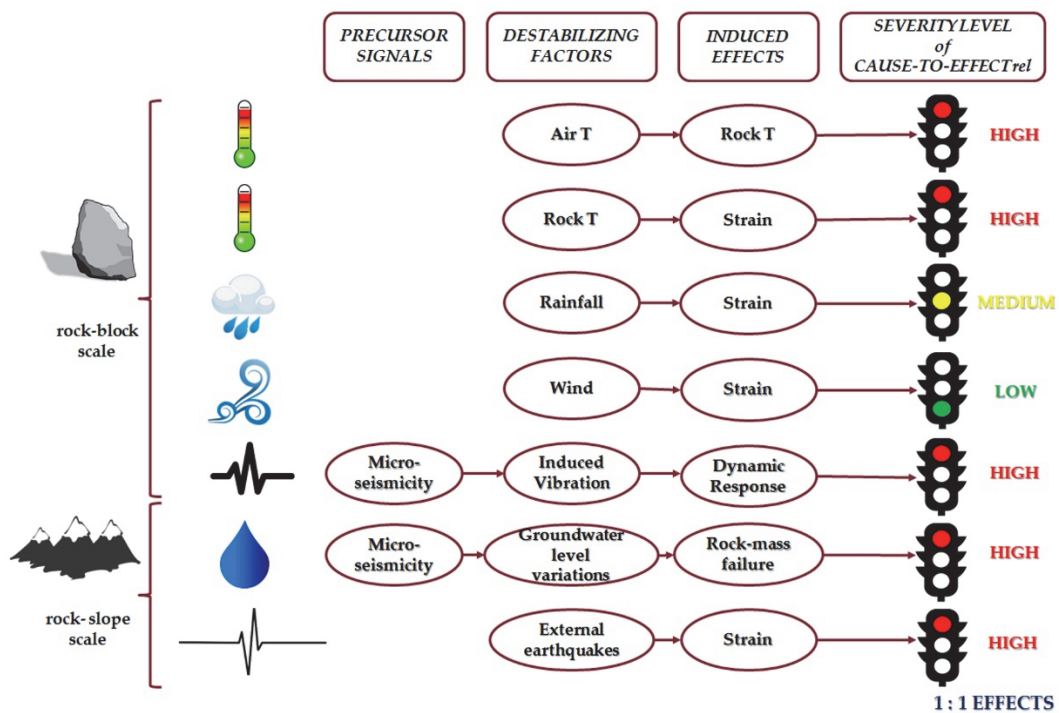


Fig. 85: OBA results derived by both test-sites with associated a cause-to-effect relations severity level.

Applying the OBA approach is also possible to detect and verify some chain effects on monitored time-series. A lesson learned of this topic derive by the first test-site, where a chain effect occurs is the case of the air temperature that is in cause-to-effect relation to rock temperature, which in turn is in cause-to-effect relation to strain of the rock mass. In addition, the rainfall and the strong wind are in cause-to-effect relation to rock temperature, which in turn are in cause-to-effect relation to rock mass deformation. In fact, the occurrence of these events lowers the rock temperature and decreases the amplitude of the thermal cycle. However, rainfall and strong wind do not completely stop the associated rock mass deformative response Fig. 86.

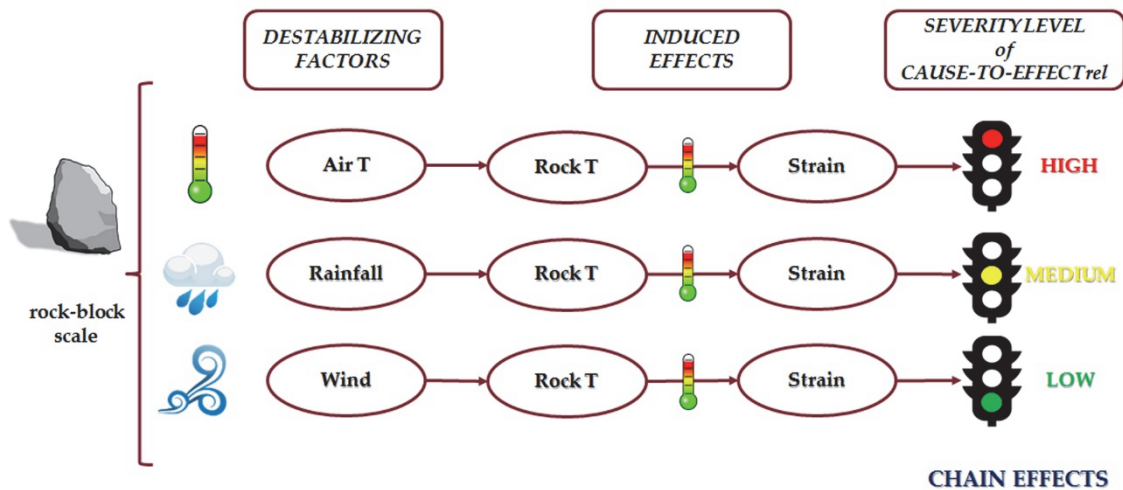


Fig. 86: OBA results with highlighted the verify chain effects in cause-to-effect relations.

A statistically based analysis, following the proposed SBA approach, was also carried out in order to define which rate series are cross-correlated with each other. The power of statistical approach is to automatically verifying the occurrence of cross-correlation among several rate series, with a high level of objectivity, both on block rock scale both on entire slope. The SBA approach is also very useful to estimate the time in which two rate series are cross-correlated, expressed as LAG unit (the time shift in which a rate series influences the other). In this case, very important is the concept of

rate, that is, how a natural physical process varies over-time influencing others. In order to carry out cross-correlation among different parameters to point out anomalies of continuous or cumulative values, a rate variation on different data was calculated. All rate series of destabilizing actions have been cross-correlated with the related rate series of induced effects, as joints and micro-fractures displacement. The results from first test-site, show a good cross correlation between some environmental destabilizing factors (like as temperature) and deformational response of rock mass, both on daily thermal cycle and on seasonal thermal trend. A statistical analysis in order to detect possible variation of seismic noise rate occurring at slope-scale, shortly before the occurrence of micro-seismic crises, was also performed. In this case, the trend analysis followed very well the seasonal response of rock-mass to deformational processes acting on middle-period time-window (Fig. 87). Following SBA approach results to be very difficult detect the precursory signals. In fact, these kind of events are clustered in time, while a continuous rate series is needed for apply a statistical cross-correlation analysis.

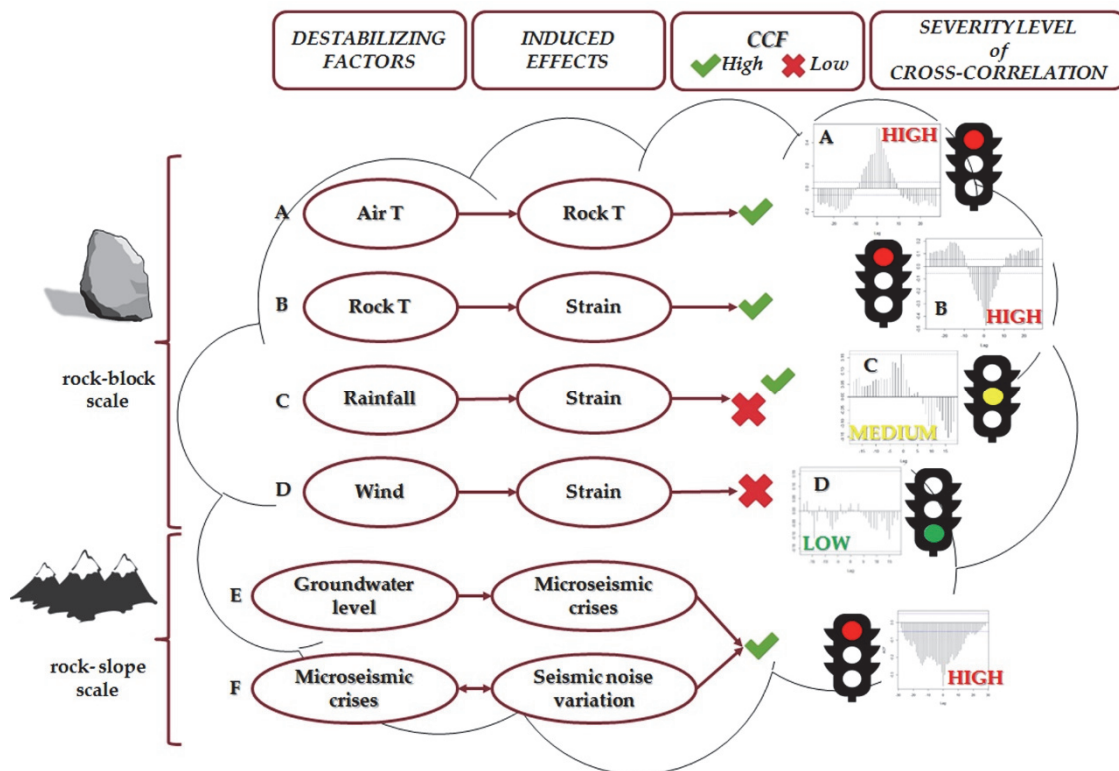


Fig. 87: SBA results derived by the both test-site whit associated a cause-to-effect relations severity level.

Summarizing the obtained results of OBA approach and of SBA approach for data analysis from multi-parametric monitoring system installed at rock-block dimensional scale, a high and significance value of cross-correlation functions were defined between rate series of air and rock temperature as well as between rate series of rock temperature and deformative response of rock mass. The OBA approach can obtain the same results, comparing the time sequence of air and rock temperature and of micro-strain and rock temperature. In fact, using the OBA approaches possible to see that the destabilizing factors always precedes rock deformations, thus confirming the influence of them on the rock mass behavior. In particular, as it results by the cross-correlation and by the objective cause-to-effect relations, the rock temperature represent a main *preparatory factor* (*sensu* Gunzburger et al., 2005) since its variation systematically anticipates joint deformations in daily cycle and in seasonal trend of exposed rock-block and in a short-period and cyclical time window. The advantage of the SBA approach with respect to OBA approach is to provide the temporal LAG in which a destabilizing factors influence the deformational response of rock mass. Both OBA approach and SBA approach have allowed to identify several *predisposition factors*, *preparatory factors* and *trigger factors* (*sensu* Gunzburger et al., 2005) active on rock mass and how can affect its deformation response. Summarizing the obtained results of OBA approach and of SBA approach for data analysis from multi-parametric monitoring system applied to entire-slope dimensional scale, the OBA approach turned out to be very useful for identifying and characterizing cause-to-effect relation between groundwater level and occurrence of micro-seismic events that are the expression of the ongoing gravity-induced deformation process. Moreover, OBA approach results to be very useful in order to detect scattered precursor signals that not show a continuous trend. The SBA approach turned out to be very suitable for detecting, with statistical significance, the trend of average seismic noise rate and seismic noise base level in relation with the occurrence of micro-seismic events at seasonal scale, showing that the seismic rate variations anticipates and highlighted in the time collapse crises that are incipient. In this way, the seismic noise rate variation can be interpreted itself as the precursor signal of a collapse crisis (Fig. 88).

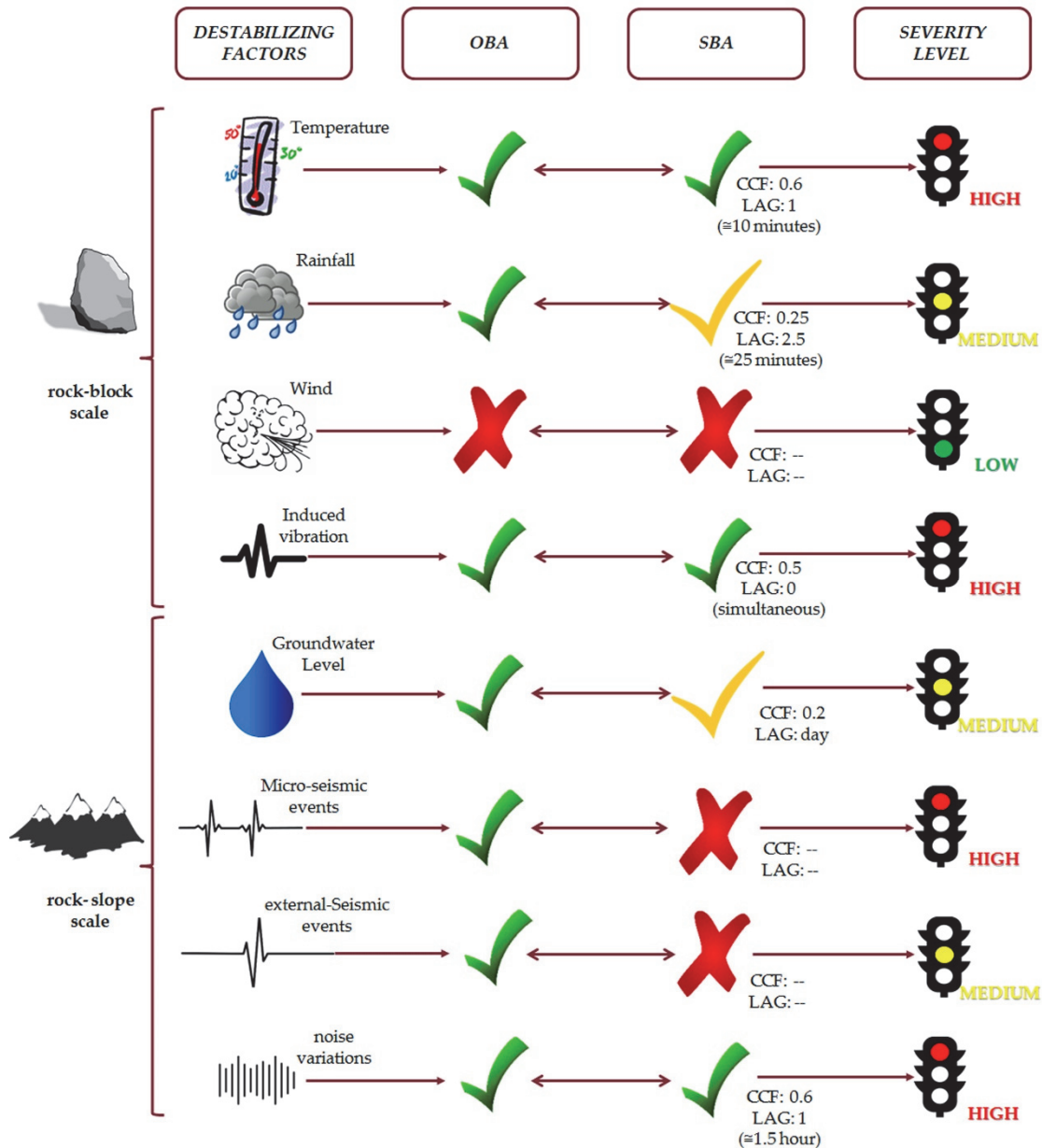


Fig. 88: Sketch representing the reliability of the OBA and SBA approaches for identifying destabilizing actions on slope stability at different dimensional scale.

As is it apparent from the experiments conducted, both the OBA approach and SBA approach have demonstrated the possibility to detect destabilizing factors to slope stability and provide an early warning. In order to use the OBA approach for implementation of an early warning system, greater is the cause-to-effect relation between destabilizing factor and induced deformation, more that destabilizing factor is

considered as an *alert* in the early-warning criteria. In statistical analysis, every possible rate series of destabilizing action (as temperature, rainfall, wind, induced vibration) is cross-correlated with the rate series of each strain sensor (strain gauges and extensometers). In order to implement an early warning system calibrated on results from statistical approach, when the number of verify cross-correlation between destabilizing action and induced deformation increase, then the severity of the alert increase. The LAG time between the event detection and the alert signal is well identified by the CCF value obtained by application of SBA approach. Since the process of calculating the rate series and of cross-correlation is automated, the use of SBA approach of data analysis in risk management and in infrastructure administration result to be very useful. The outputs from this PhD Thesis suggest that future multi-parametric records could provide better constrains to the evidences collected so far and allow to evaluate the possible role of precursor signals in early warning practice, i.e. by extending the “advice time” for the risk management. In conclusion, it can be said that both of the applied approaches identified very well which forcing actions is a destabilizing factors and influence monitored strain effects. In future development, the most significant destabilizing factors identified through the application of two different approaches will be the basis of the threshold parameters for a hypothetical early warning system (EWS), pointing out their suitability and the corresponding reliability level for different scenarios of rock fall trigger. Regarding the second test-site, an early-warning system has been developed and is already present in published literature (Lenti et al., 2012). It is based on the occurrence of vibrational events, following a Control Index that take into account three different factors: a time-frequency of earthquakes, a time-frequency of microseismic events that are originated within the slope and, finally, on the cumulative values of Arias Intensity of the recorded microseismic events. With the advent of permanent SNS array, the alarm system for the Peschiera drainage plant has been recalibrated due to the increase of resolution respect to the conventional accelerometric network. Starting from the August 2016, the alarm system of the Peschiera Spring slope was active only relying on SNS array, and the Control Index has been increased by a factor of 4 (Fiorucci et al.,

2016). Future developments may relate to the implementation of the Control Index presented above implementing results from SBA approach. In particular, can be taken into account the seismic noise rate variation results: the automatic calculation procedure is very suitable to be implemented in an alert system based on the recognition of precursor signals of main microseismic events related to ongoing gravity-induced slope deformation.

From a preliminary analysis following the SEA approach, it is possible understand that the gravity-induced deformational process described above is not attributable only to the destabilizing factors acting in short- and middle- time window, but depends also on time-dependent processes. These act in a time much longer than the scale of daily or annual observation. More in particular, a difference between the two test-sites was noticed. In fact, in the second test-site the long-time deformation processes are attributable only to traditional creep phenomena. Instead, in the first test site the long-time behaviour is mainly due to effects of load/unload thermal cycles on rock mass that cumulate plastic deformations on rock joints. In this way, the SEA approach is very suitable to evaluate the long-period behaviour of the monitored rock-slope, taking into account the several destabilizing factors (given by the sum of *predisposing factors* and of *preparatory factors*) that act on slope stability in various time windows.

The data analysis carried out following the three proposed approaches, has allowed to recognize a multilevel dynamics of the deformational processes. As an example, here is reported the Peschiera Spring slope test-site. Firstly, long-term evolutionary processes mainly related to rock mass creep processes that affect the entire slope. These types of processes can be easily investigated using the SEA approach. Secondly, middle-term evolutionary processes related to aquifer dynamics and to seasonal groundwater level excursion that influence the occurrence of micro-seismic crises and seismic noise variations. These types of processes can be easily investigated through the use of SBA approach and of OBA approach. Finally, short-term evolutionary processes due to external and transitory actions, like ad earthquakes in near or far field. These types of processes can be easily investigated applying OBA approach (Fig. 89).

:



















		<i>data analysis approaches</i>		
		<i>OBA</i>	<i>SBA</i>	<i>SEA</i>
 rock-block scale	<i>temperature</i>	 <i>daily</i> 	 <i>daily</i> 	 <i>daily</i>  <i>cumulative value</i>
	<i>rainfall</i>			
	<i>wind</i>			
	<i>induced vibrations</i>			
 rock-slope scale	<i>external actions (like earthquakes)</i>			
	<i>aquifer dynamics</i>	 <i>seasonal</i> 		
	<i>seismic noise variations</i>		 <i>seasonal</i> 	
	<i>creep</i>			

Fig. 89: Summary table of the applicability of the proposed approaches to detection of factors that influence slope deformation. The clock indicates the time window in which these factors are active: from short- to long-term. The loop arrow indicate if the considered process is cyclic.

7. Conclusion

This Ph.D. thesis presented three different approaches of data analysis from multi-parametric monitoring system applied to rock falls and gravity-induced landslides phenomena at different dimensional scale, in order to reduce the geological risk that involve main infrastructures.

The challenge of these approaches is to forecast the slope evolution, will provide alert levels suitable for managing infrastructures in order to mitigate the landslide risk and reduce the “advice” time for interventions.

Three different strategies can be defined in this regard:

- I. an Observation-Based Approach (OBA) that is based on searching cause-to-effect relation among destabilizing factors (both *predisposition factors* and *preparatory factors* and *trigger factors*) and induced deformation;
- II. a Statistic-Based Approach (SBA) that is focused on statistical significance cross-correlations among different parameters and their rate variation to point out anomalies of continuous trend or cumulative values;
- III. a Semi-Empirical Approach (SEA) that is based on simplified rheological creep models calibrated time-by-time.

At this aim, several experiments have been carried out at different dimensional scales, in particular on rock-block scale and entire slope scale, and on different landslide phenomena of two test-sites, which have in common the presence of an infrastructure exposed to natural risk.

Multi-parametric monitoring systems were installed in the two test-sites and were composed by several kind of devices including extensometers, strain gauges, rock-thermometers for detecting changes in rock properties and detecting stress-strain changes, as well as rain gauges, anemometers for wind speed and wind direction, hygrometers, air-thermometers, micro- or nano- accelerometers and piezometers for detecting possible destabilizing factors.

The results from both test-sites show how both the OBA approach and the SBA approach, and secondly the SEA approach, demonstrate the possibility to detect the destabilizing actions responsible for deformative effects on rock joints and provide an early warning. The LAG time between the event detection and the alert signal is well identified by the CCF (cross-correlation factor) obtained by application of SBA approach on rate time series of several factors.

In Acuto test-site, the data analysis following the three different approaches has been carried out to understand and mitigate geological risk due to rock falls phenomena from much fractured rock mass. During monitoring period was observed that the temperature variations play a significant role for detectable strains of rock mass joints. In fact, thermo-elastic behaviour of rock mass strain were recognized both on daily cycle and on seasonal period. On the contrary, precipitation and the wind velocity do not seem to trigger strain responses on the rock mass joints. Moreover, experiments were carried out in forced conditions, applying dynamic actions and monitoring seismic wave propagation within the rock wall. These experiments have allowed to understand the fractured rock mass behaviour under induced vibrations.

In Peschiera Spring slope test-site, the data analysis following the three different approaches has been carried out to understand and mitigate geological risk due to ongoing gravity-induced deformation processes. During monitoring period was observed that several factors act on slope deformation processes at different time windows. The evolutionary process of the slope is a multi-level temporal type in which play a significant role both long term processes due to creep, and detectable using SEA approach, middle term processes due to influence of groundwater level variation and short term processes due to external factors detectable by SBA and OBA approaches. The deformation processes were also understood by the study of micro-seismicity generated inside the slope. Failures and collapses of the rock mass, related to creep processes and to hydrogeological factors are continuously monitored thanks to an innovative nano-seismic network, called SNS array, installing inside the drainage plant and devoted to monitor the micro-seismic activity starting from 2015. An automatic

process for continuous monitoring of seismic noise variation has allowed to understand the behaviour of entire rock mass slope during the main collapse crises. Drop and variation of the seismic noise amplitude was concomitant with the occurrence of micro-seismic crises. At this aim, a SBA approach devoted to detect seismic noise rate variation result to be very useful to implement the early-warning procedure, already existing and based only on OBA analysis.

The presented approaches, applied to two test-site, has allowed to identify the continuous forcing (like as temperature, groundwater level variation, creep and inelastic phenomena) and the transient forcing (like as rainfall, wind, induced vibrations) acting on rock mass deformation on both dimensional observation scale. More in particular the OBA approach was useful to detect impulsive event that predispose the rock mass to instability, from short to middle term. The SBA approach was useful to detect rate variations of predisposing factors respect induce effects, from short to long term. The SEA approach is useful for detecting rheological trend changes due to creep processes only in long-term geological phenomena. In this way, the OBA approach results very suitable also to detect precursor signals related to higher deformational episodes. Furthermore, the presented approaches are able to provide an early-warning for landslide phenomena because: i) identify precursor signals, ii) analyse cause-to-effect relations between predisposing factors and related strain, iii) compute, through the cross-correlation function, the time in which two or more rate series influence the deformative response of the rock mass, iv) describe the long-period behaviour of the landslide mass over different time-window. Finally, the approaches here presented are suitable to rock landslides at various dimensional scales (i.e. rock slopes, cliff slopes and roadway made cuts) where is possible to install a multi-parametric monitoring system.

8. References

- Accordi, G., Carbone, F., Civitelli, G., Corda, L., De Rita, D., Esu, D., Funicello, R., Kotsakis, T., Mariotti, G., Sposato, A., 1986. Lithofacies map of Latium- Abruzzi and neighbouring areas. Quaderno C.N.R. "La Ricerca Scientifica", Roma, 114 (5), pp. 223
- Amitrano, D., Arattano, M., Chiarle, M., Mortara, G., Occhiena, C., Pirulli, M., Scavia, C., 2010. Microseismic activity analysis for the study of the rupture mechanisms in unstable rock masses. *Nat. Hazards Earth Syst. Sci.* 10, 831–841. doi:10.5194/nhess-10-831-2010
- Antonello, G., Casagli, N., Farina, P., Leva, D., Nico, G., Sieber, A.J., Tarchi, D., 2004. Ground-based SAR interferometry for monitoring mass movements. *Landslides* 1, 21–28. doi:10.1007/s10346-003-0009-6
- Arosio, D., Longoni, L., Papini, M., Scaioni, M., Zanzi, L., Alba, M., 2009. Towards rockfall forecasting through observing deformations and listening to microseismic emissions. *Nat. Hazards Earth Syst. Sci.* 9, 1119–1131. doi:10.5194/nhess-9-1119-2009
- Bakun-Mazor, D., Hatzor, Y.H., Glaser, S.D., Carlos Santamarina, J., 2013. Thermally vs. seismically induced block displacements in Masada rock slopes. *Int. J. Rock Mech. Min. Sci.* 61, 196–211. doi:10.1016/j.ijrmms.2013.03.005
- Bigarré, P., Verdel, T., Klein, E., Gueniffey, Y., 2011. Cloud monitoring®: an innovative approach for the prevention of landslide risks. *Proc. Second World Landslide Forum - 3-7 Oct. 2011, Rome* 1–5.
- Bigi, S., Costa Pisani, P., 2002. Structural setting of the Cicolano-M. Calvo area (Central Apennines, Italy). *Boll Soc Geol Ital Spec*, 1, 141-149
- Boni, C.F., Bono, P., Capelli, G., 1986. Schema idrogeologico dell'Italia Centrale. *Mem Soc Geol Ital*, 35, 991-1012
- Boni, C.F., Capelli, G., Petitta, M., 1995. Carta idrogeologica dell'alta e media Valle del F. Velino. Elaborazione cartografica e stampa System Cart, Roma
- Bottelin, P., Lévy, C., Baillet, L., Jongmans, D., Guéguen, P., 2013. Modal and thermal analysis of les arches unstable rock column (vercors massif, french alps). *Geophys. J. Int.* 194, 849–858. doi:10.1093/gji/ggt046
- Butler, R., 2003. The Hawaii-2 observatory: observation of nanoearthquakes. *Seismol Res Lett* 74, 290-297
- Casini, S., Martino, S., Petitta, M., Prestininzi, A., 2006. A physical analogue model to analyse interactions between tensile stresses and dissolution in carbonate slopes. *Hydrogeol. J.* 14, 1387–1402. doi:10.1007/s10040-006-0064-x
- Chigira, M., 1992. Long-term gravitational deformation of rocks by mass rock creep. *Eng. Geol.* 32, 157–184. doi:10.1016/0013-7952(92)90043-X
- Ciotoli, G., Di Filippo, M., Nisio, S., Romagnoli, C., 2001. La Piana di S. Vittorino: dati preliminari sugli studi geologici, strutturali, geomorfologici, geofisici e geochimici. *Mem Soc Geol Ital*, 56, 297-308
- Civitelli, G., Corda, L., Mariotti G., 1986. Il bacino sabino:3) evoluzione sedimentaria ad inquadramento regionale dall'Oligocene al Serravalliano. *Mem. Soc. Gol. It.* 35:

399-406

- Collins, B.D., Stock, G.M., 2016. Rockfall triggering by cyclic thermal stressing of exfoliation fractures. *Nat. Geosci.* 2686. doi:10.1038/ngeo2686
- Contrucci, I., Klein, E., Bigarré, P., Lizeur, A., Lomax, A., Bennani, M., 2010. Management of post-mining large-scale ground failures: Blast swarms field experiment for calibration of permanent microseismic early-warning systems. *Pure Appl. Geophys.* 167, 43–62. doi:10.1007/s00024-009-0005-4
- Contrucci, I., Klein, E., Cao, N.-T., Daupley, X., Bigarré, P., 2011. Multi-parameter monitoring of a solution mining cavern collapse: First insight of precursors. *Comptes Rendus Geosci.* 343, 1–10. doi:10.1016/j.crte.2010.10.007
- Corda, L., Mariotti G., 1986. Il Bacino Sabino: 1) Fenomeni di risedimentazione nella serie di Osteria Tancia. *Boll. Soc. Geol. It.*, 105 (1-2): 41-63
- Cornelius, R.R., Voight, B., 1995. Graphical and PC-software analysis of volcano eruption precursors according to the Materials Failure Forecast Method (FFM). *J. Volcanol. Geotherm. Res.* 64, 295–320. doi:10.1016/0377-0273(94)00078-U
- Cosentino, D., Cipollari, C., 2006. La paleogeografia neogenica del Mediterraneo centrale: vincoli geologici dall'Appennino centrosettentrionale. *Biogeographia* 27, 11–34.
- Cruden, D.M., Varnes, D.J., 1996. Landslides types and processes. *Landslides Investigation and Mitigation*. Transportation Research Board, Turner AK, Shuster RL (eds), National Research Council, Special Report 247. National Research Council: Washington, DC, 36-75
- Curi, L., 2017. Monitoraggio dei versanti in frana attraverso l'utilizzo di accelerometri. 2nd level University Master degree
- Devoto, G., 1970. Sguardo geologico dei monti simbruini (Lazio Nord-orientale). *Geol. Rom.*, IX, pp. 127-136
- Evans, S., Mugnozza, G.S., Strom, A., 2006. Landslides from massive rock slope failure. *Nato Science Series. Springer, Netherlands. Series IV: Earth Environ Sci*, vol 49, p 662
- Fantini, A., Magrini, M., Martino, S., Moroni, D., Pieri, G., Prestininzi, A., Salvetti, O., 2015. EXPERIENCING EMBEDDED SENSORS NETWORK FOR THE EARLY WARNING MANAGEMENT OF NATURAL RISKS DUE TO FAST-FAILURES ALONG RAILWAYS. *Proc. 5th Int. Work. Image Mining. Theory Appl.* Berlin, Ger. 85–91.
- Fiorucci, M., Iannucci, R., Lenti, L., Martino, S., Paciello, A., Prestininzi, A., Rivellino, S., 2016. Nanoseismic monitoring of gravity-induced slope instabilities for the risk management of an aqueduct infrastructure in Central Apennines (Italy). *Nat. Hazards*. doi:10.1007/s11069-016-2516-5
- Fiorucci, M., Iannucci, R., Lenti, L., Martino, S., Paciello, A., Prestininzi, A., Rivellino, S., 2015. Experiment of an innovative nanoseismic monitoring applied to gravity-induced slope instabilities in a karstified rock mass. *Rend. Online Soc. Geol. Ital.* 35. doi:10.3301/ROL.2015.82
- Fukuzono, T., 1985. A new method for predicting the failure time of a slope. *Proc. of 4th intern. conf. and field workshop on landslides*, Tokyo: 145–150
- Funiciello, R., Parotto, M., 1978. Il substrato sedimentario nell'area dei Colli Albani:

- considerazioni geodinamiche e paleogeografiche sul margine tirrenico dell'Appennino centrale. *Geol. Rom.*
- Gaffet, S., Guglielmi, Y., Cappa, F., Pambrun, C., Monfret, T., Amitrano, D., 2010. Use of the simultaneous seismic, GPS and meteorological monitoring for the characterization of a large unstable mountain slope in the southern French Alps. *Geophys. J. Int.* 182, 1395–1410. doi:10.1111/j.1365-246X.2010.04683.x
- Galadini, F., Messina, P., 1994. Plio-Quaternary tectonics of the Fucino basin and surroundings areas (central Italy). *G. di Geol.* 56/2, 73–99.
- Gischig, V., Amann, F., Moore, J.R., Loew, S., Eisenbeiss, H., Stempfhuber, W., 2011. Composite rock slope kinematics at the current Randa instability, Switzerland, based on remote sensing and numerical modeling. *Eng. Geol.* 118, 37–53. doi:10.1016/j.enggeo.2010.11.006
- Gischig, V.S., Moore, J.R., Evans, K.F., Amann, F., Loew, S., 2011a. Thermomechanical forcing of deep rock slope deformation: 1. Conceptual study of a simplified slope. *J. Geophys. Res. Earth Surf.* 116, 1–18. doi:10.1029/2011JF002006
- Gischig, V.S., Moore, J.R., Evans, K.F., Amann, F., Loew, S., 2011b. Thermomechanical forcing of deep rock slope deformation: 2. the Randa rock slope instability. *J. Geophys. Res. Earth Surf.* 116, 1–17. doi:10.1029/2011JF002007
- Got, J.-L., Mourot, P., Grangeon, J., 2010. Pre-failure behaviour of an unstable limestone cliff from displacement and seismic data. *Nat. Hazards Earth Syst. Sci.* 10, 819–829. doi:10.5194/nhess-10-819-2010
- Greif, V., Brcek, M., Vlcko, J., Varilova, Z., Zvelebil, J., 2016. Thermomechanical behavior of Pravcicka Brana Rock Arch (Czech Republic). *Landslides* 1–15. doi:10.1007/s10346-016-0784-5
- Gunzburger, Y., Merrien-Soukatchoff, V., 2011. Near-surface temperatures and heat balance of bare outcrops exposed to solar radiation. *Earth Surf. Process. Landforms* 36, 1577–1589. doi:10.1002/esp.2167
- Gunzburger, Y., Merrien-Soukatchoff, V., Guglielmi, Y., 2005. Influence of daily surface temperature fluctuations on rock slope stability: Case study of the Rochers de Valabres slope (France). *Int. J. Rock Mech. Min. Sci.* 42, 331–349. doi:10.1016/j.ijrmms.2004.11.003
- Hatzor, Y.H., 2003. Keyblock Stability in Seismically Active Rock Slopes—Snake Path Cliff, Masada. *J. Geotech. Geoenvironmental Eng.* 129, 697–710. doi:10.1061/(ASCE)1090-0241(2003)129:8(697)
- Hutchinson, J.N., 1988. General report: morphological and geotechnical parameters of landslides in relation to geology and hydrogeology. In: *Proceedings of 5th international symposium on landslides, Lausanne, Balkema, Rotterdam*, 3–36
- Jenkins, G.M., Watts, D.G., 1968. *Spectral Analysis and its Applications*, Holden-Day, Oakland, Calif., 525
- Joswig, M., 2008. Nanoseismic monitoring fills the gap between microseismic networks and passive seismic. *First Break* 26, 121–128.
- Kilburn, C.R.J., Petley, D.N., 2003. Forecasting giant, catastrophic slope collapse: Lessons from Vajont, Northern Italy. *Geomorphology* 54, 21–32. doi:10.1016/S0169-555X(03)00052-7
- Klein, E., Nadim, C., Bigarré, P., Dünner, C., 2008. Global monitoring strategy applied

- to ground failure hazards 1925–1931.
- Lague, D., Brodu, N., Leroux, J., 2013. Accurate 3D comparison of complex topography with terrestrial laser scanner: application to the Rengitikei canyon (N-Z). *ISPRS, Journal of Photogrammetry and Remote Sensing*
- Lai, X.P., Cai, M.F., Xie, M.W., 2006. In situ monitoring and analysis of rock mass behavior prior to collapse of the main transport roadway in Linglong Gold Mine, China. *Int. J. Rock Mech. Min. Sci.* 43, 640–646. doi:10.1016/j.ijrmms.2005.09.015
- Lenti, L., Martino, S., Paciello, A., Prestininzi, A., Rivellino, S., 2015. Recorded displacements in a landslide slope due to regional and teleseismic earthquakes. *Geophys. J. Int.* 201, 1335–1345. doi:10.1093/gji/ggv063
- Lenti, L., Martino, S., Paciello, A., Prestininzi, A., Rivellino, S., 2012. Microseismicity within a karstified rock mass due to cracks and collapses as a tool for risk management. *Nat. Hazards* 64, 359–379. doi:10.1007/s11069-012-0245-y
- Macciotta, R., Hendry, M., Martin, C.D., 2016. Developing an early warning system for a very slow landslide based on displacement monitoring. *Nat. Hazards* 81, 887–907. doi:10.1007/s11069-015-2110-2
- Maffei, A., Martino, S., Prestininzi, A., 2005. From the geological to the numerical model in the analysis of gravity-induced slope deformations: An example from the Central Apennines (Italy). *Eng. Geol.* 78, 215–236. doi:10.1016/j.enggeo.2004.12.009
- Martino, S., Mazzanti, P., 2014. Integrating geomechanical surveys and remote sensing for sea cliff slope stability analysis: The Mt. Pucci case study (Italy). *Nat. Hazards Earth Syst. Sci.* 14, 831–848. doi:10.5194/nhess-14-831-2014
- Martino, S., Prestininzi, A., Scarascia Mugnozza, G., 2004. Geological-evolutionary model of a gravity-induced slope deformation in the carbonate Central Apennines (Italy). *Q. J. Eng. Geol. Hydrogeol.* 37, 31–47. doi:10.1144/1470-9236/03-030
- Mattei, M., Funicello, R., Parotto, M., 2008. Rome and recent geodynamic evolution of Central Italy. *S.EL.CA.* 80/1, 13-24
- Mazzanti, P., Bozzano, F., Cipriani, I., Prestininzi, A., 2014. New insights into the temporal prediction of landslides by a terrestrial SAR interferometry monitoring case study. *Landslides* 12, 55–68. doi:10.1007/s10346-014-0469-x
- Merrien-Soukatchoff, V., Gasc-Barbier, M., 2017. Consequences of daily and annual thermal cycles on fracture propagation and rock slope stability. *Proc. of Progressive rock failure conference, Monte Verità, 5-9 June 2017*, 02F-01:12-14
- Modanesi, S., 2016. Suscettibilità al distacco di blocchi da pareti in roccia valutata attraverso analisi di stabilità e metodi di verifica della compatibilità cinematica basata su rilievi geostretturali con tecniche dirette e da remoto applicata ad un sito sperimentale. 2nd level University Master degree
- Moretto, S., Bozzano, F., Esposito, C., Mazzanti, P., Rocca, A., 2017. Assessment of Landslide Pre-Failure Monitoring and Forecasting Using Satellite SAR Interferometry. *Geosciences* 7, 36. doi:10.3390/geosciences7020036
- Parotto, M., 1980. Appennino centrale. *Simpl. Pubbl. 26 Congr. Geol. Int. di Parigi*: 33-37
- R Core Team, 2015. R: A language and environment for statistical computing. R Foundation for Statistical Computing, Vienna, Austria (<http://www.R-project.org/>)

- Rosi, A., Berti, M., Bicocchi, N., Castelli, G., Corsini, A., Mamei, M., Zambonelli, F., 2011. Landslide monitoring with sensor networks: experiences and lessons learnt from a real-world deployment. *Int. J. Sens. Networks* 10, 111. doi:10.1504/IJSNET.2011.042195
- Savage, W.Z., Varnes D.J., 1987. Mechanism of gravitational spreading of steep-sided ridges ("sackung"). *Bull Int As Eng Geol*, 35, 31-36
- Sick, B., Walter, M., Joswig, M., 2014. Visual Event Screening of Continuous Seismic Data by Supersonograms. *Pure Appl. Geophys.* 171, 549–559. doi:10.1007/s00024-012-0618-x
- Szwedzicki, T., 2003. Rock mass behaviour prior to failure. *Int. J. Rock Mech. Min. Sci.* 40, 573–584. doi:10.1016/S1365-1609(03)00023-6
- Szwedzicki, T., 2001. Geotechnical precursors to large-scale ground collapse in mines. *Int. J. Rock Mech. Min. Sci.* 38, 957–965. doi:10.1016/S1365-1609(01)00062-4
- Vila, J., Macià, R., Kumar, D., Ortiz, R., Moreno, H., Correig, A.M., 2006. Analysis of the unrest of active volcanoes using variations of the base level noise seismic spectrum. *J. Volcanol. Geotherm. Res.* 153, 11–20. doi:10.1016/j.jvolgeores.2005.10.011
- Voight B., 1989. A relation to describe rate-dependent material failure. *Science*, 243(4888): 200–203
- Walter, M., Arnhardt, C., Joswig, M., 2012a. Seismic monitoring of rockfalls, slide quakes, and fissure development at the Super-Sauze mudslide, French Alps. *Eng. Geol.* 128, 12–22. doi:10.1016/j.enggeo.2011.11.002
- Walter, M., Schwaderer, U., Joswig, M., 2012b. Seismic monitoring of precursory fracture signals from a destructive rockfall in the Vorarlberg Alps, Austria. *Nat. Hazards Earth Syst. Sci.* 12, 3545–3555. doi:10.5194/nhess-12-3545-2012
- Xu, N.W., Li, T.B., Dai, F., Li, B., Zhu, Y.G., Yang, D.S., 2015. Microseismic monitoring and stability evaluation for the large scale underground caverns at the Houziyan hydropower station in Southwest China. *Eng. Geol.* 188, 48–67. doi:10.1016/j.enggeo.2015.01.020
- Zischinsky, U., 1969. *Über Sackungen*. *Rock Mech*, 1, 30-52

Aknowledgements

Al termine di questa avventura, se mi fermo per un attimo e mi volto indietro rivedo un percorso fatto di persone, di cose, di luoghi, di sapori difficili da dimenticare e che hanno costantemente accompagnato questi tre anni di studio.

Voglio ringraziare innanzitutto il Prof. Salvatore Martino, mentore e tutor del mio Dottorato, per essere stato una guida attenta e disponibile in ogni momento e, soprattutto, per la fiducia sempre riposta nei miei confronti. Un ringraziamento particolare va anche al Prof. Alberto Prestininzi, docente co-tutor, per l'attenzione che mai mi ha fatto mancare. Grazie alla Prof.ssa Francesca Bozzano, direttrice del Centro di Ricerca CERI, per il supporto dato in questi tre anni di corso. Grazie, in termini più generali, a tutti i componenti la sezione di Geologia Applicata di questo Dipartimento, per la scienza e la conoscenza che in questi anni di studio, fin dalla laurea triennale, mi hanno trasmesso ed insegnato.

Un grazie particolarmente sentito va a Gigi e Luigi: senza la loro disponibilità e la loro passione non sarebbe stato possibile realizzare il "sogno" di Acuto. Un altro grazie particolarmente vivo va ad Antonella Paciello per la presenza costante e per l'aiuto che in questi anni ha sempre dato a me ed ai miei colleghi: l'insegnamento più prezioso che ci lascia e di cui faccio tesoro è la dedizione al lavoro e l'entusiasmo messo in tutte le attività fatte e proposte. Grazie ad Andrea Fantini, per la presenza, l'aiuto e la stima sempre accordatami. Grazie a Stefano Rivellino, collega ed amico: la sua costante e discreta presenza è stata preziosa e fondamentale durante questi anni. Grazie a tutti i colleghi dottorandi che con me hanno condiviso questo percorso più o meno da vicino, ognuno di voi mi ha arricchito del vostro affetto, del vostro aiuto e della vostra amicizia.

Pilastro e fondamenta della mia vita sono sempre stati tutti i miei amici. Da voi ho ricevuto un bene grande ed incondizionato: vi custodisco indistintamente nel mio cuore, come una cosa preziosa. Grazie innanzitutto agli amici che l'università stessa mi ha dato e che sono diventati presenza costante nella mia vita: Andrea, Roberto (M.) e Lorenzo, Chiara. Grazie a Roberto (I.) con cui ho condiviso un tempo ben più lungo dei tre anni di dottorato ed iniziato fin dalla laurea triennale. Grazie agli amici storici David, Daniel ed Eleonora perché da anni sono affianco a me, donandomi un affetto inestimabile. Un grazie particolare va a tutti i miei amici di Pesaro perché accompagnano da sempre molti passaggi della mia vita. Sono tanti... scrivere il nome di ognuno in questa pagina risulterebbe eccessivo, ma ognuno di loro è impresso chiaramente nel mio cuore. Un grazie speciale va al gruppo degli SD... questa tesi è dedicata anche a noi e alla nostra amicizia.

Grazie a Cocu, amico da quasi tutta la vita, perché la sua presenza è sempre stata una certezza che testimonia un'amicizia sincera, inseparabile e caratterizzata da grande affetto.

Grazie a mamma Elisa e papà Domenico per avermi educato e cresciuto con amore e determinazione, accompagnandomi sempre nelle vita ma lasciandomi libero di scegliere la mia strada. Grazie a Silvia, sorella minore, per il legame profondo che si accresce sempre. Grazie a zia Stefania, anche lei sempre pronta a starmi affianco con grande affetto.

Il Grazie più grande va a Giammi, amico e fratello nella vita (il mio *Frates...*), perché con me ha condiviso ogni momento di questa avventura e più in generale degli ultimi tre anni, insegnandomi, più di ogni altro, il valore inestimabile della vera amicizia. Un bambino ischitano, con innocenza e genuinità, ha colto perfettamente il sentimento che ci lega e che è radicato in noi: "...da quanto tempo studiate insieme? da parecchio tempo... ...ma ogni giorno? sì, ogni giorno... ...ah (sorridendo) ...allora siete migliori amici!". La nostra indissolubile e fraterna amicizia è la preziosa eredità che questo dottorato mi lascia e che custodirò nel mio cuore per tutta la vita (e si sa... l'amicizia va anche in paradiso!). Un grande Grazie va poi a Francesca, la sua compagna, per il grande affetto, la grande amicizia e la grande stima che da sempre mi accorda e mi dimostra.

Infine Grazie ai miei nonni... so che il vostro amore non mi abbandonerà mai!

